NASA
Technical
Paper
2922 C#2

August 1989

Longitudinal Aerodynamic Characteristics of a Subsonic, Energy-Efficient Transport Configuration in the National Transonic Facility

Peter F. Jacobs
and Blair B. Gloss

NASA

NASA
Technical
Paper
2922

1989

Longitudinal Aerodynamic Characteristics of a Subsonic, Energy-Efficient Transport Configuration in the National Transonic Facility

Peter F. Jacobs
and Blair B. Gloss
Langley Research Center
Hampton, Virginia

NASA
National Aeronautics and
Space Administration
Office of Management
Scientific and Technical
Information Division

Summary

An investigation has been conducted in the National Transonic Facility (NTF) at the Langley Research Center to determine Reynolds number, aeroelasticity, boundary-layer transition, and nonadiabatic wall temperature effects for a subsonic, energy-efficient transport model. The model was tested over a Mach number range from 0.50 to 0.86 and a Reynolds number range from 1.9×10^6 to approximately 23.0×10^6 (based on mean geometric chord). The majority of the data were taken using cryogenic nitrogen. (Data at a Reynolds number of 1.9×10^6 were taken in air.) Longitudinal force and moment, wing pressure, and wing thermocouple data are presented in this report. The data indicate that increasing the Reynolds number resulted in greater effective camber of the supercritical wing and horizontal tail, thus resulting in greater lift and pitching-moment coefficients at nearly all angles of attack for a Mach number (M) of 0.82. As Reynolds number was increased, untrimmed lift-drag ratio (L/D) increased, the angle of attack for maximum L/D decreased, drag creep was reduced significantly, and drag-divergence Mach number increased slightly. Data repeatabilty for both modes of operation of the NTF (air and cryogenic nitrogen) was generally very good, and nonadiabatic wall effects were estimated to be small. Transition-free and transition-fixed configurations had significantly different force and moment data at $M = 0.82$ for low Reynolds numbers, and very small differences were noted at high Reynolds numbers.

Introduction

To aid in the checkout of the data acquisition systems of the National Transonic Facility (NTF) and for a tunnel-to-tunnel comparison, several cryogenic tunnel models were built. These models were based on existing NASA Langley wind-tunnel models for which a large data base existed. One of these models, the Pathfinder I, is representative of a subsonic, energy-efficient transport (EET) with a wide-body fuselage and an aspect-ratio-9.8 supercritical wing (fig. 1). The Pathfinder I model, which was based on one of the EET configurations developed by Whitcomb and Bartlett (refs. 1 and 2) in the late 1970's, was designed for a cruise Mach number of 0.82 at a cruise lift coefficient (wing-body configuration) of 0.55. The Pathfinder I has been used extensively in the NTF, not only in the checkout of tunnel systems but also as a research model for high Reynolds number and cryogenic flow phenomena. For the present investigation, the primary objectives were to determine Reynolds number, aeroelasticity, boundary-layer transition, and nonadiabatic wall temperature effects. The model was tested over a Mach number range from 0.50 to 0.86 and a Reynolds number range from 1.9×10^6 to approximately 23.0×10^6 (based on mean geometric chord). The majority of the data were taken using nitrogen as the test gas; however, the data at a Reynolds number of 1.9×10^6 were taken in the air mode of operation.

Symbols

Force and moment data presented in this paper have been reduced to conventional coefficient form based on the wing trapezoidal planform area (extended to the fuselage centerline). Longitudinal aerodynamic characteristics are referred to the stability-axis system. Moments are referenced to the quarter-chord of the mean geometric chord. All dimensional values are given in U.S. Customary Units. The symbols are defined as follows:

b	wing span, 52.97 in.
C_D	drag coefficient, Drag/qS
C_L	lift coefficient, Lift/qS
C_m	pitching-moment coefficient, Pitching moment/$qS\bar{c}$
C_p	pressure coefficient, $(p - p_\infty)/q$
c	local streamwise chord of wing, in.
$\bar{c}$	mean geometric chord of reference wing panel, 5.74 in.
E	Young's modulus of elasticity
i_H	horizontal tail incidence, positive for leading edge up, deg
L/D	lift-drag ratio
M	free-stream Mach number
p	local static pressure, psi
p_T	total pressure, psia
p_∞	free-stream static pressure, psia
q	free-stream dynamic pressure, psf
$R_{\bar{c}}$	Reynolds number based on mean geometric chord
r	fuselage cross-section radius, in.
S	wing planform reference (trapezoidal) area, 1.988 ft^2
T	absolute temperature of wing from thermocouples, °R
T_{aw}	absolute adiabatic wall temperature, °R

T_T total temperature, °F

x chordwise distance, positive aft, in.

y spanwise distance from model centerline, in.

z vertical coordinate of airfoil, positive upward, in.

z_o waterline (W.L.) of leading edge for wing coordinates in table II, in.

z' coordinate of vertical tail airfoil (see table V), in.

α angle of attack, deg

Δ incremental value

η semispan station, $2y/b$

Subscripts:

le leading edge

min minimum value

Abbreviations:

F.S. fuselage station, in.

L.S. lower surface

U.S. upper surface

W.L. waterline, in. (fuselage centerline is W.L. 0.00; positive direction is up)

Experimental Apparatus and Procedures

Test Facility

The National Transonic Facility (NTF) at the Langley Research Center is a closed-circuit, continuous-flow, cryogenic pressure tunnel. The test section is 8.2 ft by 8.2 ft and 25 ft long with slots in the floor and ceiling. The NTF has a Mach number range from 0.2 to 1.2, a total pressure range from approximately 15 to 125 psia, and a temperature range from 320°F to 150°F. Actual test conditions for this investigation are presented in table I.

The test gas may be either dry air or nitrogen. For the air mode of operation, heat is removed by a water-cooled heat exchanger located at the upstream end of the settling chamber. For the cryogenic mode of operation, heat is removed by evaporating liquid nitrogen, which is sprayed into the tunnel circuit upstream of the fan. When nitrogen is injected into the tunnel, venting is used to maintain constant total pressure. To minimize energy consumption and reduce thermal cycling of the pressure shell, thermal insulation in the NTF is installed internal to the pressure shell.

In order to maintain good flow quality and aerodynamic efficiency over the wide operating range of the NTF, the test-section floor and ceiling walls, the reentry flaps, and the step height for reentering slot flow can be varied remotely. In addition, there are four turbulence damping screens in the settling chamber and a 15:1 contraction from the settling chamber to the nozzle throat to reduce turbulence. Acoustic treatment upstream and downstream of the fan helps minimize fan noise effects. Further details of the tunnel can be found in reference 3.

Model Description

The Pathfinder I model is representative of a subsonic, energy-efficient transport (EET) with a wide-body fuselage and supercritical wing. This configuration was designed for a cruise Mach number of 0.82 at a lift coefficient (wing-body) of 0.55. A sketch of the model is shown in figure 2.

The supercritical wing has a span of 52.97 in., a trapezoidal planform area of 1.98 ft^2, an aspect ratio of 9.8, 35° of sweep at the quarter-chord, and 5° of dihedral. The wing has thickness-chord ratios of 0.145 at the root, 0.120 at the geometric break, and 0.106 at the tip. Wing coordinates are presented in table II. The fuselage is 50.00 in. long and has a maximum diameter of 5.75 in. The fuselage geometry is presented in table III.

The all-moving supercritical horizontal tail has a span of 19.59 in., a planform area of 0.70 ft^2, an aspect ratio of 3.82, 32.5° of sweep at the quarter-chord, 10° of dihedral, and a thickness-chord ratio of 0.10. The incidence of the horizontal tail was set at 0° throughout the investigation. The supercritical vertical tail has a span of 10.00 in., a planform area of 0.42 ft^2, an aspect ratio of 1.65, 35° of sweep at the quarter-chord, and a thickness-chord ratio of 0.10. Coordinates of the horizontal and vertical tails are presented in tables IV and V, respectively.

This small-scale model was designed to be tested at near-flight Reynolds numbers, and therefore a very smooth model surface was required. The surface finish was 8 10 μin. (root-mean-square) over the entire model.

Instrumentation includes a three-axis accelerometer and six, 32-port, electronically scanned pressure (ESP) modules housed in the nose of the fuselage, a six-component strain-gauge balance, three balance thermocouples, and nine wing and fuselage thermocouples.

Transition Strips

Transition strips consisting of sparsely distributed No. 180 carborundum grit set in a plastic adhesive were applied to the wing, tails, and fuselage of the Pathfinder I model for most of the test. The strips were approximately 0.1 in. wide and were located 1.0 in. aft of the nose of the fuselage and at 10 percent of the local chord on the wing and tails.

The grit was sized based on charts developed for the NTF that use the ideal-gas equations of references 4 and 5. Use of the real-gas equations was considered unnecessary, because real-gas corrections are small except at very high Reynolds numbers (where transition strips probably are not needed), and also because the roughness particles are usually chosen to be slightly larger than the critical roughness height in order to ensure transition for a range of test conditions. However, since the viscosity of nitrogen changes significantly with pressure at low temperatures, the viscosity equations of reference 6 were used. The grit size was calculated for low Reynolds number conditions. The grit was located relatively far forward throughout most of the test because time considerations did not allow for numerous tunnel entries to relocate the transition strips. Normally, the transition strips would be located as far aft as possible for low Reynolds number conditions to simulate a higher Reynolds number. Consequently, for this investigation drag levels at low Reynolds number conditions are higher than would result for aft transition locations. As the Reynolds number is increased, the wing boundary layer gets thinner and eventually the transition strip height exceeds the calculated flat-plate boundary-layer thickness.

Measurements

Aerodynamic force and moment data were obtained with a six-component, electrical strain-gauge balance. The quoted accuracy of the balance is 0.5 percent of the full-scale values (normal force, 3400 lb; axial force, 300 lb; pitching moment, 10 000 in-lb; rolling moment, 5000 in-lb; yawing moment, 5000 in-lb; and side force, 1000 lb). However, the repeatability of the data was generally better than the quoted accuracy.

A three-axis accelerometer package attached to the balance block was used to measure roll angle and angle of attack. Static pressures were measured in the model along the sting cavity by using differential-pressure transducers referenced to tunnel plenum static pressure.

The Pathfinder I has a total of 173 wing-surface pressure taps located in six spanwise rows ($\eta = 0.131$, 0.282, 0.432, 0.640, 0.829, and 0.961). Nominal chordwise pressure orifice locations are presented in chart A. Because of model strength and construction considerations, the upper- and lower-surface pressures were located on left and right wing panels, respectively. The wing pressures were measured with six, 32-port, electronically scanned pressure (ESP) modules. Three of the modules had a full-scale range of ±30 psid, and three had a range of ±15 psid. Accuracy of the modules over their full pressure range is ±0.25 percent of full scale.

Chart A

x/c	
U.S.	L.S.
0.025	0.025
.075	.075
.125	.125
.200	.200
.300	.300
.400	.400
.450	.500
.500	.600
.550	.700
.600	.800
.650	
.700	
.800	
.900	

The thermocouples on the model were type T (copper-constantan). The wing thermocouples were located at $\eta = 0.2$, 0.5, and 0.8 at $x/c \approx 0.4$.

Corrections

The angle of attack of the model was corrected for flow angularity in the tunnel test section. This correction was obtained from upright and inverted tests of the model. Drag data presented herein have been adjusted to correspond to the condition of free-stream static pressure acting in the balance chamber and at the base of the fuselage. No correction has been made to the data to account for wall interference effects.

The wind-tunnel floor and ceiling walls were set at the proper angles (from tunnel-empty calibrations) to eliminate pressure gradients and buoyancy effects in the test section. Also, the solid-blockage ratio of the model was sufficiently small to minimize blockage effects based on conventional criteria.

During previous cryogenic investigations of the Pathfinder I in the NTF, a "frostlike" substance was observed on the model. This substance was later shown to be water vapor that was released from the internal insulation of the NTF and then formed frost on the model. After an extensive study of the problem and several operational procedure changes, the amount of water vapor being released was greatly reduced. Pressure distributions from the current investigation are presented in reference 7 and show that frost effects on model surface pressures are very small. The errors in pressure measurements due to frost at design conditions are on the same order as those due to Mach number differences of less than 0.001 or angle-of-attack differences of approximately 0.01°. Thus, since it is unlikely that frost effects are discernible, no corrections have been made to the data of this investigation.

Discussion of Results

A typical map of test conditions for a cruise Mach number of 0.82 is shown in figure 3. Since it is more cost-effective to make cryogenic runs at low pressure (less nitrogen consumption), most of the Reynolds number effect data are taken at approximately 30 psia. However, as shown in figure 3, the Reynolds number range that can be achieved by a reduction of gas temperature increases significantly with pressure. The data taken at a total pressure of approximately 30 psia have a Reynolds number range from 4.8×10^6 to 17.9×10^6. To achieve a Reynolds number of 22.7×10^6, the total pressure was increased to approximately 40 psia. Data were taken at both pressures for a Reynolds number of 17.9×10^6 in order to determine model aeroelastic effects.

Because the steel used in the Pathfinder I model becomes stiffer (the modulus of elasticity (E) increases) as temperature decreases, the test points showing the Reynolds number effect are not run at a constant dynamic pressure. Instead, the total pressure is increased slightly as temperature is decreased to maintain a constant ratio of dynamic pressure to modulus of elasticity (q/E). Test points for other Mach numbers are similar to those in figure 3.

Repeatability

The repeatability of the longitudinal aerodynamic data taken during separate runs in the air mode and cryogenic mode of operation at $M = 0.82$ is shown in figures 4–6 and figures 7–9, respectively.

In the air mode, the variations of C_L versus α (fig. 4) and C_m versus C_L (fig. 5) show exceptional repeatability for values of C_L up to the initial break in the lift curve, and good agreement is shown beyond the break. The variation of C_D versus C_L (fig. 6) shows good repeatability, with a maximum difference in drag coefficient of approximately 0.0004. It should be noted that this increment in drag is equivalent to approximately 0.5 lb and that the axial-force capacity of the balance is 300 lb. Thus, the repeatability for these data is better than the quoted accuracy for the balance of 0.5 percent of full scale.

In the cryogenic mode of operation, the lift data (fig. 7) and pitching-moment data (fig. 8) show very good repeatability. The drag data (fig. 9) have a similar maximum variation as in the air mode for lift coefficients up to the lift-curve break. The increment in drag increases after the lift-curve break possibly because of small differences in Mach number between the repeat runs.

Aeroelasticity

One of the advantages of a cryogenic pressure tunnel is that Reynolds number and aeroelastic effects may be studied independently. For the Pathfinder I, the effect of a variation in total pressure at nearly constant Reynolds number on the longitudinal force and moment data and the chordwise pressure distributions is presented in figures 10–12 and figure 13, respectively. Data are presented for a Mach number of 0.82 at total pressures of approximately 31.2 and 40.0 psia. The lift and pitching-moment data in figures 10 and 11, respectively, indicate essentially negligible aeroelastic effects. Some exaggeration of the effect in figures 10 and 11 occurs because the cubic-spline fairings are affected by the differences in data density at values of C_L greater than 0.7. A comparison of pressure distributions at an angle of attack of approximately 3.2° (fig. 13) reveals a very slight unloading of the wing outboard of $\eta = 0.432$ for the higher dynamic pressure data. However, it should be noted that some of the differences between the data in figure 13 are due to small angle-of-attack and Mach number variations ($\Delta\alpha = 0.008$ and $\Delta M = 0.0019$). Small differences in drag level (fig. 12) are due to base-pressure correction differences that cannot be explained.

Transition Effects

Longitudinal force and moment data for the clean wing (transition off) and transition-fixed (transition on) configurations at a Mach number of 0.82 are presented in figures 14–16, and chordwise pressure distributions at a Reynolds number of approximately 22×10^6 are presented in figure 17.

Low Reynolds number data. At a Reynolds number of 4.8×10^6, the variation of C_L versus α (fig. 14(a)) indicates that the clean wing has greater effective camber because of a thinner boundary layer and thus generates more lift. The effectiveness of aft-cambered supercritical wings is sensitive to boundary-layer transition location, as was shown in references 8–10. At $\alpha \approx 1°$, the transition point on the upper surface of the clean wing moves forward and causes a loss of lift. However, the average natural transition point on the clean wing remains aft of the transition for the transition-fixed configuration (0.1c). At the highest angles of attack tested, the clean wing has reduced trailing-edge separation and significantly higher lift than the transition-fixed configuration. The data trends shown in the lift data are also evident in the variations of C_m versus C_L and C_D versus C_L (figs. 15(a) and 16(a), respectively). Because the clean wing has a thinner boundary layer and more effective camber, it produces a more negative pitching moment and lower drag than the transition-fixed data. As the transition point for the clean wing moves forward, the pitching moments become less negative and the drag level increases.

The clean-wing force and moment data underscore the importance of transition fixing for low Reynolds number tests. The natural transition point for configurations like the Pathfinder I can move around significantly with angle of attack, thus making data analysis and extrapolation very difficult.

High Reynolds number data. Longitudinal force and moment data are presented in figures 14(b), 15(b), and 16(b) for the clean wing and the transition-fixed configuration at a Mach number of 0.82 and Reynolds numbers of 22.7×10^6 and 21.5×10^6, respectively. The dynamic pressure and Reynolds number for these two configurations are not identical ($\Delta q \approx 1$ percent); however, the small differences should not significantly affect the data comparisons. The variation of C_L versus α (fig. 14(b)) and of C_m versus C_L (fig. 15(b)) indicates that the transition points for both configurations are nearly identical.

The drag data (fig. 16(b)) indicate that the increment in drag coefficient between the transition-fixed and clean wing configurations is approximately 0.0010 to 0.0020. However, only a portion of this increment can be considered "trip drag" in the classical sense. Some of the drag increment is probably due to increased trailing-edge separation for the transition-fixed configuration. Evidence of trailing-edge separation is shown in figure 17(b) at $\eta = 0.640$, where the shock wave for the transition-fixed configuration has moved forward of the clean wing shock wave. The transition strips (which were sized for low Reynolds number conditions) may have some effect on local surface pressures near the leading edge of the outboard pressure rows. It should be noted that the lower-surface pressures for the clean wing configuration were not available because of ESP instrumentation malfunction.

An estimation of the trip drag penalty has been made in the following manner. Minimum drag values ($C_{D,\text{min}}$) were determined from a series of transition-fixed polars at $M = 0.82$ and Reynolds numbers from 1.9×10^6 to 21.5×10^6. The values of C_L corresponding to the values of $C_{D,\text{min}}$ were less than 0.1 and were approximately the same. Therefore, an assumption was made that the induced-drag portion of $C_{D,\text{min}}$ was essentially the same for each Reynolds number and was small enough to neglect. Using the Somer and Short T$'$ method of reference 11, flat-plate turbulent-skin-friction values were computed for boundary layers starting at the leading edge of the wing and at 0.1c. No estimate was made for laminar skin friction on the first 10 percent of the chord in the latter case. All skin-friction values were then multiplied by the ratio of $C_{D,\text{min}}$ (with $R_{\bar{c}} = 1.9 \times 10^6$) to the 90-percent turbulent-skin-friction value (with $R_{\bar{c}} = 1.9 \times 10^6$). The data are presented in figure 18 and indicate that for Reynolds numbers greater than approximately 3.0×10^6, the transition on the wing moves forward of 0.1c. Also, it would appear that for Reynolds numbers higher than approximately 12.0×10^6, the boundary layer is fully turbulent and some trip drag is present. At a Reynolds number of 21.5×10^6, the trip drag increment is approximately 0.0008.

Nonadiabatic Wall Effects

The influence of nonadiabatic wall conditions on skin friction and boundary-layer properties is well-known. In cryogenic tunnels such as the NTF, the model should be nearly stabilized in temperature to minimize nonadiabatic wall effects. The instrumentation of the Pathfinder I model included thermocouples on the wing and fuselage to monitor model temperatures. Typical wing temperature data for a series of runs at $M = 0.82$ are presented in figure 19 for three wingspan stations ($\eta = 0.2$, 0.5, and 0.8) at $x/c \approx 0.4$. Each symbol represents a different angle of attack in a pitch polar. The method of Johnson and Adcock (ref. 12) was used to calculate the adiabatic wall temperature. It should be noted that the wing thermocouples were buried in the wing, not on the surface. It is reasonable to assume then that the thermocouple response would lag the surface-temperature variations caused by changes in local flow conditions with angle of attack. Therefore, the data in figure 19 are considered to be conservative and actual surface temperatures should be closer to the adiabatic wall temperatures.

For relatively warm surface-temperature data ($T_T > -100°\text{F}$), the wing temperatures are within approximately 2 percent of the adiabatic wall temperatures; and for the coldest surface-temperature data ($T_T < -250°\text{F}$), the wing temperatures are less than 8 percent higher than the adiabatic wall temperatures. Data from references 13 and 14 indicate that for configurations with transition near the leading edge, values of T/T_{aw} of the same magnitude do not significantly affect the data. Thus, any error due to nonadiabatic wall effects should be well within the balance accuracy and within the balance repeatability as well.

Reynolds Number Effects

The effects of Reynolds number ($R_{\bar{c}}$) on the longitudinal aerodynamic characteristics of the Pathfinder I (with transition fixed) at a cruise Mach number of 0.82 are presented in figures 20–23. The Reynolds number ranged from 1.9×10^6 to 21.5×10^6. It has been shown that aeroelastic effects for a total pressure range of approximately 31 to 40 psia (i.e., the data from a Reynolds number range between 4.8×10^6 and 21.5×10^6) are small. However, because of tunnel operational constraints, the data at $R_{\bar{c}} = 1.9 \times 10^6$ and 3.0×10^6 were run at significantly lower values of q/E. Therefore, data comparisons with the higher Reynolds number data involve unknown aeroelastic effects.

The lift data (fig. 20) demonstrate the effective camber increase with Reynolds number for the highly aft-cambered supercritical wing of the Pathfinder I. Although the shape of the lift curves is fairly constant, the curves translate in the positive C_L direction with increasing Reynolds number. Some of the difference is a function of the forward transition strip location. If the transition strips had been located farther aft (i.e., in a thinner boundary layer) for the lower Reynolds number data, the extent of the translation of the curves would be reduced. The increase in the aft loading and in the extent of the upper-surface pressure plateau with Reynolds number is evident in the pressure distributions of figure 24.

The variation of C_m versus C_L and of C_m versus α (figs. 21 and 22, respectively) indicates more positive (nose-up) pitching moments with increasing Reynolds number. The increase in effective camber of the wing with Reynolds number, which would tend to produce a more negative C_m, is offset by increased negative loading on the horizontal tail resulting in a more positive C_m. It should be noted that at $R_{\bar{c}} = 21.5 \times 10^6$, the α required for any C_L is approximately 0.4° less than the α required at $R_{\bar{c}} = 1.9 \times 10^6$ (fig. 20). Thus, for constant C_L, the incidence of the horizontal tail would be 0.4° lower at $R_{\bar{c}} = 21.5 \times 10^6$ than at 1.9×10^6; and because the horizontal tail has inverted airfoils (negative camber), the negative load on the tail would increase with Reynolds number. In addition, the load on the horizontal tail would also increase with Reynolds number because of greater effective camber. A comparison of pitching-moment data for the Pathfinder I with data taken in the NASA Langley 8-Foot Transonic Pressure Tunnel for the geometrically similar Pathfinder I prototype configuration of reference 2 is shown in figure 25. The Pathfinder I data have been recomputed using approximately the same static margin as the data from reference 2. The data in figure 25 indicate that the increase in C_m due to an increase in Reynolds number for the Pathfinder I is remarkably similar to the increase in C_m due to a decrease in horizontal tail incidence of 0.5° for the Pathfinder I prototype ($R_{\bar{c}} = 2.4 \times 10^6$).

The smoothness of the untrimmed drag data (fig. 23) is adversely affected by unresolved base pressure fluctuations and also by small errors in the test conditions that were introduced by manual control of the wind tunnel. It should be noted that the NTF integrated control system (simultaneous control of M, p_T, and T_T) was not fully operational during this investigation, and manual control was often required. The shape of the drag polars for the Pathfinder I does not change significantly with Reynolds number for $C_L < 0.6$. However, the increased trailing-edge separation present at low Reynolds numbers for $C_L > 0.6$ results in a more rapid increase in drag than for higher Reynolds numbers. Also, as previously discussed, some trip drag was present at the higher Reynolds numbers that would affect overall drag level.

The untrimmed lift-drag ratio (L/D) data for the Pathfinder I (with tails) in figures 26 and 27 indicate that the maximum L/D occurs at $C_L \approx 0.6$ regardless of Reynolds number. The angle of attack for the maximum L/D decreases slightly with increasing Reynolds number as would be expected.

Drag data for Mach number sweeps at Reynolds numbers of 3.0×10^6 and approximately 23.0×10^6 (fig. 28) were used to determine the effects of Reynolds number on the untrimmed drag rise characteristics of the Pathfinder I (fig. 29). The high Reynolds number data (fig. 29(b)) show significantly less drag creep than the low Reynolds number data (fig. 29(a)), even though some trip drag is present in the high Reynolds number data. For $C_L = 0.6$, the drag creep between $M = 0.5$ and $M = 0.82$ is 0.0050 and 0.0021 for the low and high Reynolds numbers, respectively. The drag-divergence Mach number is based on $\Delta C_D/\Delta M = 0.1$ and is indicated by a tick mark in figure 29. The drag-divergence Mach number at $C_L = 0.6$ increased slightly with Reynolds number from 0.821 to 0.825.

Summary of Results

An investigation has been conducted in the National Transonic Facility (NTF) at the Langley Research Center to determine Reynolds number, aeroelasticity, boundary-layer transition, and non-adiabatic wall temperature effects for a subsonic, energy-efficient transport model. The model was tested over a Mach number range from 0.50 to 0.86 and a Reynolds number range from 1.9×10^6 to approximately 23.0×10^6 (based on mean geometric chord). The majority of the data were taken using cryogenic nitrogen. (Data at a Reynolds number of 1.9×10^6 were taken in air.) Longitudinal force and moment, wing pressure, and wing thermocouple data are presented in this report. The results of this investigation may be summarized as follows:

1. Increasing the Reynolds number resulted in greater effective camber of the supercritical wing and horizontal tail, thus resulting in greater lift and pitching-moment coefficients at nearly all angles of attack for a Mach number (M) of 0.82.

2. As Reynolds number was increased, untrimmed lift-drag ratio (L/D) increased and the angle of attack for maximum L/D decreased.

3. Drag creep was reduced significantly and drag-divergence Mach number increased slightly with increasing Reynolds number.

4. NTF data repeatability for both air and cryogenic nitrogen modes of operation was generally very good.

5. Comparisons of force and moment data at $M = 0.82$ for transition-free and transition-fixed configurations showed significant differences at a Reynolds number of 4.8×10^6 and very small differences at a Reynolds number of approximately 21.6×10^6.

6. Nonadiabatic wall effects were estimated to be small.

NASA Langley Research Center
Hampton, VA 23665-5225
June 14, 1989

References

1. Bartlett, Dennis W.: *Wind-Tunnel Investigation of Several High Aspect-Ratio Supercritical Wing Configurations on a Wide-Body-Type Fuselage.* NASA TM X-71996, 1977.
2. Jacobs, Peter F.: *Experimental Trim Drag Values and Flow-Field Measurements for a Wide-Body Transport Model With Conventional and Supercritical Wings.* NASA TP-2071, 1982.
3. Fuller, Dennis E.: *Guide for Users of the National Transonic Facility.* NASA TM-83124, 1981.
4. Chapman, Dean R.; and Rubesin, Morris, W.: Temperature and Velocity Profiles in the Compressible Laminar Boundary Layer With Arbitrary Distribution of Surface Temperature. *J. Aeronaut. Sci.*, vol. 16, no. 9, Sept. 1949, pp. 547–565.
5. Braslow, Albert L.; and Knox, Eugene C.: *Simplified Method for Determination of Critical Height of Distributed Roughness Particles for Boundary-Layer Transition at Mach Numbers From 0 to 5.* NACA TN 4363, 1958.
6. Kilgore, Robert Ashworth: *The Cryogenic Wind Tunnel for High Reynolds Number Testing.* Ph.D. Thesis, Univ. of Southampton, 1974. (Available as NASA TM X-70207.)
7. Gloss, Blair B.; and Bruce, Robert A.: A Solution to Water Vapor in the National Transonic Facility. AIAA-89-0152, Jan. 1989.
8. Anglin, Ernie L.; and Byrdsong, Thomas A.: Wing Flap-Type Control Effectiveness and Effects of Control Hinge Gap Seals for a Supercritical Wing. AIAA-82-0960, June 1982.
9. Jacobs, Peter F.: *Aileron Effectiveness for a Subsonic Transport Model With a High-Aspect-Ratio Supercritical Wing.* NASA TM-85674, 1983.
10. Jacobs, Peter F.: *Effect of Aileron Deflections on the Aerodynamic Characteristics of a Semispan Model of a Subsonic Energy-Efficient Transport.* NASA TP-2478, 1985.
11. Peterson, John B., Jr.: *A Comparison of Experimental and Theoretical Results for the Compressible Turbulent-Boundary-Layer Skin Friction With Zero Pressure Gradient.* NASA TN D-1795, 1963.
12. Johnson, Charles B.; and Adcock, Jerry B.: Measurement of Recovery Temperature on an Airfoil in the Langley 0.3-m Transonic Cryogenic Wind Tunnel. AIAA-81-1062, June 1981.
13. Johnson, Charles B.: Study of Nonadiabatic Boundary-Layer Stabilization Time in a Cryogenic Tunnel for Typical Wing and Fuselage Models. *J. Aircr.*, vol. 18, no. 11, Nov. 1981, pp. 913–919.
14. Lynch, F. T.; Fancher, M. F.; Patel, D. R.; and Inger, G. R.: Nonadiabatic Model Wall Effects on Transonic Airfoil Performance in a Cryogenic Wind Tunnel. *Wind Tunnels and Testing Techniques*, AGARD-CP-348, Feb. 1984, pp. 14-1–14-11.

Table I. Test Conditions

M	R_c	p_T, psia	T_T, °F
0.50	3.0×10^6	26.3	26
.50	23.0	57.5	−262
.60	3.0	22.9	26
.60	23.2	49.8	−263
.70	3.0	20.8	25
.70	22.9	44.5	−262
.75	3.0	19.9	27
.75	22.9	42.8	−261
.80	3.0	19.2	28
.80	23.0	41.4	−262
.82	1.9	14.7	100
.82	3.0	19.0	27
.82	4.8	30.0	22
.82	4.8	30.2	27
.82	6.0	30.0	−52
.82	7.3	30.5	−101
.82	7.7	38.9	−50
.82	7.8	26.3	−153
.82	7.8	20.4	−200
.82	9.0	26.9	−175
.82	13.1	30.0	−224
.82	17.4	40.0	−224
.82	17.8	31.2	−263
.82	21.5	40.4	−254
.82	22.7	40.0	−263
.82	22.8	40.4	−262
.84	3.0	18.8	28
.84	23.0	40.3	−262
.86	3.0	18.5	27
.86	23.1	39.8	−263

Table II. Wing Coordinates

(a) $\eta = 0$; $c = 13.58$ in.; $x_{le} = 17.56$ in.; z_o = W.L. −2.145 in.

x/c	z/c U.S.	z/c L.S.	x/c	z/c U.S.	z/c L.S.
0.000	0.00000	0.00000	0.360	0.06127	−0.08318
.002	.01006	−.00683	.380	.05963	−.08349
.005	.01542	−.01339	.420	.05577	−.08328
.010	.02076	−.02004	.460	.05135	−.08203
.020	.02835	−.02779	.500	.04656	−.07990
.030	.03383	−.03292	.520	.04407	−.07853
.040	.03784	−.03690	.540	.04154	−.07692
.050	.04135	−.04020	.560	.03900	−.07504
.060	.04456	−.04318	.580	.03645	−.07294
.070	.04741	−.04599	.600	.03388	−.07062
.080	.04992	−.04867	.620	.03131	−.06814
.090	.05211	−.05118	.640	.02876	−.06541
.100	.05401	−.05354	.660	.02623	−.06240
.110	.05569	−.05577	.680	.02370	−.05922
.120	.05718	−.05789	.700	.02117	−.05580
.130	.05850	−.05992	.720	.01864	−.05226
.140	.05972	−.06186	.740	.01610	−.04858
.150	.06079	−.06374	.760	.01352	−.04485
.160	.06166	−.06551	.780	.01090	−.04109
.170	.06250	−.06717	.800	.00822	−.03747
.180	.06319	−.06875	.820	.00550	−.03408
.190	.06379	−.07027	.840	.00273	−.03099
.200	.06433	−.07162	.860	−.00008	−.02823
.220	.06501	−.07408	.880	−.00296	−.02604
.240	.06540	−.07621	.900	−.00590	−.02442
.260	.06551	−.07804	.920	−.00890	−.02351
.280	.06526	−.07959	.940	−.01196	−.02327
.300	.06470	−.08084	.960	−.01510	−.02378
.320	.06383	−.08191	.980	−.01828	−.02525
.340	.06269	−.08271	1.000	−.02152	−.02778

Table II. Continued

(b) $\eta = 0.109$; $c = 11.40$ in.; $x_{le} = 19.74$ in.; $z_o =$ W.L. -1.893 in.

x/c	z/c U.S.	z/c L.S.	x/c	z/c U.S.	z/c L.S.
0.000	0.00000	0.00000	0.360	0.06127	−0.08318
.002	.01006	−.00683	.380	.05963	−.08349
.005	.01542	−.01339	.420	.05577	−.08328
.010	.02076	−.02004	.460	.05135	−.08203
.020	.02835	−.02779	.500	.04656	−.07990
.030	.03383	−.03292	.520	.04407	−.07853
.040	.03784	−.03690	.540	.04154	−.07692
.050	.04135	−.04020	.560	.03900	−.07504
.060	.04456	−.04318	.580	.03645	−.07294
.070	.04741	−.04599	.600	.03388	−.07062
.080	.04992	−.04867	.620	.03131	−.06814
.090	.05211	−.05118	.640	.02876	−.06541
.100	.05401	−.05354	.660	.02623	−.06240
.110	.05569	−.05577	.680	.02370	−.05922
.120	.05718	−.05789	.700	.02117	−.05580
.130	.05850	−.05992	.720	.01864	−.05226
.140	.05972	−.06186	.740	.01610	−.04858
.150	.06079	−.06374	.760	.01352	−.04485
.160	.06166	−.06551	.780	.01090	−.04109
.170	.06250	−.06717	.800	.00822	−.03747
.180	.06319	−.06875	.820	.00550	−.03408
.190	.06379	−.07027	.840	.00273	−.03099
.200	.06433	−.07162	.860	−.00008	−.02823
.220	.06501	−.07408	.880	−.00296	−.02604
.240	.06540	−.07621	.900	−.00590	−.02442
.260	.06551	−.07804	.920	−.00890	−.02351
.280	.06526	−.07959	.940	−.01196	−.02327
.300	.06470	−.08084	.960	−.01510	−.02378
.320	.06383	−.08191	.980	−.01828	−.02525
.340	.06269	−.08271	1.000	−.02152	−.02778

Table II. Continued

(c) $\eta = 0.132$; $c = 10.92$ in.; $x_{le} = 20.22$ in.; $z_o =$ W.L. -1.840 in.

x/c	z/c		x/c	z/c	
	U.S.	L.S.		U.S.	L.S.
0.000	0.00000	0.00000	0.360	0.06073	−0.08128
.002	.00971	−.00799	.380	.05926	−.08141
.005	.01525	−.01414	.420	.05579	−.08092
.010	.02075	−.02050	.460	.05178	−.07948
.020	.02830	−.02800	.500	.04741	−.07721
.030	.03358	−.03298	.520	.04513	−.07578
.040	.03747	−.03687	.540	.04279	−.07411
.050	.04085	−.04012	.560	.04041	−.07219
.060	.04391	−.04305	.580	.03801	−.07005
.070	.04664	−.04581	.600	.03557	−.06769
.080	.04906	−.04845	.620	.03310	−.06516
.090	.05118	−.05093	.640	.03063	−.06239
.100	.05304	−.05325	.660	.02816	−.05938
.110	.05469	−.05544	.680	.02568	−.05620
.120	.05615	−.05751	.700	.02318	−.05282
.130	.05746	−.05949	.720	.02065	−.04931
.140	.05865	−.06137	.740	.01810	−.04568
.150	.05969	−.06319	.760	.01550	−.04201
.160	.06056	−.06490	.780	.01286	−.03833
.170	.06139	−.06650	.800	.01016	−.03478
.180	.06206	−.06802	.820	.00740	−.03145
.190	.06265	−.06945	.840	.00459	−.02842
.200	.06317	−.07076	.860	.00172	−.02574
.220	.06387	−.07312	.880	−.00120	−.02361
.240	.06429	−.07512	.900	−.00419	−.02208
.260	.06442	−.07683	.920	−.00725	−.02129
.280	.06423	−.07827	.940	−.01038	−.02121
.300	.06375	−.07939	.960	−.01360	−.02189
.320	.06299	−.08031	.980	−.01687	−.02353
.340	.06199	−.08095	1.000	−.02019	−.02618

Table II. Continued

(d) $\eta = 0.150$; $c = 10.54$ in.; $x_{le} = 20.60$ in.; $z_o =$ W.L. -1.799 in.

x/c	z/c U.S.	z/c L.S.	x/c	z/c U.S.	z/c L.S.
0.000	0.00000	0.00000	0.360	0.06025	−0.07965
.002	.00940	−.00896	.380	.05894	−.07963
.005	.01509	−.01481	.420	.05579	−.07890
.010	.02073	−.02090	.460	.05215	−.07730
.020	.02825	−.02819	.500	.04813	−.07490
.030	.03336	−.03304	.520	.04603	−.07341
.040	.03715	−.03684	.540	.04384	−.07169
.050	.04041	−.04005	.560	.04162	−.06974
.060	.04335	−.04293	.580	.03935	−.06756
.070	.04598	−.04566	.600	.03701	−.06517
.080	.04831	−.04827	.620	.03463	−.06260
.090	.05036	−.05071	.640	.03223	−.05980
.100	.05219	−.05301	.660	.02981	−.05679
.110	.05381	−.05515	.680	.02737	−.05362
.120	.05526	−.05719	.700	.02490	−.05026
.130	.05656	−.05911	.720	.02238	−.04679
.140	.05771	−.06095	.740	.01980	−.04320
.150	.05873	−.06271	.760	.01719	−.03958
.160	.05961	−.06438	.780	.01453	−.03596
.170	.06041	−.06593	.800	.01181	−.03247
.180	.06108	−.06739	.820	.00901	−.02920
.190	.06166	−.06876	.840	.00617	−.02622
.200	.06217	−.07002	.860	.00325	−.02362
.220	.06287	−.07230	.880	.00028	−.02154
.240	.06331	−.07418	.900	−.00275	−.02008
.260	.06347	−.07579	.920	−.00586	−.01940
.280	.06333	−.07713	.940	−.00905	−.01947
.300	.06292	−.07815	.960	−.01233	−.02030
.320	.06226	−.07893	.980	−.01568	−.02207
.340	.06136	−.07944	1.000	−.01908	−.02484

Table II. Continued

(e) $\eta = 0.188$; $c = 9.79$ in.; $x_{le} = 21.35$ in.; z_o = W.L. -1.711 in.

x/c	z/c U.S.	z/c L.S.	x/c	z/c U.S.	z/c L.S.
0.000	0.00000	0.00000	0.360	0.05922	−0.07602
.002	.00872	−.01112	.380	.05826	−.07564
.005	.01476	−.01630	.420	.05583	−.07438
.010	.02072	−.02181	.460	.05298	−.07242
.020	.02814	−.02860	.500	.04975	−.06975
.030	.03288	−.03317	.520	.04803	−.06815
.040	.03644	−.03679	.540	.04621	−.06632
.050	.03946	−.03988	.560	.04430	−.06428
.060	.04211	−.04269	.580	.04231	−.06201
.070	.04452	−.04533	.600	.04021	−.05956
.080	.04666	−.04784	.620	.03804	−.05689
.090	.04858	−.05025	.640	.03577	−.05404
.100	.05035	−.05246	.660	.03348	−.05101
.110	.05190	−.05451	.680	.03112	−.04785
.120	.05331	−.05646	.700	.02871	−.04456
.130	.05457	−.05831	.720	.02620	−.04117
.140	.05567	−.06003	.740	.02361	−.03768
.150	.05663	−.06166	.760	.02097	−.03417
.160	.05750	−.06321	.780	.01827	−.03070
.170	.05827	−.06466	.800	.01548	−.02735
.180	.05892	−.06599	.820	.01261	−.02420
.190	.05948	−.06721	.840	.00967	−.02134
.200	.05995	−.06837	.860	.00666	−.01888
.220	.06069	−.07046	.880	.00359	−.01692
.240	.06118	−.07210	.900	.00048	−.01565
.260	.06138	−.07348	.920	−.00276	−.01519
.280	.06137	−.07461	.940	−.00609	−.01557
.300	.06111	−.07538	.960	−.00950	−.01674
.320	.06067	−.07586	.980	−.01302	−.01883
.340	.06004	−.07607	1.000	−.01660	−.02184

Table II. Continued

(f) $\eta = 0.226$; $c = 9.03$ in.; $x_{le} = 22.11$ in.; $z_o =$ W.L. -1.623 in.

x/c	z/c U.S.	z/c L.S.	x/c	z/c U.S.	z/c L.S.
0.000	0.00000	0.00000	0.360	0.05929	−0.07075
.002	.00862	−.01115	.380	.05866	−.07041
.005	.01443	−.01622	.420	.05696	−.06919
.010	.02034	−.02158	.460	.05482	−.06727
.020	.02777	−.02826	.500	.05218	−.06456
.030	.03258	−.03281	.520	.05074	−.06289
.040	.03606	−.03639	.540	.04916	−.06095
.050	.03896	−.03938	.560	.04747	−.05883
.060	.04151	−.04201	.580	.04568	−.05643
.070	.04383	−.04446	.600	.04374	−.05388
.080	.04587	−.04678	.620	.04171	−.05111
.090	.04769	−.04895	.640	.03958	−.04818
.100	.04935	−.05094	.660	.03739	−.04507
.110	.05075	−.05279	.680	.03515	−.04184
.120	.05202	−.05452	.700	.03284	−.03844
.130	.05316	−.05612	.720	.03041	−.03498
.140	.05417	−.05762	.740	.02788	−.03148
.150	.05508	−.05902	.760	.02531	−.02797
.160	.05588	−.06032	.780	.02265	−.02455
.170	.05660	−.06155	.800	.01991	−.02128
.180	.05724	−.06267	.820	.01706	−.01827
.190	.05778	−.06372	.840	.01415	−.01560
.200	.05829	−.06470	.860	.01116	−.01335
.220	.05911	−.06643	.880	.00811	−.01169
.240	.05969	−.06780	.900	.00498	−.01068
.260	.06005	−.06894	.920	.00177	−.01042
.280	.06021	−.06982	.940	−.00150	−.01093
.300	.06021	−.07041	.960	−.00486	−.01221
.320	.06007	−.07076	.980	−.00832	−.01432
.340	.05977	−.07087	1.000	−.01186	−.01727

Table II. Continued

(g) $\eta = 0.254$; $c = 8.46$ in.; $x_{le} = 22.68$ in.; $z_o =$ W.L. -1.559 in.

x/c	z/c U.S.	z/c L.S.	x/c	z/c U.S.	z/c L.S.
0.000	0.00000	0.00000	0.360	0.05939	−0.06614
.002	.00849	−.01113	.380	.05905	−.06584
.005	.01410	−.01613	.420	.05795	−.06472
.010	.01998	−.02136	.460	.05639	−.06285
.020	.02744	−.02797	.500	.05426	−.06013
.030	.03229	−.03250	.520	.05304	−.05840
.040	.03572	−.03604	.540	.05168	−.05636
.050	.03853	−.03894	.560	.05018	−.05415
.060	.04100	−.04142	.580	.04856	−.05166
.070	.04322	−.04370	.600	.04678	−.04901
.080	.04516	−.04585	.620	.04486	−.04616
.090	.04690	−.04782	.640	.04284	−.04317
.100	.04847	−.04959	.660	.04075	−.03998
.110	.04975	−.05126	.680	.03862	−.03667
.120	.05091	−.05283	.700	.03639	−.03317
.130	.05196	−.05421	.720	.03401	−.02964
.140	.05290	−.05550	.740	.03156	−.02614
.150	.05376	−.05667	.760	.02903	−.02263
.160	.05452	−.05777	.780	.02642	−.01924
.170	.05520	−.05880	.800	.02373	−.01605
.180	.05582	−.05975	.820	.02089	−.01316
.190	.05637	−.06063	.840	.01800	−.01065
.200	.05691	−.06144	.860	.01503	−.00859
.220	.05781	−.06285	.880	.01199	−.00719
.240	.05846	−.06399	.900	.00884	−.00641
.260	.05895	−.06491	.920	.00566	−.00633
.280	.05927	−.06557	.940	.00243	−.00696
.300	.05949	−.06602	.960	−.00087	−.00832
.320	.05961	−.06626	.980	−.00427	−.01046
.340	.05958	−.06630	1.000	−.00778	−.01334

Table II. Continued

(h) $\eta = 0.282$; $c = 7.89$ in.; $x_{le} = 23.25$ in.; $z_o =$ W.L. -1.494 in.

x/c	z/c U.S.	z/c L.S.	x/c	z/c U.S.	z/c L.S.
0.000	0.00000	0.00000	0.360	0.06059	−0.06439
.002	.00839	−.01079	.380	.06040	−.06415
.005	.01407	−.01568	.420	.05965	−.06313
.010	.01989	−.02084	.460	.05834	−.06127
.020	.02735	−.02739	.500	.05650	−.05847
.030	.03227	−.03191	.520	.05543	−.05664
.040	.03579	−.03544	.540	.05423	−.05451
.050	.03861	−.03835	.560	.05290	−.05216
.060	.04099	−.04084	.580	.05142	−.04947
.070	.04306	−.04305	.600	.04980	−.04658
.080	.04488	−.04512	.620	.04808	−.04348
.090	.04652	−.04699	.640	.04625	−.04022
.100	.04800	−.04869	.660	.04430	−.03677
.110	.04931	−.05029	.680	.04225	−.03319
.120	.05050	−.05179	.700	.04005	−.02949
.130	.05159	−.05313	.720	.03772	−.02576
.140	.05257	−.05437	.740	.03527	−.02209
.150	.05348	−.05550	.760	.03272	−.01853
.160	.05432	−.05654	.780	.03006	−.01513
.170	.05509	−.05751	.800	.02731	−.01196
.180	.05580	−.05838	.820	.02444	−.00912
.190	.05644	−.05921	.840	.02148	−.00673
.200	.05704	−.05995	.860	.01842	−.00484
.220	.05806	−.06124	.880	.01526	−.00356
.240	.05889	−.06225	.900	.01202	−.00289
.260	.05955	−.06308	.920	.00871	−.00294
.280	.06004	−.06373	.940	.00533	−.00372
.300	.06039	−.06415	.960	.00188	−.00522
.320	.06062	−.06440	.980	−.00169	−.00750
.340	.06068	−.06449	1.000	−.00537	−.01056

Table II. Continued

(i) $\eta = 0.339$; $c = 6.83$ in.; $x_{le} = 24.39$ in.; $z_o =$ W.L. -1.362 in.

x/c	z/c U.S.	z/c L.S.	x/c	z/c U.S.	z/c L.S.
0.000	0.00000	0.00000	0.360	0.06413	−0.06157
.002	.00832	−.00935	.380	.06421	−.06129
.005	.01385	−.01429	.420	.06405	−.06020
.010	.01947	−.01949	.460	.06330	−.05818
.020	.02680	−.02613	.500	.06208	−.05523
.030	.03179	−.03059	.520	.06130	−.05332
.040	.03539	−.03411	.540	.06041	−.05113
.050	.03833	−.03700	.560	.05938	−.04865
.060	.04076	−.03951	.580	.05822	−.04585
.070	.04285	−.04168	.600	.05691	−.04273
.080	.04469	−.04366	.620	.05549	−.03942
.090	.04638	−.04543	.640	.05398	−.03588
.100	.04791	−.04704	.660	.05231	−.03219
.110	.04930	−.04855	.680	.05052	−.02837
.120	.05061	−.04994	.700	.04856	−.02450
.130	.05181	−.05122	.720	.04646	−.02062
.140	.05294	−.05239	.740	.04418	−.01681
.150	.05399	−.05348	.760	.04178	−.01314
.160	.05497	−.05446	.780	.03922	−.00964
.170	.05588	−.05536	.800	.03654	−.00640
.180	.05675	−.05618	.820	.03372	−.00346
.190	.05756	−.05695	.840	.03076	−.00098
.200	.05829	−.05765	.860	.02767	.00102
.220	.05960	−.05882	.880	.02440	.00245
.240	.06073	−.05974	.900	.02103	.00330
.260	.06170	−.06049	.920	.01738	.00329
.280	.06249	−.06105	.940	.01374	.00262
.300	.06312	−.06141	.960	.00995	.00117
.320	.06362	−.06161	.980	.00598	−.00124
.340	.06393	−.06167	1.000	.00183	−.00457

Table II. Continued

(j) $\eta = 0.375$; $c = 6.19$ in.; $x_{le} = 25.11$ in.; $z_o =$ W.L. -1.279 in.

x/c	z/c		x/c	z/c	
	U.S.	L.S.		U.S.	L.S.
0.000	0.00000	0.00000	0.360	0.06702	−0.05969
.002	.00825	−.00796	.380	.06730	−.05934
.005	.01361	−.01303	.420	.06752	−.05806
.010	.01907	−.01841	.460	.06718	−.05589
.020	.02624	−.02515	.500	.06643	−.05285
.030	.03124	−.02955	.520	.06585	−.05094
.040	.03490	−.03307	.540	.06520	−.04878
.050	.03798	−.03596	.560	.06436	−.04629
.060	.04050	−.03846	.580	.06341	−.04352
.070	.04273	−.04063	.600	.06219	−.04056
.080	.04468	−.04259	.620	.06099	−.03719
.090	.04647	−.04433	.640	.05968	−.03359
.100	.04812	−.04591	.660	.05821	−.02984
.110	.04959	−.04733	.680	.05666	−.02600
.120	.05098	−.04868	.700	.05493	−.02210
.130	.05231	−.04992	.720	.05305	−.01821
.140	.05353	−.05105	.740	.05101	−.01435
.150	.05469	−.05210	.760	.04883	−.01057
.160	.05578	−.05305	.780	.04643	−.00697
.170	.05679	−.05394	.800	.04389	−.00357
.180	.05776	−.05475	.820	.04117	−.00048
.190	.05869	−.05550	.840	.03831	.00226
.200	.05951	−.05621	.860	.03529	.00453
.220	.06103	−.05734	.880	.03204	.00627
.240	.06237	−.05827	.900	.02866	.00746
.260	.06354	−.05897	.920	.02504	.00791
.280	.06453	−.05947	.940	.02124	.00747
.300	.06538	−.05977	.960	.01721	.00620
.320	.06609	−.05990	.980	.01295	.00379
.340	.06661	−.05986	1.000	.00843	.00034

Table II. Continued

(k) $\eta = 0.433$; $c = 5.72$ in.; $x_{le} = 26.07$ in.; $z_o =$ W.L. -1.145 in.

x/c	z/c U.S.	z/c L.S.	x/c	z/c U.S.	z/c L.S.
0.000	0.00000	0.00000	0.360	0.06462	−0.05399
.002	.00711	−.01008	.380	.06510	−.05350
.005	.01193	−.01492	.420	.06578	−.05208
.010	.01691	−.01970	.460	.06605	−.04994
.020	.02376	−.02553	.500	.06584	−.04698
.030	.02845	−.02932	.520	.06555	−.04510
.040	.03203	−.03233	.540	.06521	−.04285
.050	.03498	−.03480	.560	.06473	−.04025
.060	.03746	−.03692	.580	.06409	−.03730
.070	.03963	−.03881	.600	.06333	−.03404
.080	.04154	−.04051	.620	.06243	−.03059
.090	.04324	−.04199	.640	.06136	−.02700
.100	.04482	−.04326	.660	.06017	−.02332
.110	.04629	−.04444	.680	.05885	−.01964
.120	.04768	−.04553	.700	.05741	−.01595
.130	.04900	−.04652	.720	.05580	−.01230
.140	.05023	−.04744	.740	.05404	−.00878
.150	.05135	−.04831	.760	.05209	−.00534
.160	.05244	−.04910	.780	.04993	−.00201
.170	.05343	−.04982	.800	.04751	.00100
.180	.05438	−.05044	.820	.04489	.00381
.190	.05529	−.05101	.840	.04202	.00627
.200	.05617	−.05157	.860	.03894	.00836
.220	.05777	−.05243	.880	.03554	.00991
.240	.05919	−.05314	.900	.03190	.01085
.260	.06040	−.05370	.920	.02795	.01107
.280	.06148	−.05413	.940	.02366	.01045
.300	.06246	−.05432	.960	.01908	.00876
.320	.06326	−.05440	.980	.01414	.00602
.340	.06400	−.05429	1.000	.00885	.00187

Table II. Continued

(l) $\eta = 0.489$; $c = 5.46$ in.; $x_{le} = 27.00$ in.; $z_o =$ W.L. -1.016 in.

x/c	z/c U.S.	z/c L.S.	x/c	z/c U.S.	z/c L.S.
0.000	0.00000	0.00000	0.360	0.06469	−0.05322
.002	.00723	−.00988	.380	.06519	−.05273
.005	.01202	−.01471	.420	.06591	−.05126
.010	.01697	−.01951	.460	.06621	−.04909
.020	.02370	−.02531	.500	.06604	−.04609
.030	.02836	−.02906	.520	.06578	−.04418
.040	.03192	−.03205	.540	.06546	−.04194
.050	.03484	−.03448	.560	.06500	−.03932
.060	.03732	−.03659	.580	.06439	−.03638
.070	.03949	−.03844	.600	.06365	−.03314
.080	.04140	−.04010	.620	.06278	−.02968
.090	.04310	−.04158	.640	.06173	−.02610
.100	.04468	−.04284	.660	.06058	−.02245
.110	.04618	−.04401	.680	.05928	−.01877
.120	.04757	−.04508	.700	.05786	−.01507
.130	.04890	−.04606	.720	.05629	−.01140
.140	.05013	−.04696	.740	.05455	−.00788
.150	.05127	−.04780	.760	.05263	−.00444
.160	.05234	−.04860	.780	.05049	−.00110
.170	.05336	−.04930	.800	.04813	.00195
.180	.05432	−.04989	.820	.04554	.00476
.190	.05524	−.05046	.840	.04270	.00725
.200	.05612	−.05100	.860	.03966	.00934
.220	.05774	−.05182	.880	.03630	.01090
.240	.05916	−.05251	.900	.03270	.01184
.260	.06040	−.05304	.920	.02878	.01208
.280	.06149	−.05343	.940	.02453	.01147
.300	.06246	−.05360	.960	.01996	.00977
.320	.06330	−.05366	.980	.01504	.00702
.340	.06405	−.05353	1.000	.00975	.00288

Table II. Continued

(m) $\eta = 0.564$; $c = 5.10$ in.; $x_{le} = 28.24$ in.; $z_o =$ W.L. -0.843 in.

x/c	z/c U.S.	z/c L.S.	x/c	z/c U.S.	z/c L.S.
0.000	0.00000	0.00000	0.360	0.06485	−0.05202
.002	.00735	−.00954	.380	.06539	−.05150
.005	.01210	−.01442	.420	.06618	−.04997
.010	.01698	−.01920	.460	.06656	−.04773
.020	.02364	−.02494	.500	.06646	−.04464
.030	.02823	−.02864	.520	.06624	−.04273
.040	.03175	−.03159	.540	.06595	−.04044
.050	.03464	−.03398	.560	.06555	−.03782
.060	.03711	−.03606	.580	.06497	−.03490
.070	.03929	−.03788	.600	.06428	−.03165
.080	.04119	−.03952	.620	.06344	−.02821
.090	.04290	−.04096	.640	.06248	−.02464
.100	.04450	−.04220	.660	.06136	−.02097
.110	.04599	−.04335	.680	.06012	−.01727
.120	.04741	−.04439	.700	.05873	−.01357
.130	.04875	−.04534	.720	.05721	−.00990
.140	.04998	−.04624	.740	.05553	−.00634
.150	.05114	−.04707	.760	.05368	−.00286
.160	.05223	−.04783	.780	.05158	.00051
.170	.05325	−.04850	.800	.04930	.00359
.180	.05424	−.04908	.820	.04677	.00644
.190	.05517	−.04962	.840	.04399	.00896
.200	.05605	−.05012	.860	.04101	.01107
.220	.05769	−.05092	.880	.03773	.01267
.240	.05916	−.05154	.900	.03419	.01365
.260	.06042	−.05204	.920	.03034	.01391
.280	.06153	−.05238	.940	.02616	.01332
.300	.06255	−.05250	.960	.02163	.01164
.320	.06342	−.05252	.980	.01673	.00889
.340	.06419	−.05237	1.000	.01146	.00474

Table II. Continued

(n) $\eta = 0.602$; $c = 4.93$ in.; $x_{le} = 28.86$ in.; $z_o =$ W.L. −0.755 in.

x/c	z/c U.S.	z/c L.S.	x/c	z/c U.S.	z/c L.S.
0.000	0.00000	0.00000	0.360	0.06504	−0.05128
.002	.00748	−.00946	.380	.06560	−.05073
.005	.01215	−.01428	.420	.06643	−.04915
.010	.01700	−.01905	.460	.06686	−.04687
.020	.02361	−.02477	.500	.06684	−.04372
.030	.02814	−.02845	.520	.06664	−.04177
.040	.03164	−.03134	.540	.06637	−.03949
.050	.03455	−.03372	.560	.06599	−.03686
.060	.03701	−.03577	.580	.06545	−.03391
.070	.03918	−.03758	.600	.06480	−.03067
.080	.04108	−.03918	.620	.06399	−.02721
.090	.04282	−.04061	.640	.06305	−.02363
.100	.04443	−.04185	.660	.06198	−.01998
.110	.04594	−.04298	.680	.06077	−.01626
.120	.04734	−.04402	.700	.05944	−.01255
.130	.04869	−.04494	.720	.05794	−.00885
.140	.04994	−.04583	.740	.05630	−.00526
.150	.05110	−.04663	.760	.05446	−.00177
.160	.05221	−.04737	.780	.05242	.00162
.170	.05323	−.04803	.800	.05017	.00475
.180	.05422	−.04861	.820	.04768	.00762
.190	.05517	−.04913	.840	.04496	.01015
.200	.05606	−.04961	.860	.04204	.01230
.220	.05772	−.05037	.880	.03878	.01391
.240	.05919	−.05098	.900	.03529	.01490
.260	.06049	−.05142	.920	.03150	.01520
.280	.06164	−.05175	.940	.02735	.01462
.300	.06266	−.05182	.960	.02286	.01298
.320	.06357	−.05182	.980	.01799	.01022
.340	.06436	−.05163	1.000	.01272	.00609

Table II. Continued

(o) $\eta = 0.678$; $c = 4.58$ in.; $x_{le} = 30.09$ in.; $z_o =$ W.L. -0.580 in.

x/c	z/c		x/c	z/c	
	U.S.	L.S.		U.S.	L.S.
0.000	0.00000	0.00000	0.360	0.06579	−0.04928
.002	.00770	−.00908	.380	.06643	−.04865
.005	.01232	−.01394	.420	.06740	−.04695
.010	.01709	−.01868	.460	.06798	−.04450
.020	.02355	−.02430	.500	.06810	−.04122
.030	.02804	−.02791	.520	.06800	−.03919
.040	.03150	−.03074	.540	.06781	−.03684
.050	.03438	−.03305	.560	.06752	−.03417
.060	.03685	−.03503	.580	.06707	−.03117
.070	.03903	−.03678	.600	.06651	−.02790
.080	.04097	−.03834	.620	.06580	−.02443
.090	.04270	−.03974	.640	.06496	−.02084
.100	.04435	−.04093	.660	.06398	−.01712
.110	.04589	−.04203	.680	.06287	−.01336
.120	.04733	−.04302	.700	.06161	−.00960
.130	.04870	−.04391	.720	.06023	−.00585
.140	.04999	−.04475	.740	.05868	−.00220
.150	.05118	−.04551	.760	.05696	.00137
.160	.05230	−.04622	.780	.05502	.00485
.170	.05338	−.04682	.800	.05286	.00804
.180	.05439	−.04735	.820	.05050	.01100
.190	.05536	−.04783	.840	.04788	.01359
.200	.05630	−.04826	.860	.04509	.01582
.220	.05800	−.04894	.880	.04196	.01750
.240	.05956	−.04945	.900	.03859	.01858
.260	.06091	−.04981	.920	.03491	.01892
.280	.06212	−.05004	.940	.03088	.01843
.300	.06322	−.05006	.960	.02646	.01682
.320	.06417	−.04997	.980	.02165	.01411
.340	.06503	−.04971	1.000	.01645	.01003

Table II. Continued

(p) $\eta = 0.715$; $c = 4.41$ in.; $x_{le} = 30.71$ in.; $z_o =$ W.L. -0.495 in.

x/c	z/c U.S.	z/c L.S.	x/c	z/c U.S.	z/c L.S.
0.000	0.00000	0.00000	0.360	0.06636	−0.04802
.002	.00775	−.00893	.380	.06703	−.04734
.005	.01236	−.01375	.420	.06811	−.04555
.010	.01711	−.01849	.460	.06879	−.04300
.020	.02350	−.02405	.500	.06904	−.03959
.030	.02797	−.02764	.520	.06898	−.03753
.040	.03143	−.03040	.540	.06885	−.03513
.050	.03429	−.03267	.560	.06861	−.03242
.060	.03676	−.03461	.580	.06821	−.02941
.070	.03896	−.03635	.600	.06772	−.02613
.080	.04091	−.03787	.620	.06707	−.02262
.090	.04267	−.03922	.640	.06627	−.01900
.100	.04432	−.04041	.660	.06537	−.01527
.110	.04590	−.04146	.680	.06432	−.01147
.120	.04736	−.04243	.700	.06313	−.00767
.130	.04875	−.04331	.720	.06180	−.00388
.140	.05006	−.04411	.740	.06032	−.00017
.150	.05127	−.04483	.760	.05865	.00344
.160	.05242	−.04551	.780	.05680	.00697
.170	.05349	−.04610	.800	.05471	.01022
.180	.05454	−.04659	.820	.05242	.01323
.190	.05554	−.04704	.840	.04987	.01588
.200	.05648	−.04744	.860	.04715	.01815
.220	.05824	−.04808	.880	.04411	.01988
.240	.05984	−.04850	.900	.04080	.02100
.260	.06124	−.04881	.920	.03718	.02140
.280	.06250	−.04898	.940	.03324	.02093
.300	.06365	−.04894	.960	.02888	.01937
.320	.06466	−.04879	.980	.02413	.01669
.340	.06555	−.04850	1.000	.01896	.01263

Table II. Continued

(q) $\eta = 0.791$; $c = 4.06$ in.; $x_{le} = 31.95$ in.; $z_o =$ W.L. -0.319 in.

x/c	z/c U.S.	z/c L.S.	x/c	z/c U.S.	z/c L.S.
0.000	0.00000	0.00000	0.360	0.06797	−0.04481
.002	.00804	−.00848	.380	.06877	−.04403
.005	.01254	−.01331	.420	.07012	−.04198
.010	.01720	−.01800	.460	.07105	−.03917
.020	.02349	−.02345	.500	.07156	−.03549
.030	.02789	−.02693	.520	.07165	−.03331
.040	.03129	−.02959	.540	.07166	−.03080
.050	.03417	−.03174	.560	.07157	−.02800
.060	.03666	−.03360	.580	.07133	−.02492
.070	.03889	−.03524	.600	.07097	−.02154
.080	.04088	−.03668	.620	.07046	−.01799
.090	.04271	−.03794	.640	.06983	−.01431
.100	.04442	−.03907	.660	.06907	−.01048
.110	.04604	−.04007	.680	.06819	−.00660
.120	.04754	−.04097	.700	.06717	−.00269
.130	.04901	−.04177	.720	.06599	.00121
.140	.05035	−.04250	.740	.06466	.00501
.150	.05164	−.04316	.760	.06317	.00877
.160	.05284	−.04374	.780	.06144	.01243
.170	.05398	−.04425	.800	.05955	.01582
.180	.05507	−.04468	.820	.05743	.01894
.190	.05613	−.04505	.840	.05506	.02175
.200	.05715	−.04539	.860	.05252	.02411
.220	.05901	−.04586	.880	.04965	.02597
.240	.06073	−.04614	.900	.04654	.02721
.260	.06224	−.04630	.920	.04310	.02771
.280	.06364	−.04632	.940	.03931	.02738
.300	.06491	−.04615	.960	.03513	.02593
.320	.06603	−.04587	.980	.03049	.02331
.340	.06705	−.04541	1.000	.02541	.01935

Table II. Continued

(r) $\eta = 0.867$; $c = 3.71$ in.; $x_{le} = 33.18$ in.; $z_o =$ W.L. -0.144 in.

x/c	z/c U.S.	z/c L.S.	x/c	z/c U.S.	z/c L.S.
0.000	0.00000	0.00000	0.360	0.07021	−0.04067
.002	.00837	−.00798	.380	.07119	−.03974
.005	.01278	−.01275	.420	.07285	−.03736
.010	.01733	−.01742	.460	.07414	−.03420
.020	.02347	−.02270	.500	.07500	−.03018
.030	.02780	−.02605	.520	.07528	−.02782
.040	.03120	−.02854	.540	.07548	−.02519
.050	.03408	−.03059	.560	.07554	−.02224
.060	.03661	−.03231	.580	.07550	−.01906
.070	.03886	−.03383	.600	.07532	−.01560
.080	.04093	−.03517	.620	.07503	−.01194
.090	.04283	−.03635	.640	.07460	−.00817
.100	.04464	−.03738	.660	.07405	−.00424
.110	.04632	−.03827	.680	.07335	−.00023
.120	.04792	−.03909	.700	.07253	.00382
.130	.04942	−.03978	.720	.07154	.00785
.140	.05085	−.04045	.740	.07043	.01180
.150	.05221	−.04101	.760	.06912	.01573
.160	.05349	−.04151	.780	.06761	.01954
.170	.05471	−.04190	.800	.06594	.02312
.180	.05588	−.04222	.820	.06403	.02643
.190	.05701	−.04251	.840	.06192	.02937
.200	.05810	−.04274	.860	.05960	.03191
.220	.06012	−.04302	.880	.05695	.03391
.240	.06199	−.04312	.900	.05406	.03532
.260	.06368	−.04305	.920	.05086	.03595
.280	.06522	−.04288	.940	.04729	.03577
.300	.06667	−.04254	.960	.04327	.03446
.320	.06795	−.04207	.980	.03879	.03192
.340	.06912	−.04146	1.000	.03384	.02807

Table II. Continued

(s) $\eta = 0.961$; $c = 3.27$ in.; $x_{le} = 34.74$ in.; $z_o =$ W.L. 0.073 in.

x/c	z/c U.S.	z/c L.S.	x/c	z/c U.S.	z/c L.S.
0.000	0.00000	0.00000	0.360	0.07403	−0.03392
.002	.00875	−.00711	.380	.07527	−.03271
.005	.01310	−.01191	.420	.07753	−.02977
.010	.01754	−.01649	.460	.07938	−.02604
.020	.02345	−.02153	.500	.08084	−.02143
.030	.02769	−.02464	.520	.08143	−.01882
.040	.03105	−.02690	.540	.08190	−.01594
.050	.03397	−.02872	.560	.08228	−.01278
.060	.03656	−.03025	.580	.08254	−.00941
.070	.03892	−.03161	.600	.08270	−.00577
.080	.04108	−.03276	.620	.08271	−.00195
.090	.04310	−.03378	.640	.08263	.00199
.100	.04504	−.03463	.660	.08239	.00610
.110	.04685	−.03542	.680	.08203	.01031
.120	.04857	−.03608	.700	.08154	.01458
.130	.05021	−.03662	.720	.08089	.01885
.140	.05177	−.03710	.740	.08010	.02309
.150	.05326	−.03749	.760	.07912	.02730
.160	.05464	−.03785	.780	.07797	.03135
.170	.05599	−.03808	.800	.07666	.03525
.180	.05731	−.03826	.820	.07510	.03883
.190	.05858	−.03837	.840	.07336	.04203
.200	.05977	−.03842	.860	.07143	.04482
.220	.06205	−.03841	.880	.06916	.04712
.240	.06420	−.03815	.900	.06665	.04878
.260	.06618	−.03777	.920	.06382	.04968
.280	.06799	−.03727	.940	.06060	.04973
.300	.06969	−.03661	.960	.05688	.04863
.320	.07126	−.03587	.980	.05269	.04631
.340	.07268	−.03496	1.000	.04797	.04264

Table II. Concluded

(t) $\eta = 1.000$; $c = 3.12$ in.; $x_{le} = 35.37$ in.; $z_o =$ W.L. 0.163 in.

x/c	z/c U.S.	z/c L.S.	x/c	z/c U.S.	z/c L.S.
0.000	0.00000	0.00000	0.360	0.07620	−0.03019
.002	.00902	−.00672	.380	.07761	−.02885
.005	.01329	−.01152	.420	.08016	−.02560
.010	.01765	−.01602	.460	.08237	−.02158
.020	.02344	−.02092	.500	.08413	−.01662
.030	.02764	−.02392	.520	.08489	−.01384
.040	.03098	−.02604	.540	.08556	−.01082
.050	.03392	−.02778	.560	.08609	−.00753
.060	.03653	−.02920	.580	.08655	−.00405
.070	.03895	−.03042	.600	.08685	−.00032
.080	.04116	−.03148	.620	.08706	.00361
.090	.04327	−.03241	.640	.08717	.00763
.100	.04526	−.03321	.660	.08711	.01188
.110	.04716	−.03388	.680	.08696	.01622
.120	.04896	−.03446	.700	.08664	.02062
.130	.05065	−.03493	.720	.08616	.02502
.140	.05231	−.03531	.740	.08559	.02942
.150	.05385	−.03563	.760	.08478	.03376
.160	.05533	−.03588	.780	.08384	.03800
.170	.05672	−.03602	.800	.08275	.04205
.180	.05812	−.03608	.820	.08139	.04581
.190	.05947	−.03611	.840	.07986	.04919
.200	.06074	−.03610	.860	.07814	.05211
.220	.06315	−.03589	.880	.07610	.05455
.240	.06544	−.03548	.900	.07378	.05639
.260	.06758	−.03492	.920	.07118	.05740
.280	.06952	−.03423	.940	.06814	.05762
.300	.07139	−.03340	.960	.06462	.05668
.320	.07313	−.03249	.980	.06056	.05444
.340	.07470	−.03140	1.000	.05598	.05091

Table III. Fuselage Geometry

F.S., in.	r, in.	F.S., in.	r, in.
0.00	0.000	12.00	2.875
.05	.245	14.00	2.875
.10	.339	16.00	2.875
.15	.406	18.00	2.875
.20	.459	20.00	2.875
.25	.500	22.00	2.875
.30	.535	24.00	2.875
.35	.568	26.00	2.875
.40	.601	28.00	2.875
.45	.634	31.20	2.875
.50	.666	32.00	2.873
.55	.698	33.00	2.867
.60	.730	34.00	2.856
.65	.762	35.00	2.841
1.00	.974	36.00	2.820
1.50	1.253	37.00	2.795
2.00	1.507	38.00	2.765
2.50	1.735	39.00	2.730
3.00	1.940	40.00	2.690
3.50	2.123	41.00	2.646
4.00	2.284	42.00	2.596
4.50	2.425	43.00	2.543
5.00	2.546	44.00	2.484
5.50	2.648	45.00	2.421
6.00	2.730	46.00	2.352
6.50	2.794	47.00	2.279
7.00	2.839	48.00	2.201
7.50	2.866	49.00	2.119
8.00	2.875	49.50	2.075
10.00	2.875	50.00	2.030

Table IV. Horizontal Tail Coordinates

x/c	z/c L.S.	z/c U.S.	x/c	z/c L.S.	z/c U.S.
0.000	0.00000	0.00000	0.500	−0.04900	0.04650
.002	−.00760	.00760	.510	−.04880	.04600
.005	−.01160	.01160	.520	−.04850	.04540
.010	−.01550	.01550	.530	−.04820	.04470
.020	−.02070	.02070	.540	−.04790	.04400
.030	−.02420	.02420	.550	−.04760	.04320
.040	−.02690	.02690	.560	−.04720	.04230
.050	−.02910	.02910	.570	−.04680	.04130
.060	−.03100	.03100	.580	−.04640	.04030
.070	−.03270	.03270	.590	−.04590	.03920
.080	−.03420	.03420	.600	−.04540	.03810
.090	−.03555	.03560	.610	−.04490	.03690
.100	−.03680	.03690	.620	−.04430	.03570
.110	−.03790	.03810	.630	−.04370	.03440
.120	−.03890	.03920	.640	−.04310	.03310
.130	−.03990	.04020	.650	−.04250	.03170
.140	−.04080	.04110	.660	−.04180	.03030
.150	−.04160	.04200	.670	−.04110	.02890
.160	−.04240	.04280	.680	−.04040	.02750
.170	−.04310	.04350	.690	−.03960	.02610
.180	−.04380	.04420	.700	−.03880	.02470
.190	−.04440	.04490	.710	−.03800	.02330
.200	−.04500	.04550	.720	−.03720	.02190
.210	−.04560	.04600	.730	−.03630	.02050
.220	−.04610	.04650	.740	−.03540	.01910
.230	−.04660	.04700	.750	−.03450	.01770
.240	−.04700	.04740	.760	−.03360	.01630
.250	−.04740	.04780	.770	−.03260	.01490
.260	−.04780	.04810	.780	−.03160	.01350
.270	−.04810	.04840	.790	−.03060	.01210
.280	−.04840	.04870	.800	−.02960	.01070
.290	−.04870	.04890	.810	−.02850	.00930
.300	−.04890	.04910	.820	−.02740	.00790
.310	−.04910	.04930	.830	−.02630	.00650
.320	−.04930	.04940	.840	−.02520	.00510
.330	−.04950	.04950	.850	−.02410	.00380
.340	−.04960	.04960	.860	−.02290	.00250
.350	−.04970	.04970	.870	−.02170	.00130
.360	−.04980	.04970	.880	−.02050	.00020
.370	−.04990	.04970	.890	−.01930	−.00080
.380	−.05000	.04970	.900	−.01800	−.00170
.390	−.05000	.04960	.910	−.01670	−.00250
.400	−.05000	.04950	.920	−.01540	−.00310
.410	−.05000	.04940	.930	−.01410	−.00350
.420	−.05000	.04920	.940	−.01270	−.00360
.430	−.05000	.04900	.950	−.01130	−.00340
.440	−.04990	.04880	.960	−.00980	−.00290
.450	−.04980	.04850	.970	−.00830	−.00220
.460	−.04970	.04820	.980	−.00670	−.00120
.470	−.04960	.04780	.990	−.00500	.00010
.480	−.04940	.04740	1.000	−.00320	.00170
.490	−.04920	.04700			

Table V. Vertical Tail Coordinates

x/c	z'/c U.S.	z'/c L.S.	x/c	z'/c U.S.	z'/c L.S.
0.000	0.00000	0.00000	0.500	0.04840	−0.04840
.002	.00760	−.00760	.510	.04810	−.04810
.005	.01160	−.01160	.520	.04780	−.04780
.010	.01550	−.01550	.530	.04740	−.04740
.020	.02070	−.02070	.540	.04700	−.04700
.030	.02430	−.02430	.550	.04650	−.04650
.040	.02700	−.02700	.560	.04600	−.04600
.050	.02920	−.02920	.570	.04550	−.04550
.060	.03110	−.03110	.580	.04490	−.04490
.070	.03280	−.03280	.590	.04430	−.04430
.080	.03430	−.03430	.600	.04360	−.04360
.090	.03570	−.03570	.610	.04280	−.04280
.100	.03690	−.03690	.620	.04200	−.04200
.110	.03800	−.03800	.630	.04110	−.04110
.120	.03900	−.03900	.640	.04020	−.04020
.130	.04000	−.04000	.650	.03920	−.03920
.140	.04090	−.04090	.660	.03820	−.03820
.150	.04170	−.04170	.670	.03715	−.03715
.160	.04250	−.04250	.680	.03610	−.03610
.170	.04320	−.04320	.690	.03505	−.03505
.180	.04390	−.04390	.700	.03400	−.03400
.190	.04450	−.04450	.710	.03295	−.03295
.200	.04510	−.04510	.720	.03190	−.03190
.210	.04560	−.04560	.730	.03085	−.03085
.220	.04610	−.04610	.740	.02980	−.02980
.230	.04660	−.04660	.750	.02875	−.02875
.240	.04700	−.04700	.760	.02770	−.02770
.250	.04740	−.04740	.770	.02665	−.02665
.260	.04780	−.04780	.780	.02560	−.02560
.270	.04810	−.04810	.790	.02455	−.02455
.280	.04840	−.04840	.800	.02350	−.02350
.290	.04870	−.04870	.810	.02245	−.02245
.300	.04900	−.04900	.820	.02140	−.02140
.310	.04920	−.04920	.830	.02035	−.02035
.320	.04940	−.04940	.840	.01930	−.01930
.330	.04960	−.04960	.850	.01825	−.01825
.340	.04970	−.04970	.860	.01720	−.01720
.350	.04980	−.04980	.870	.01615	−.01615
.360	.04990	−.04990	.880	.01510	−.01510
.370	.05000	−.05000	.890	.01405	−.01405
.380	.05000	−.05000	.900	.01300	−.01300
.390	.05000	−.05000	.910	.01195	−.01195
.400	.05000	−.05000	.920	.01090	−.01090
.410	.05000	−.05000	.930	.00985	−.00985
.420	.04990	−.04990	.940	.00880	−.00880
.430	.04980	−.04980	.950	.00775	−.00775
.440	.04970	−.04970	.960	.00670	−.00670
.450	.04960	−.04960	.970	.00565	−.00565
.460	.04940	−.04940	.980	.00460	−.00460
.470	.04920	−.04920	.990	.00355	−.00355
.480	.04900	−.04900	1.000	.00250	−.00250
.490	.04870	−.04870			

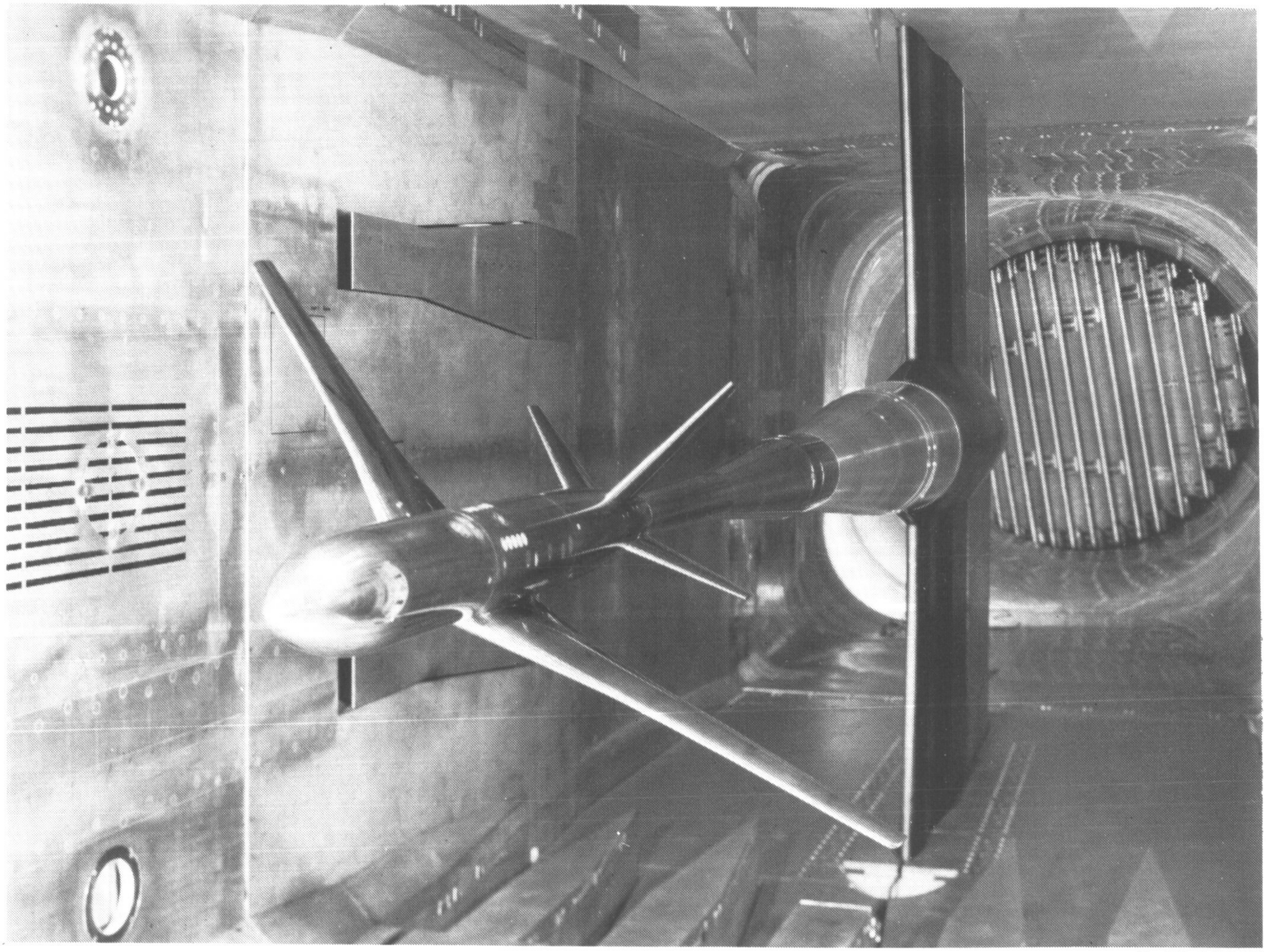

L-86-10666

Figure 1. Photograph of Pathfinder I in the NTF.

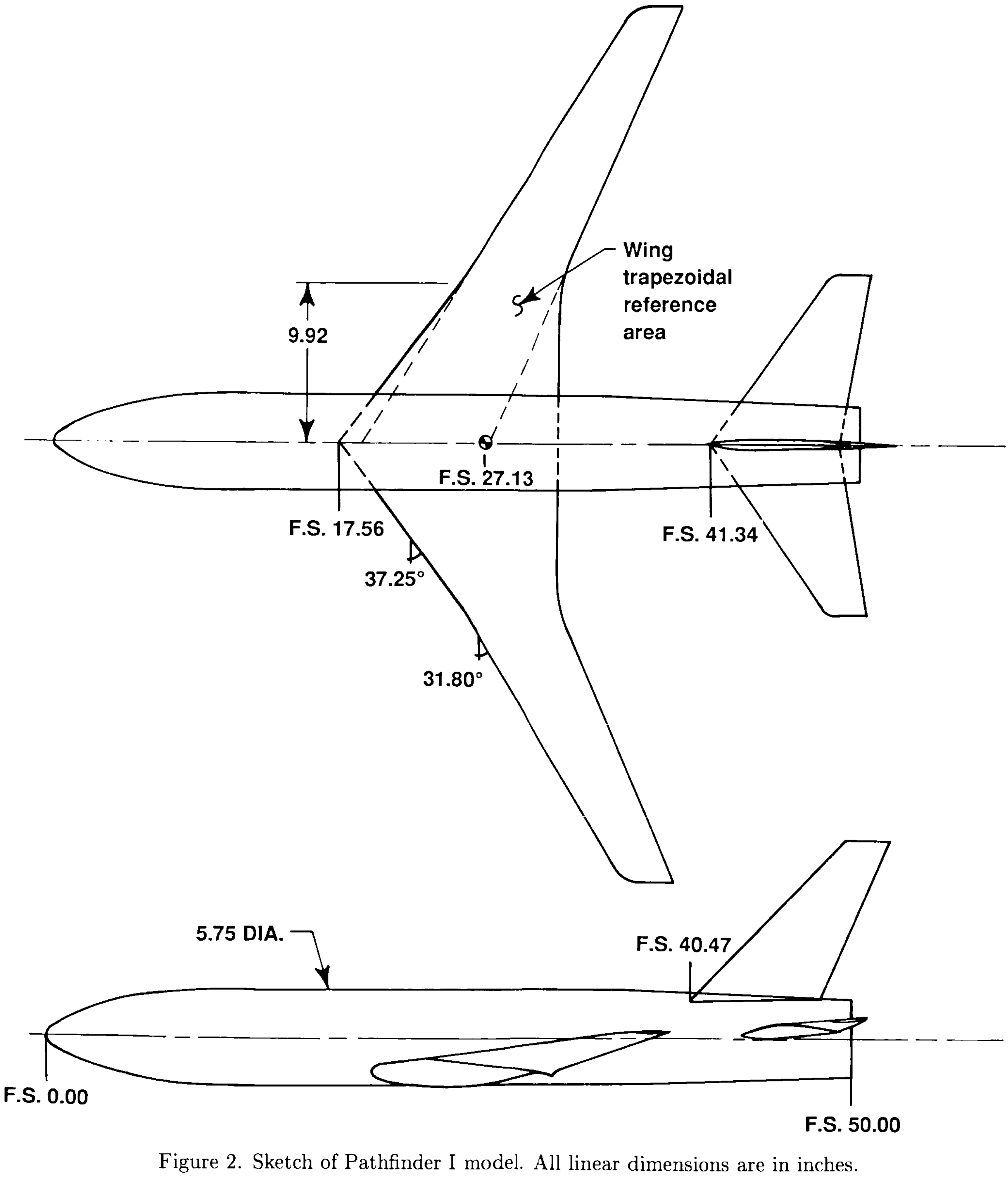

Figure 2. Sketch of Pathfinder I model. All linear dimensions are in inches.

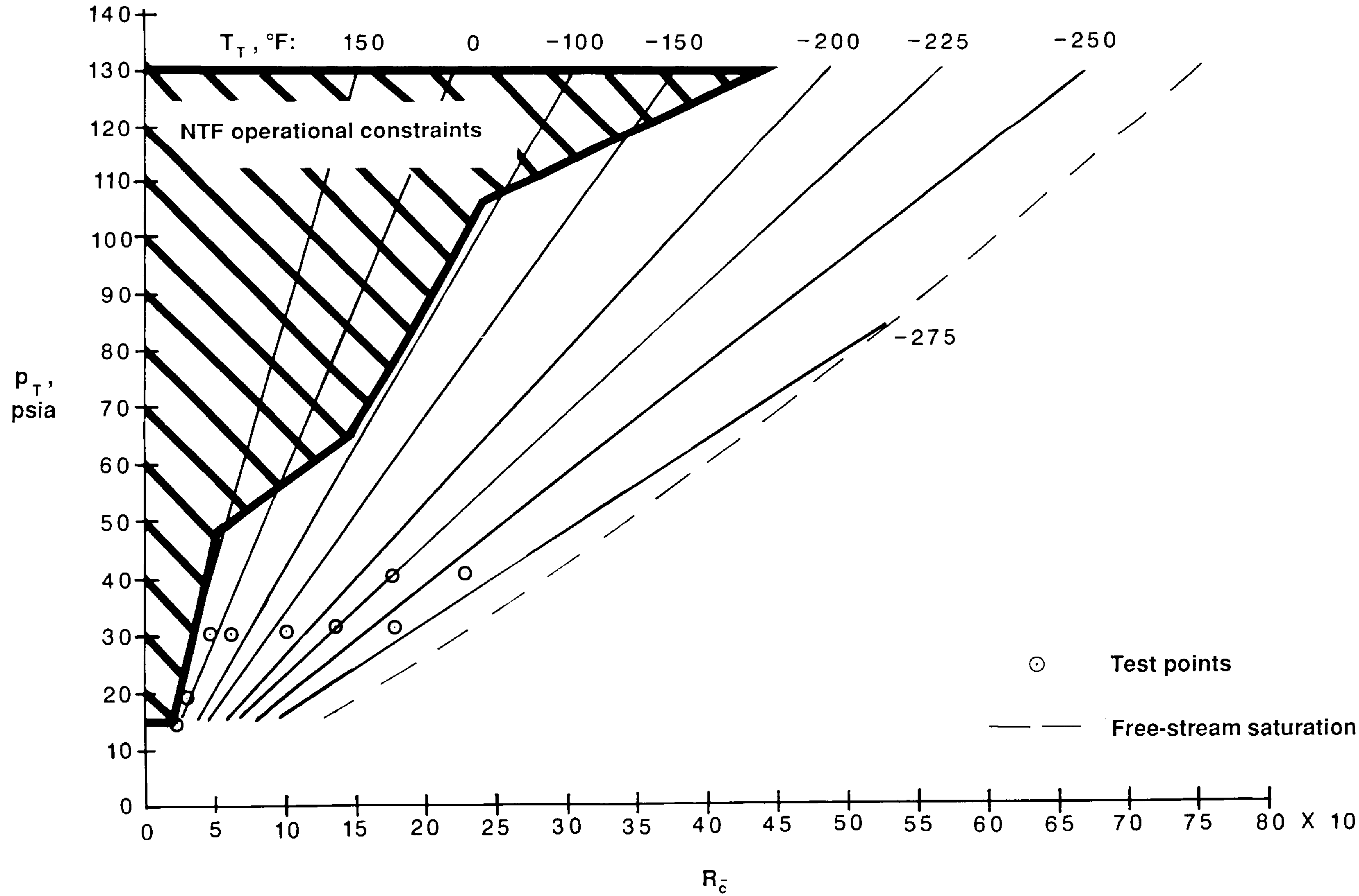

Figure 3. Typical map of test conditions at $M = 0.82$.

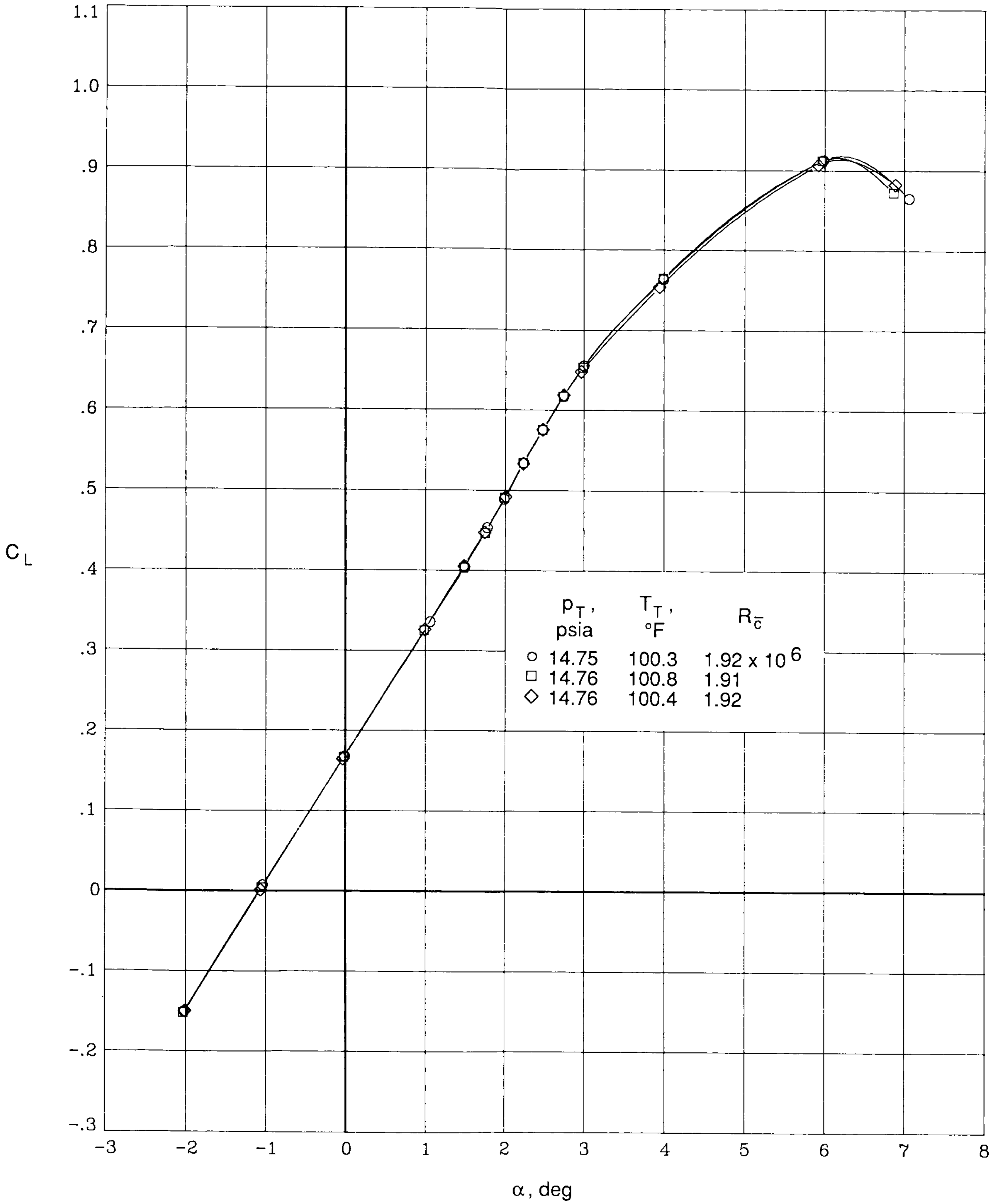

Figure 4. Air mode repeatability of lift coefficient versus angle of attack at $M = 0.82$.

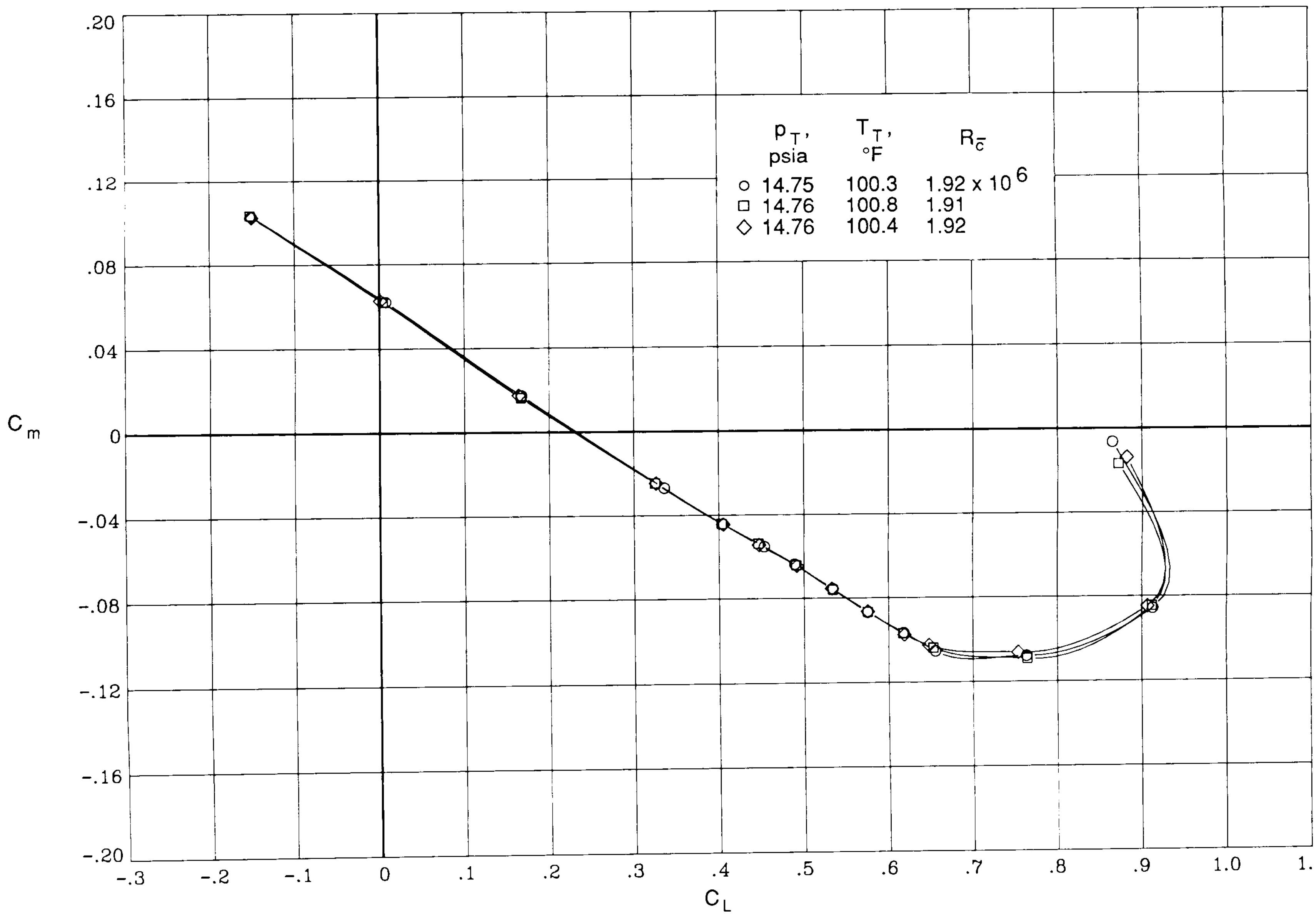

Figure 5. Air mode repeatability of pitching-moment coefficient versus lift coefficient at $M = 0.82$.

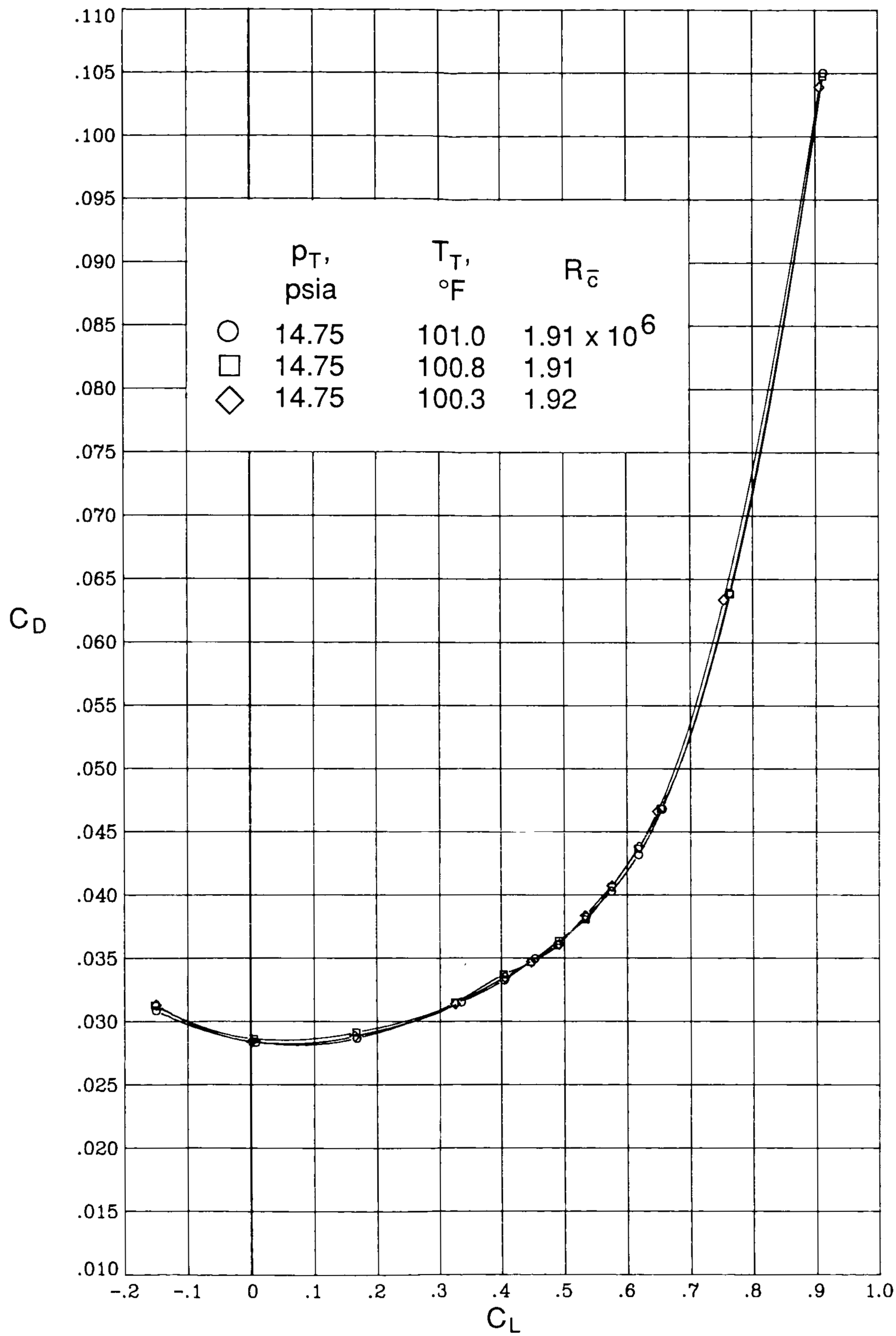

Figure 6. Air mode repeatability of drag coefficient versus lift coefficient at $M = 0.82$.

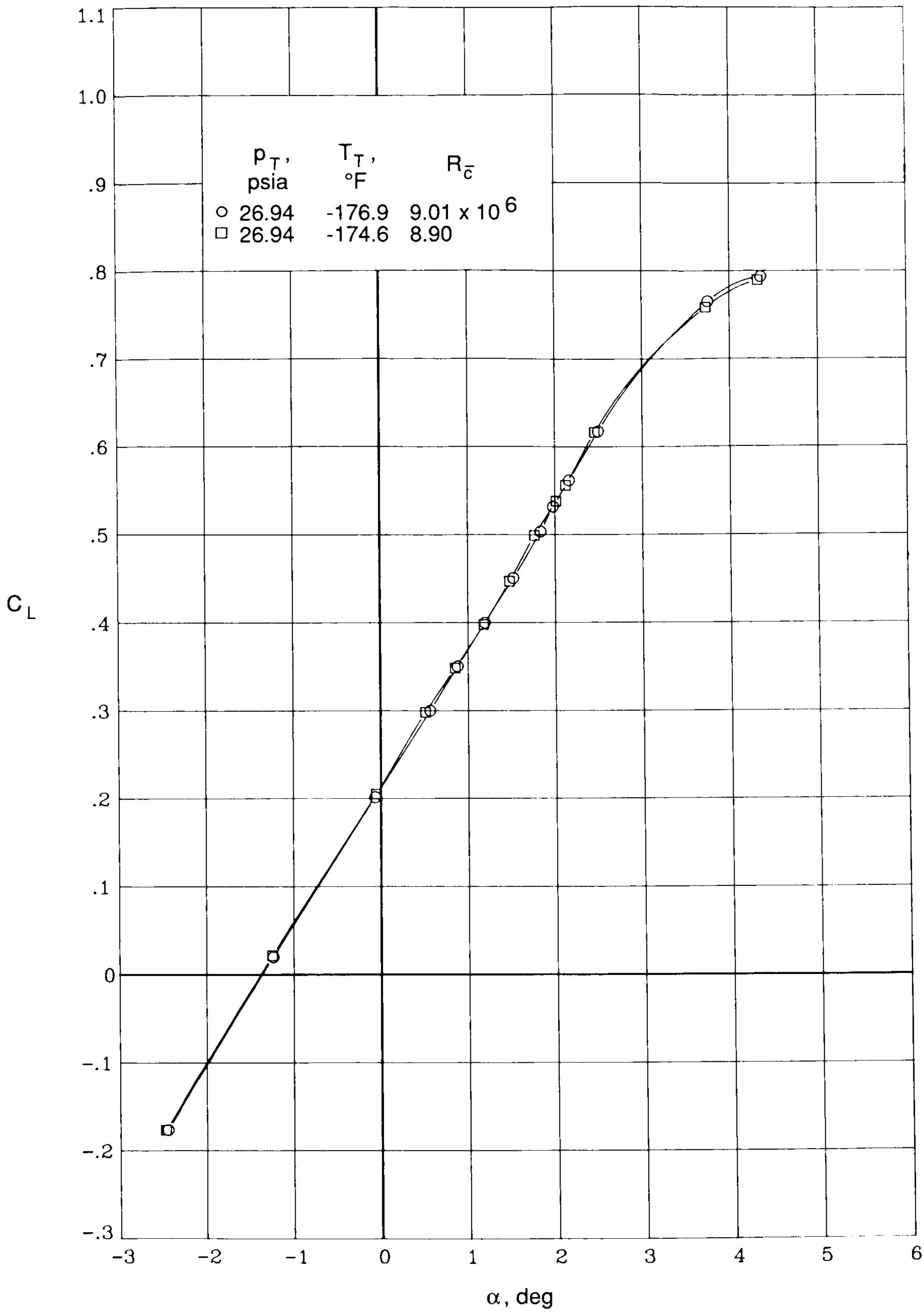

Figure 7. Cryogenic mode repeatability of lift coefficient versus angle of attack at $M = 0.82$.

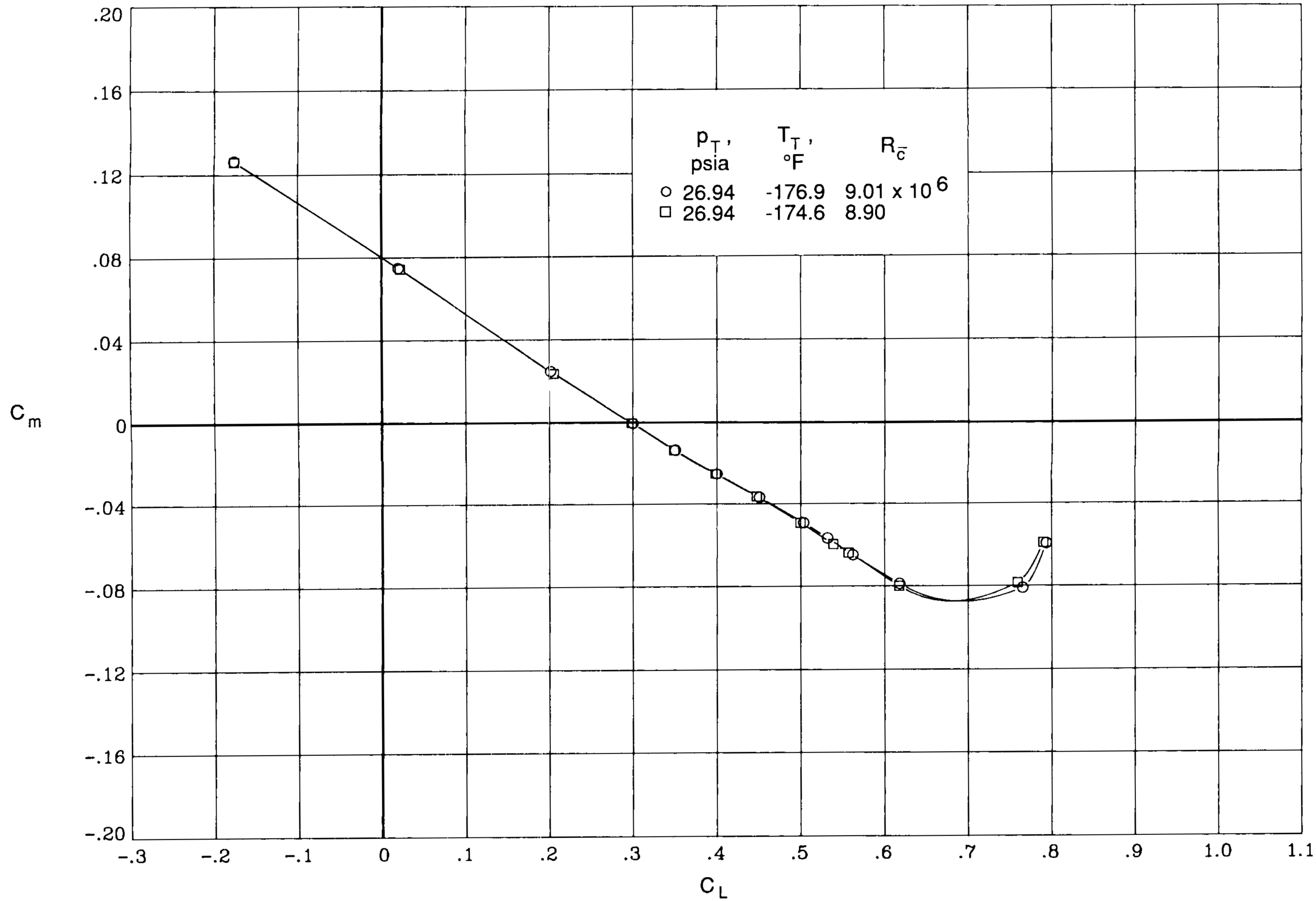

Figure 8. Cryogenic mode repeatability of pitching-moment coefficient versus lift coefficient at $M = 0.82$.

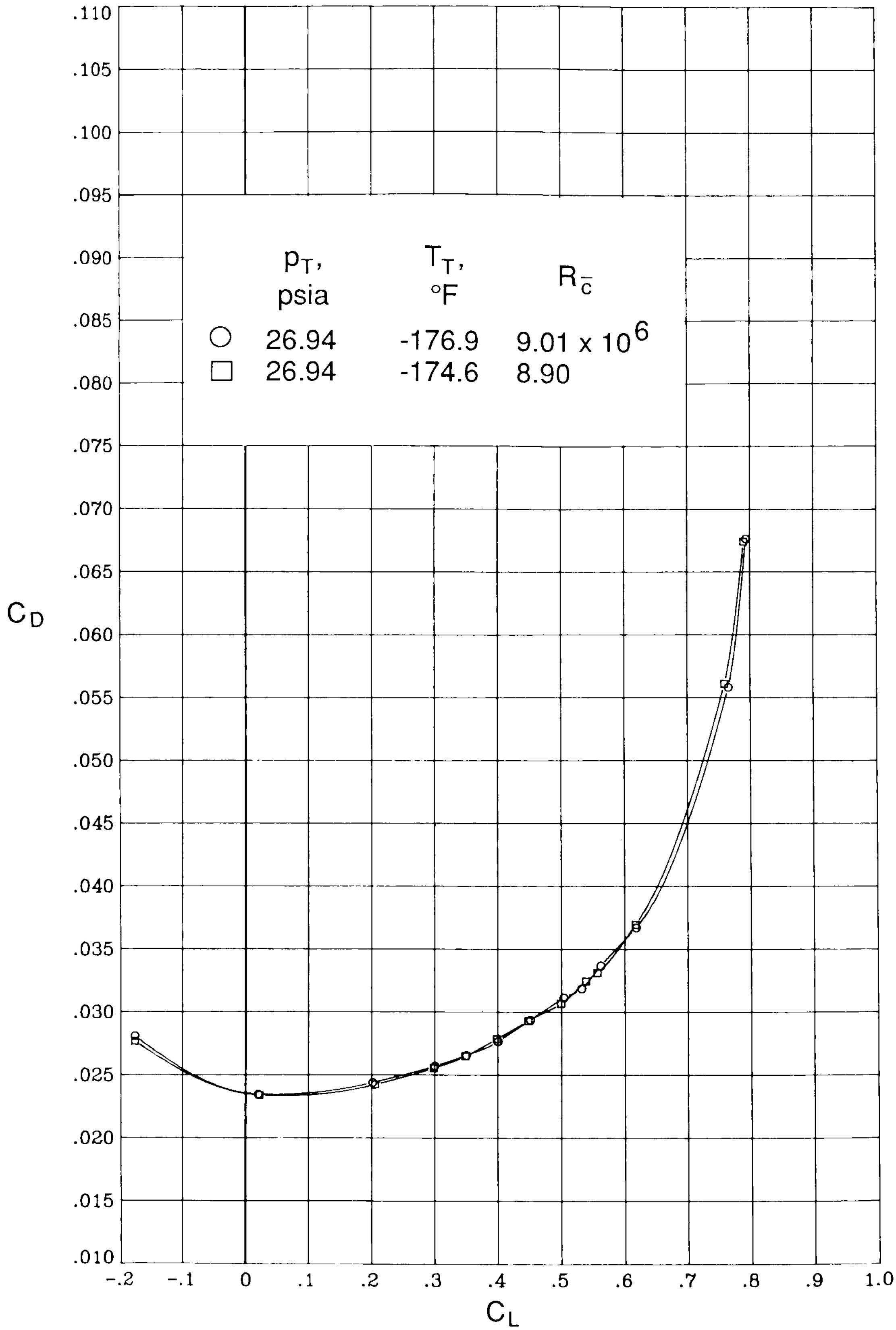

Figure 9. Cryogenic mode repeatability of drag coefficient versus lift coefficient at $M = 0.82$.

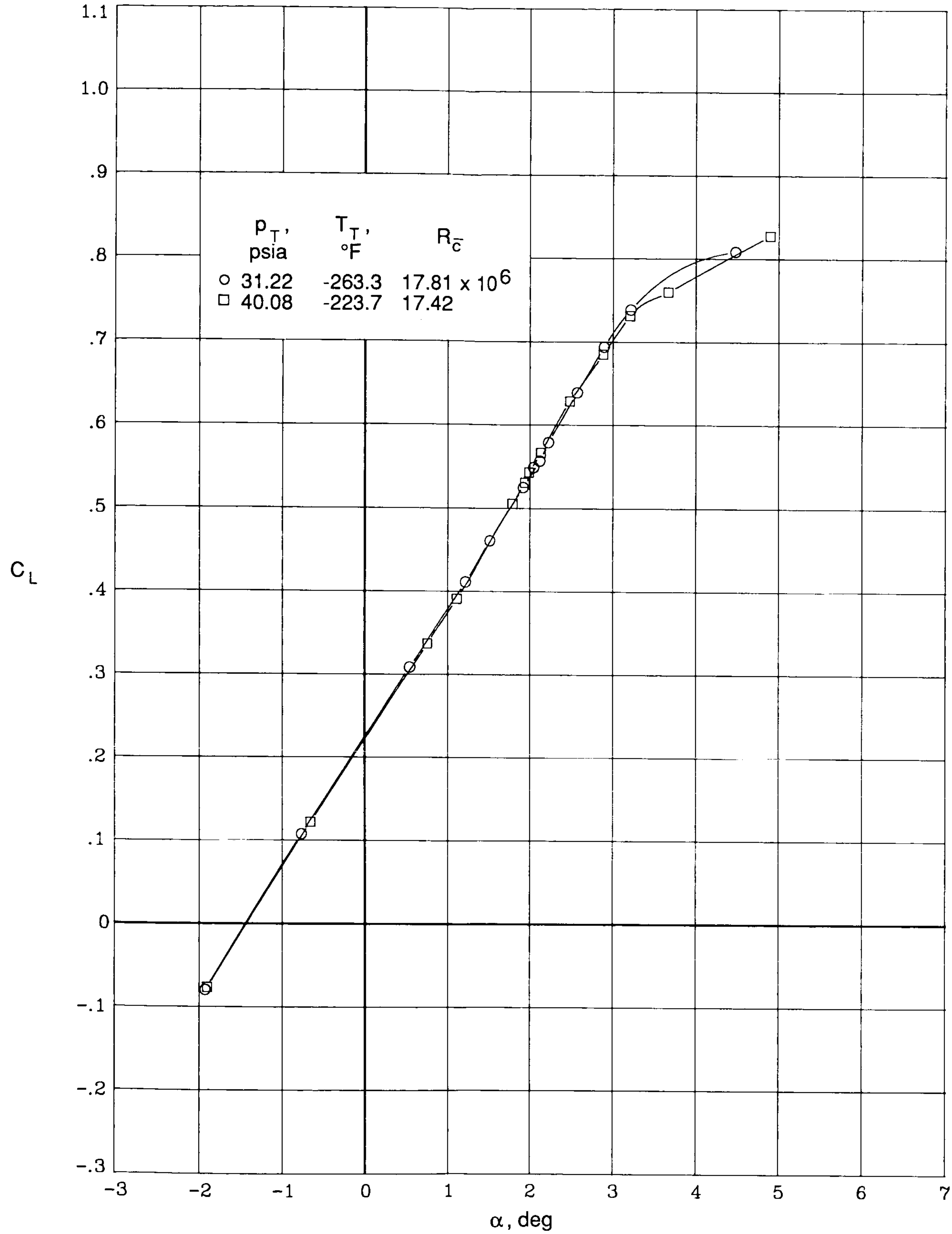

Figure 10. Aeroelasticity effects on lift coefficient versus angle of attack at $M = 0.82$.

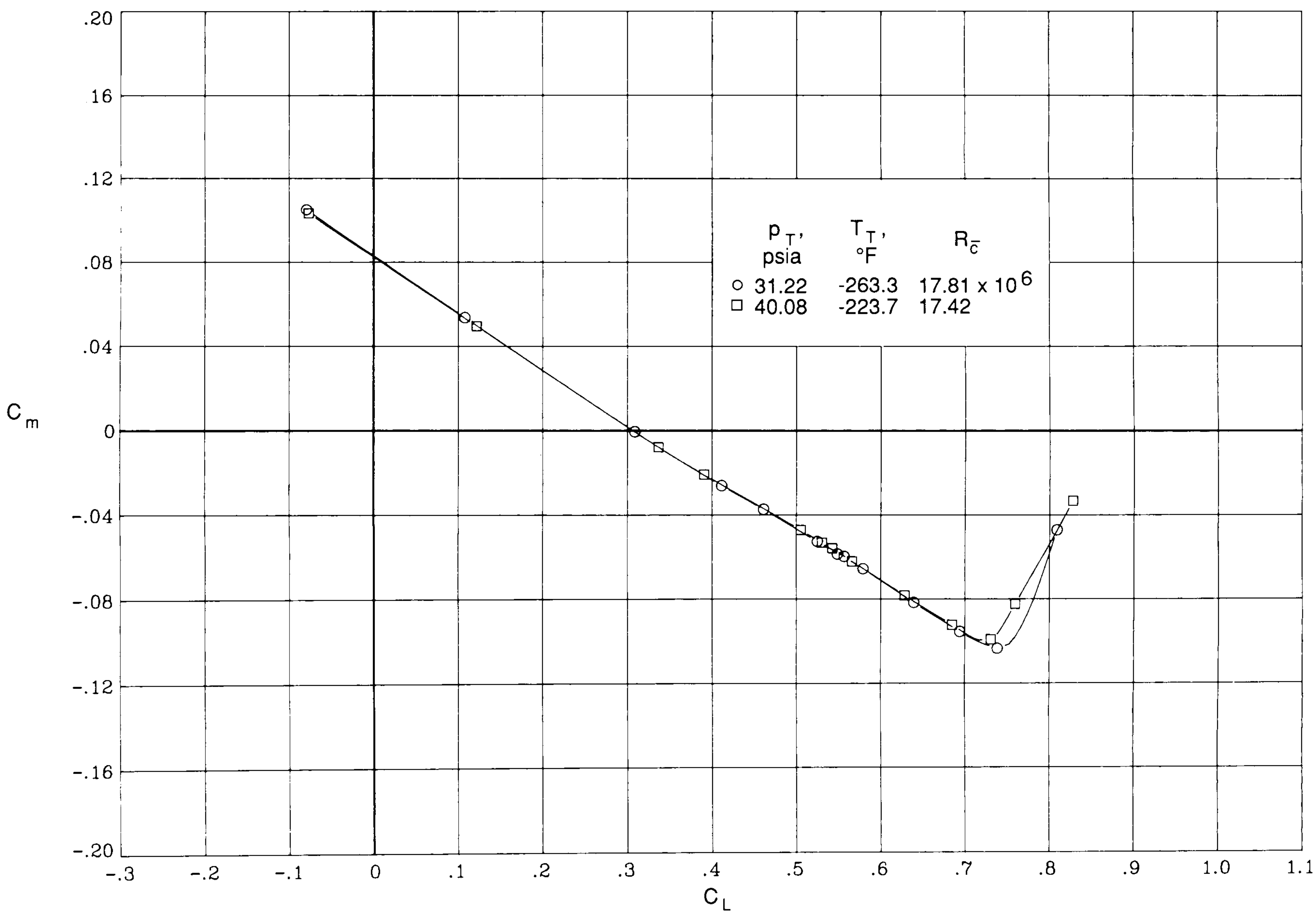

Figure 11. Aeroelasticity effects on pitching-moment coefficient versus lift coefficient at $M = 0.82$.

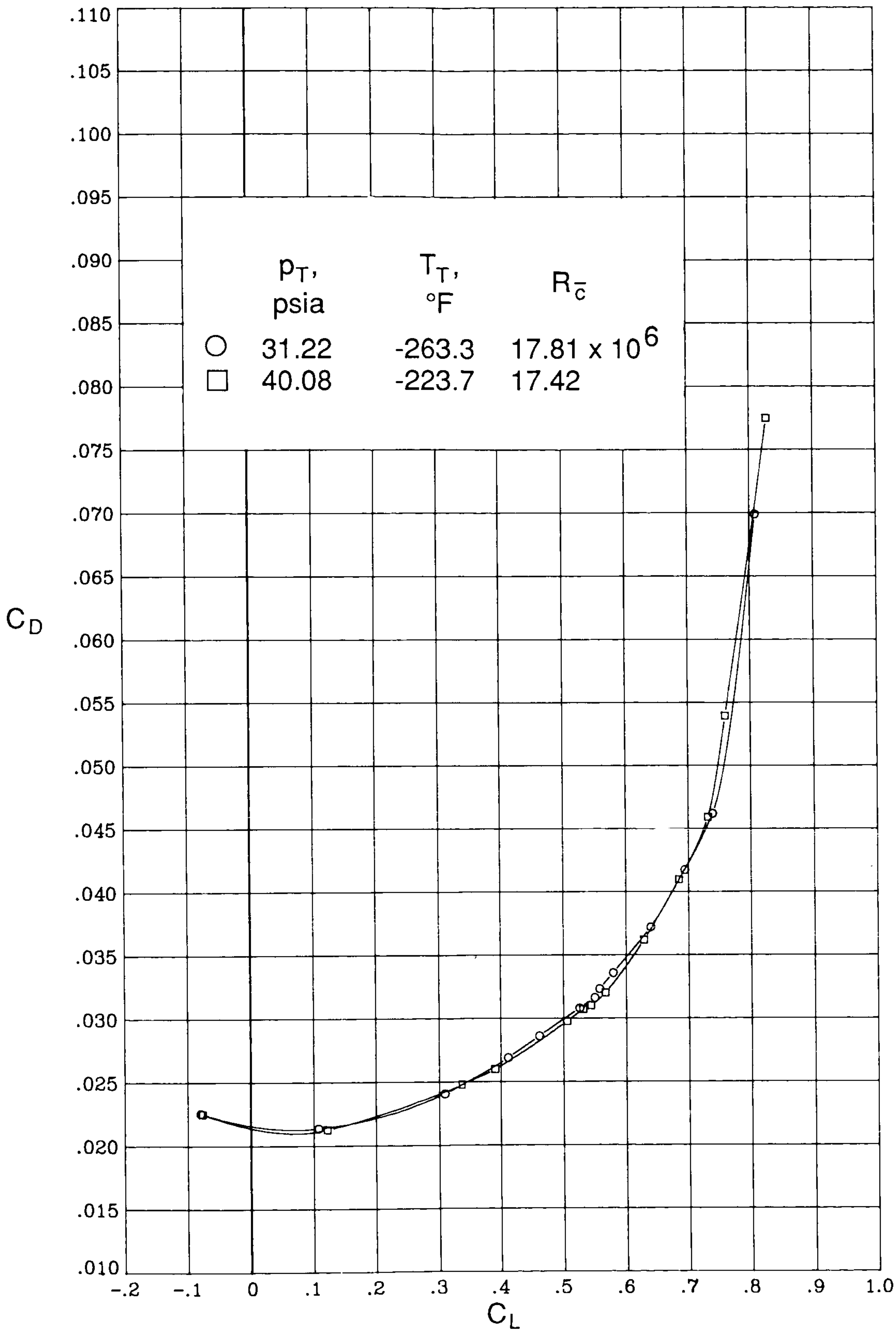

Figure 12. Aeroelasticity effects on drag coefficient versus lift coefficient at $M = 0.82$.

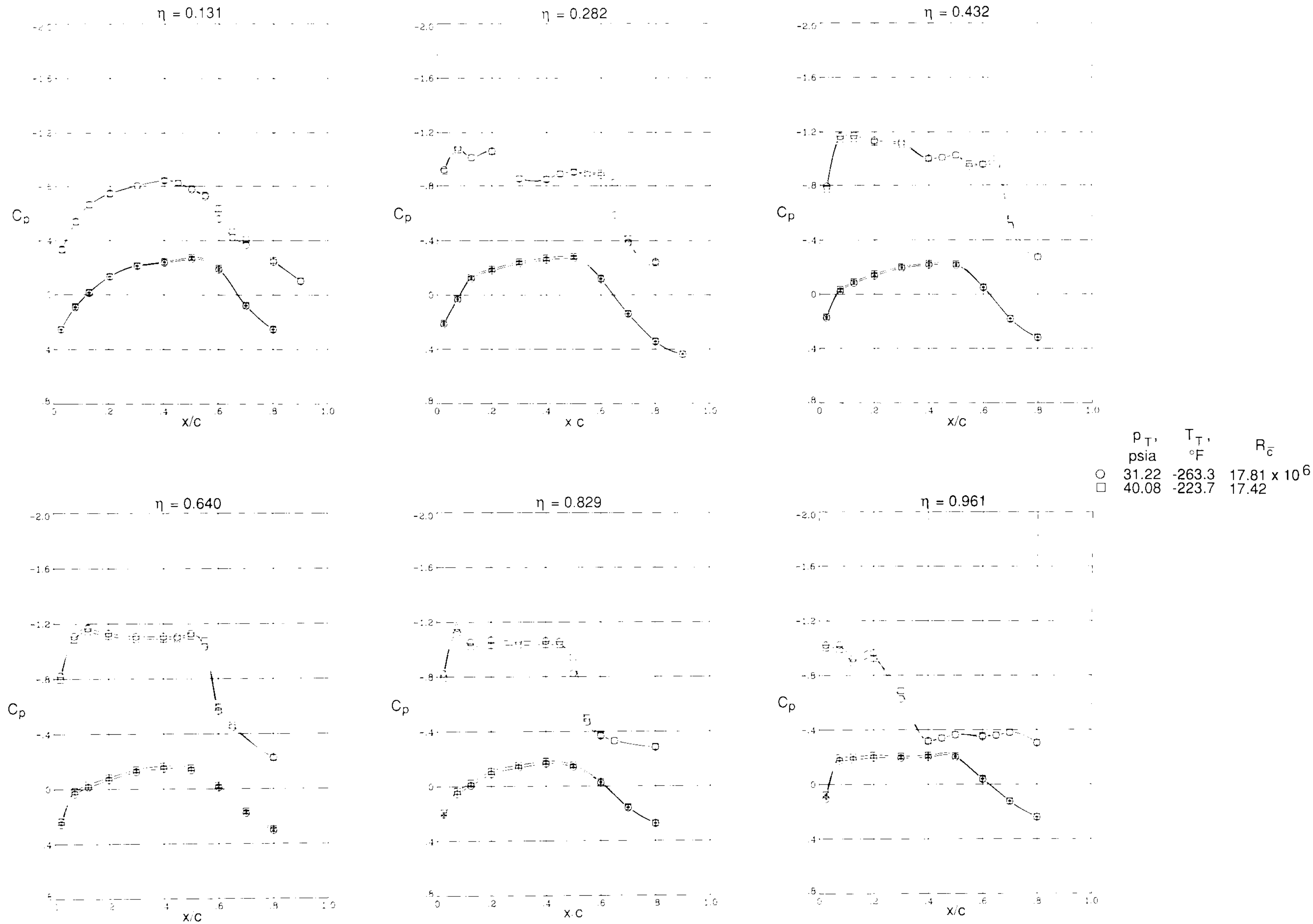

Figure 13. Aeroelasticity effects on wing chordwise pressure distributions at $M = 0.82$ and $\alpha \approx 3.2°$. Centered symbols (⊕, ⊡) represent wing lower-surface pressures.

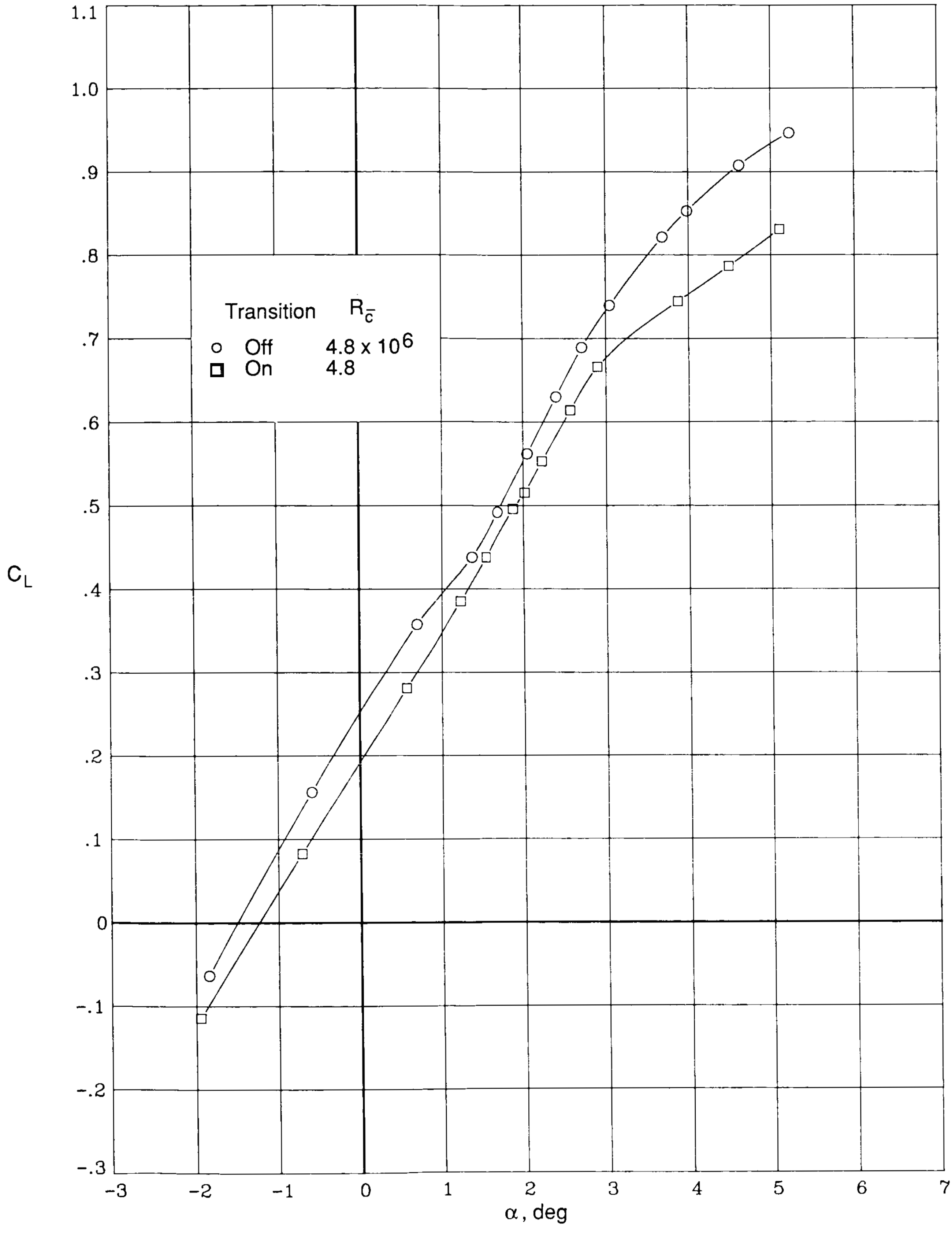

(a) Low Reynolds number.

Figure 14. Transition effects on lift coefficient versus angle of attack at $M = 0.82$.

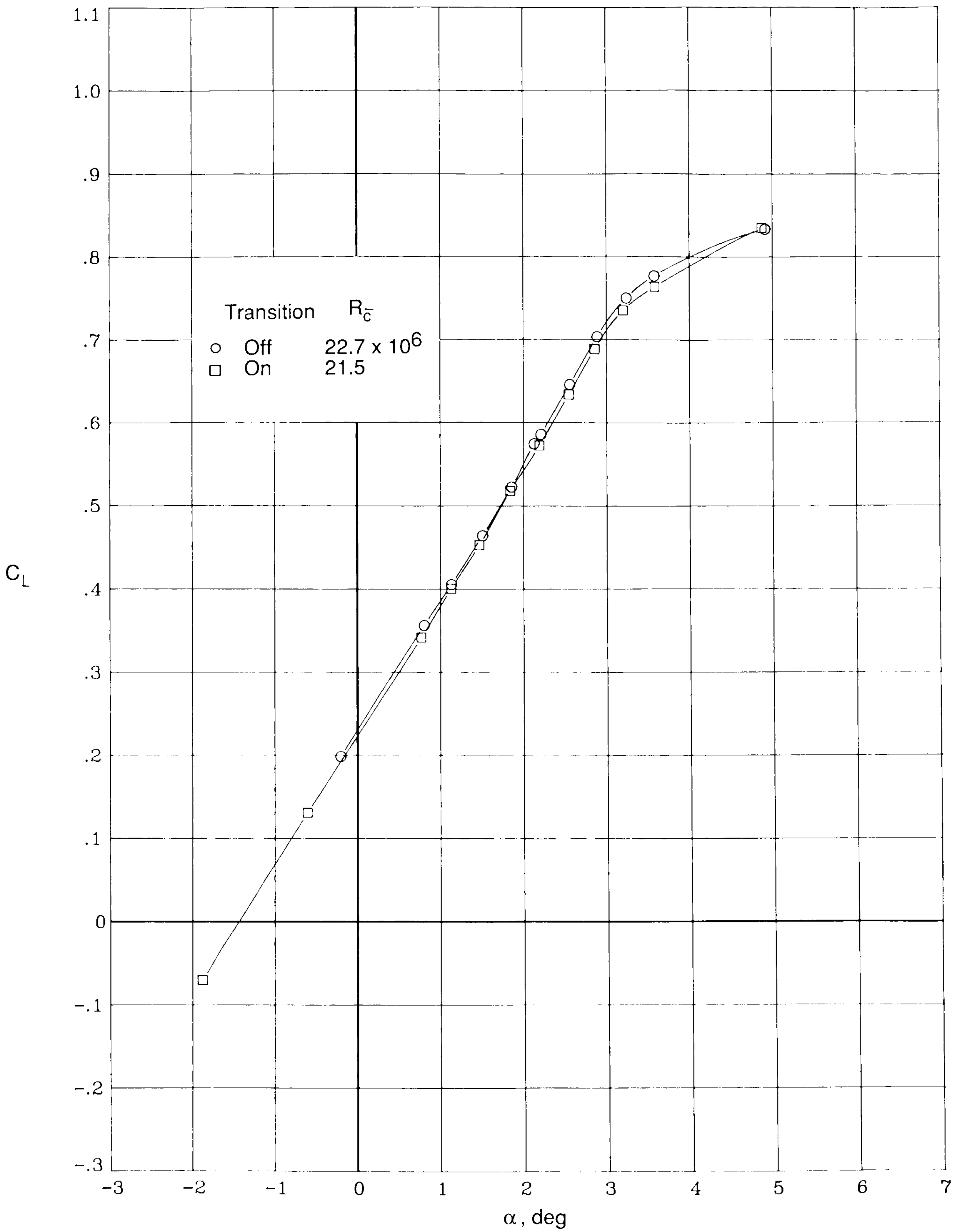

(b) High Reynolds number.

Figure 14. Concluded.

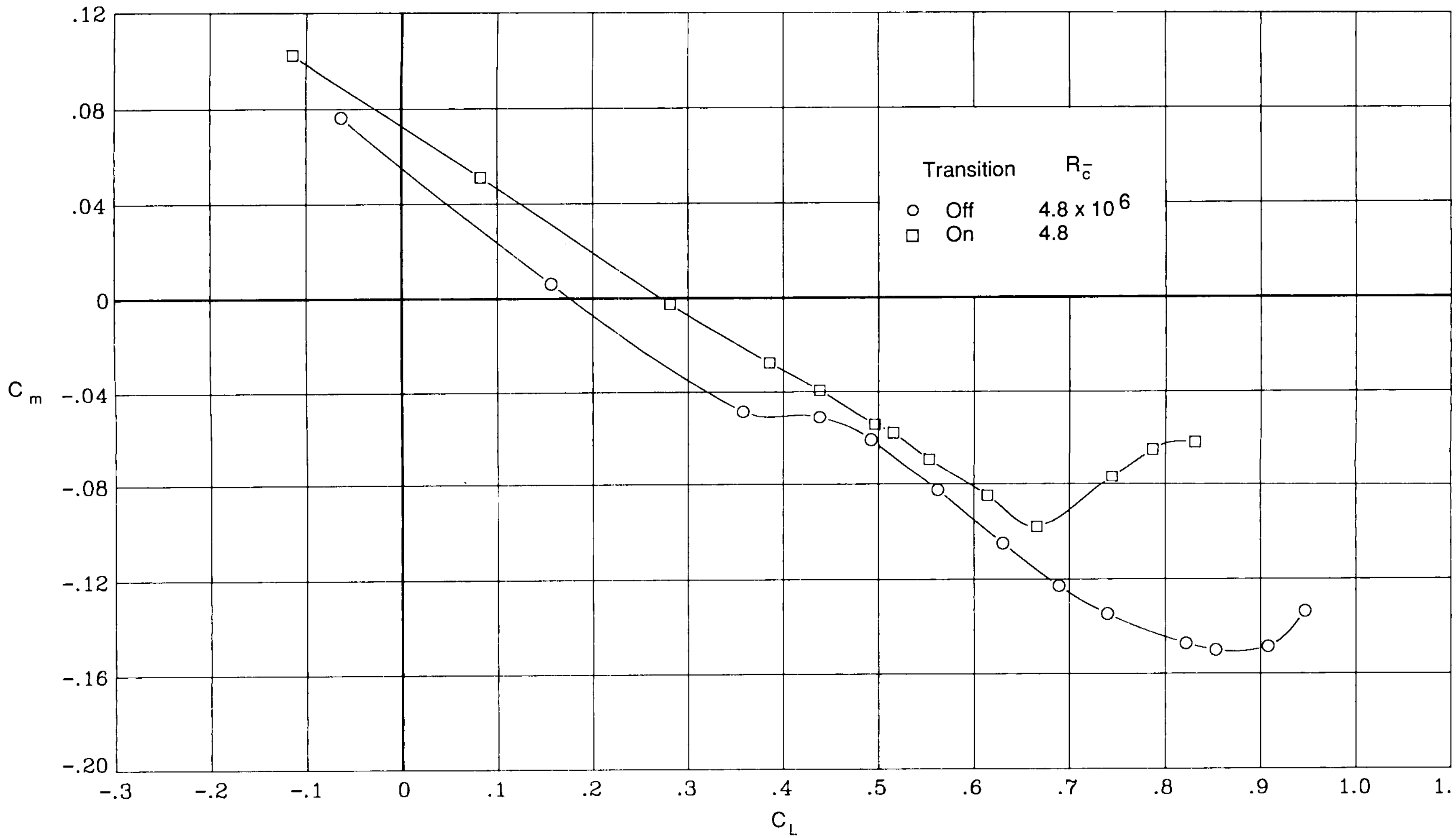

(a) Low Reynolds number.

Figure 15. Transition effects on pitching-moment coefficient versus lift coefficient at $M = 0.82$.

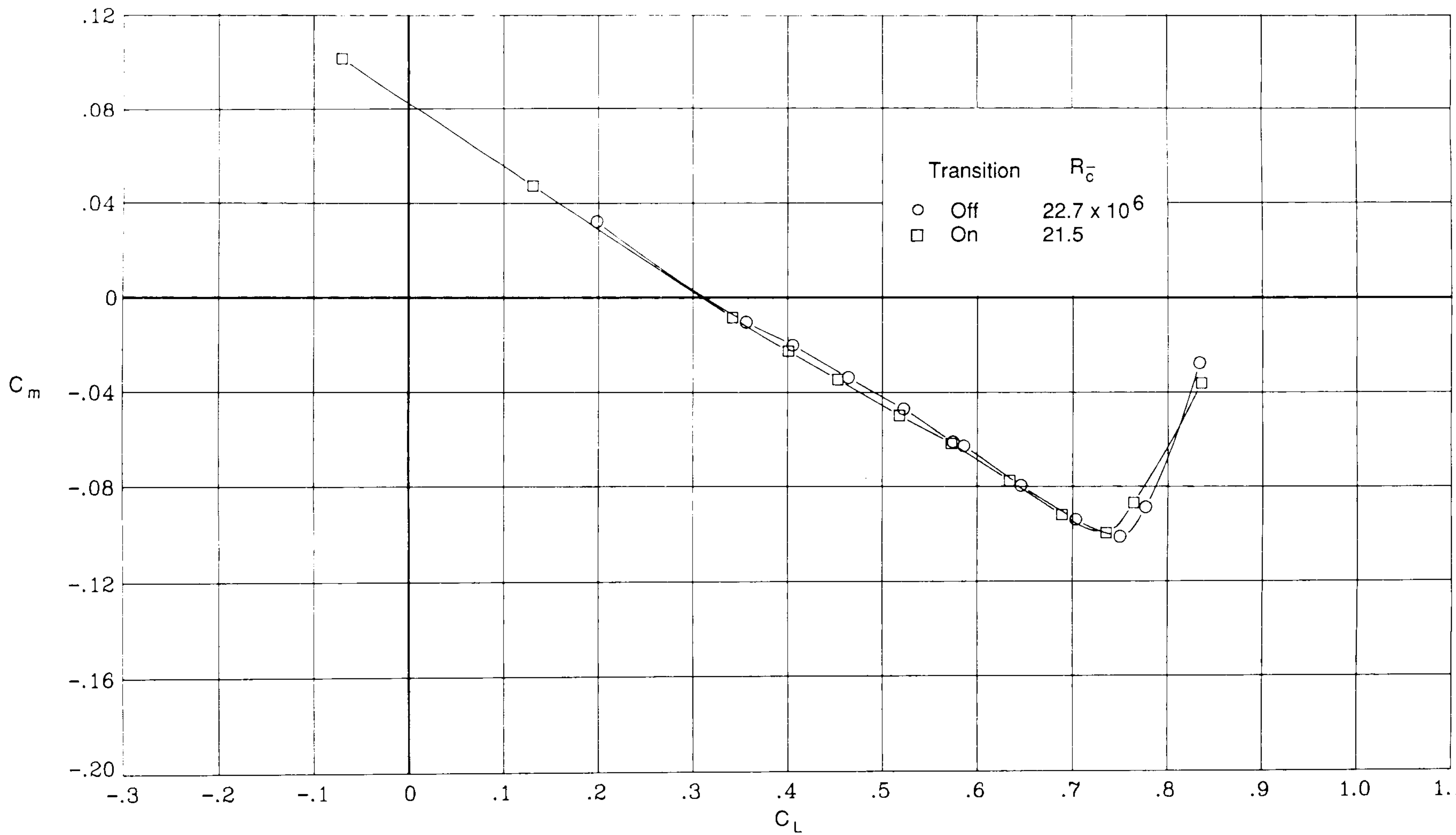

(b) High Reynolds number.

Figure 15. Concluded.

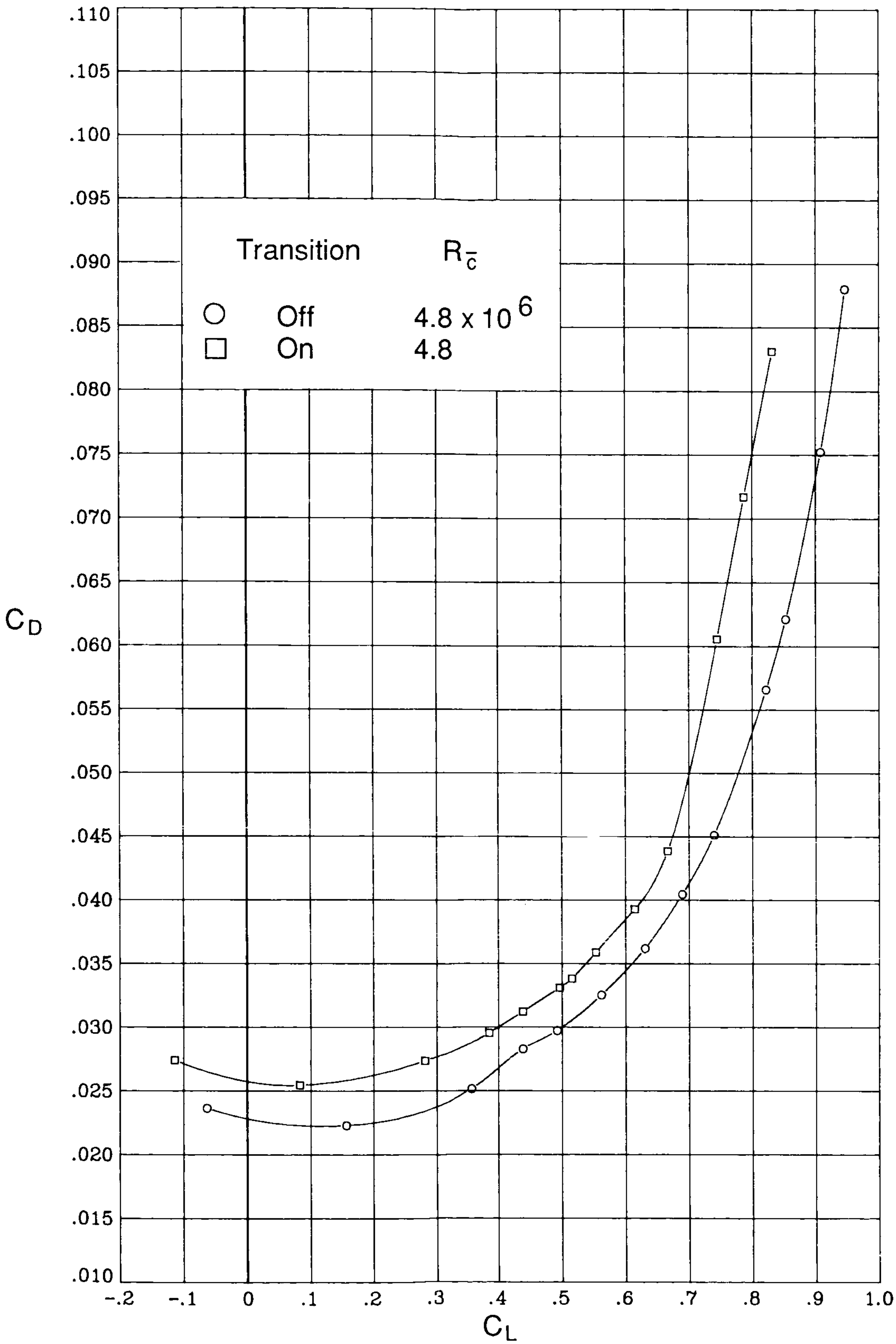

(a) Low Reynolds number.

Figure 16. Transition effects on drag co‹.ıicient versus lift coefficient at $M = 0.82$.

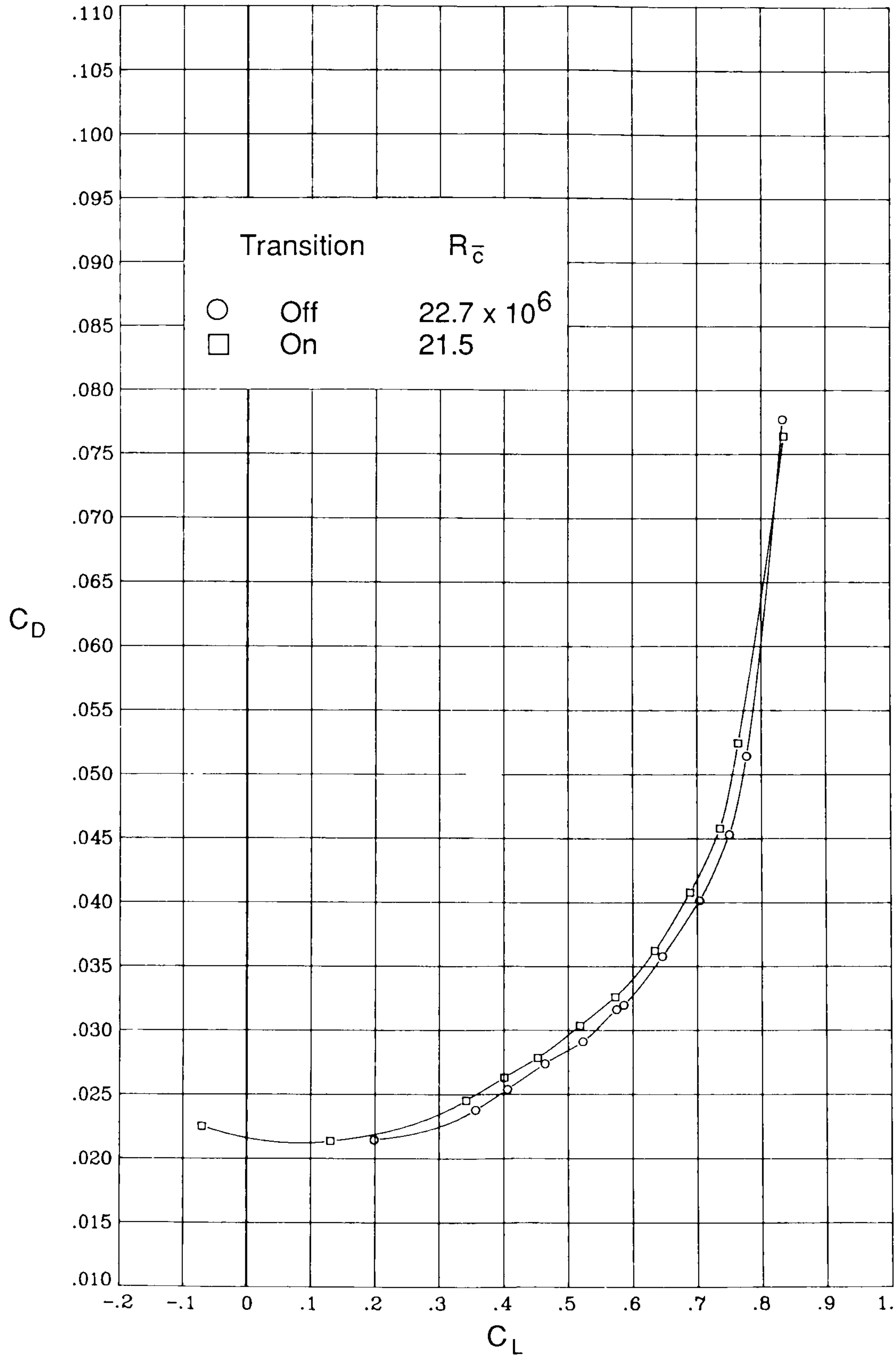

(b) High Reynolds number.

Figure 16. Concluded.

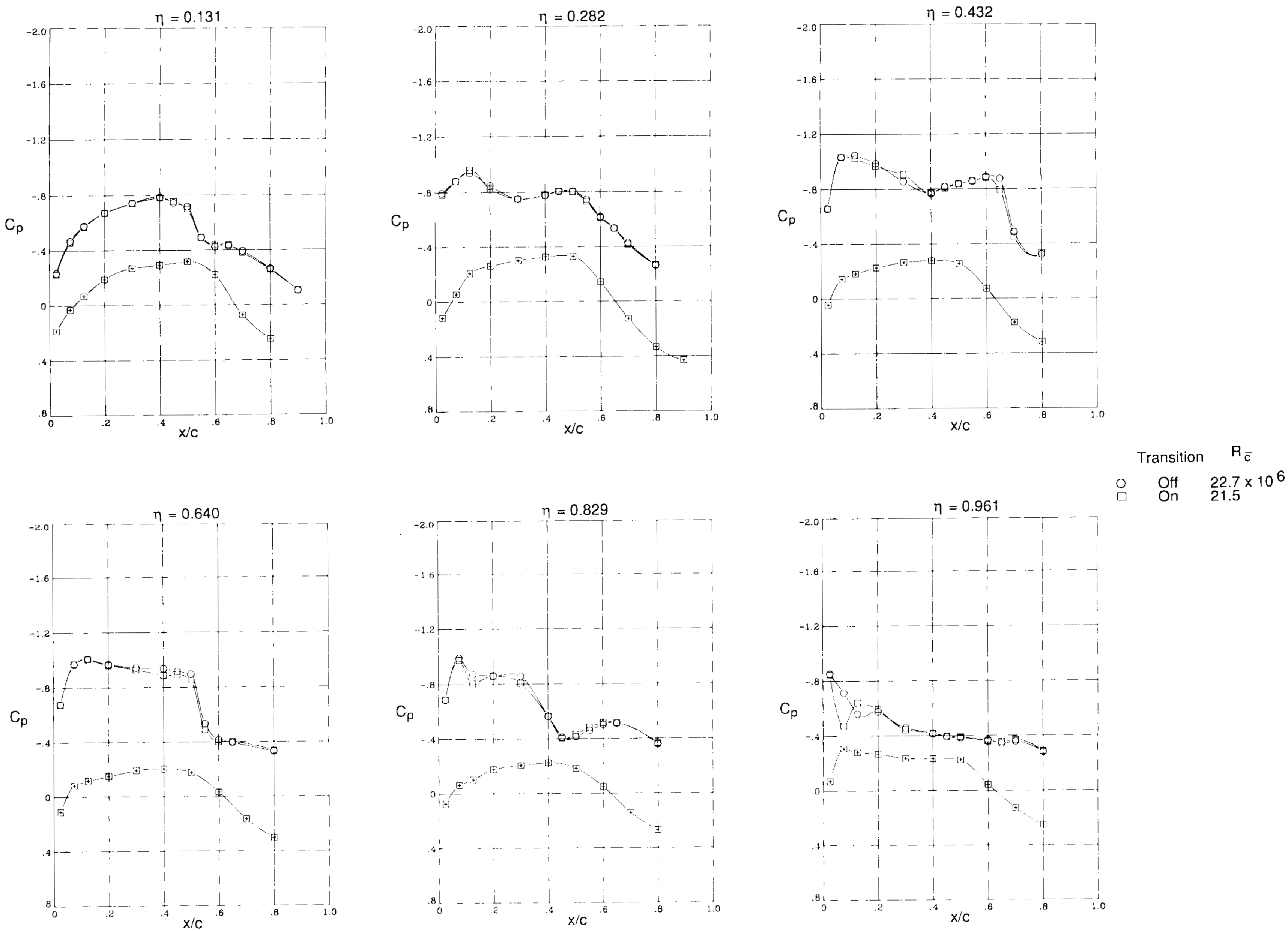

(a) $\alpha = 2.2°$.

Figure 17. Transition effects on wing chordwise pressure distributions at $M = 0.82$ with high Reynolds number. Centered symbols (⊕, ⊞) represent wing lower-surface pressures.

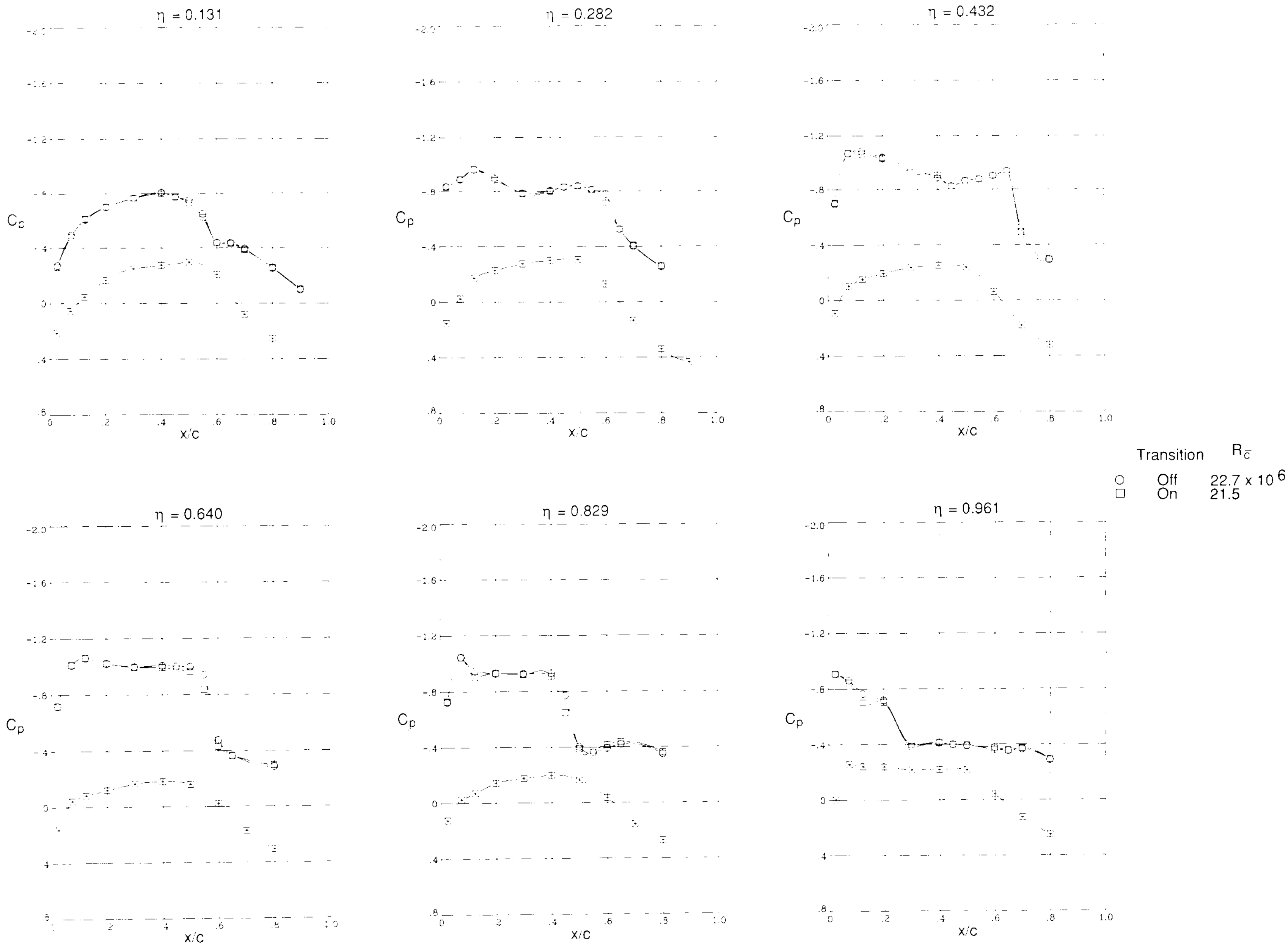

(b) $\alpha = 2.5^{\circ}$.

Figure 17. Concluded.

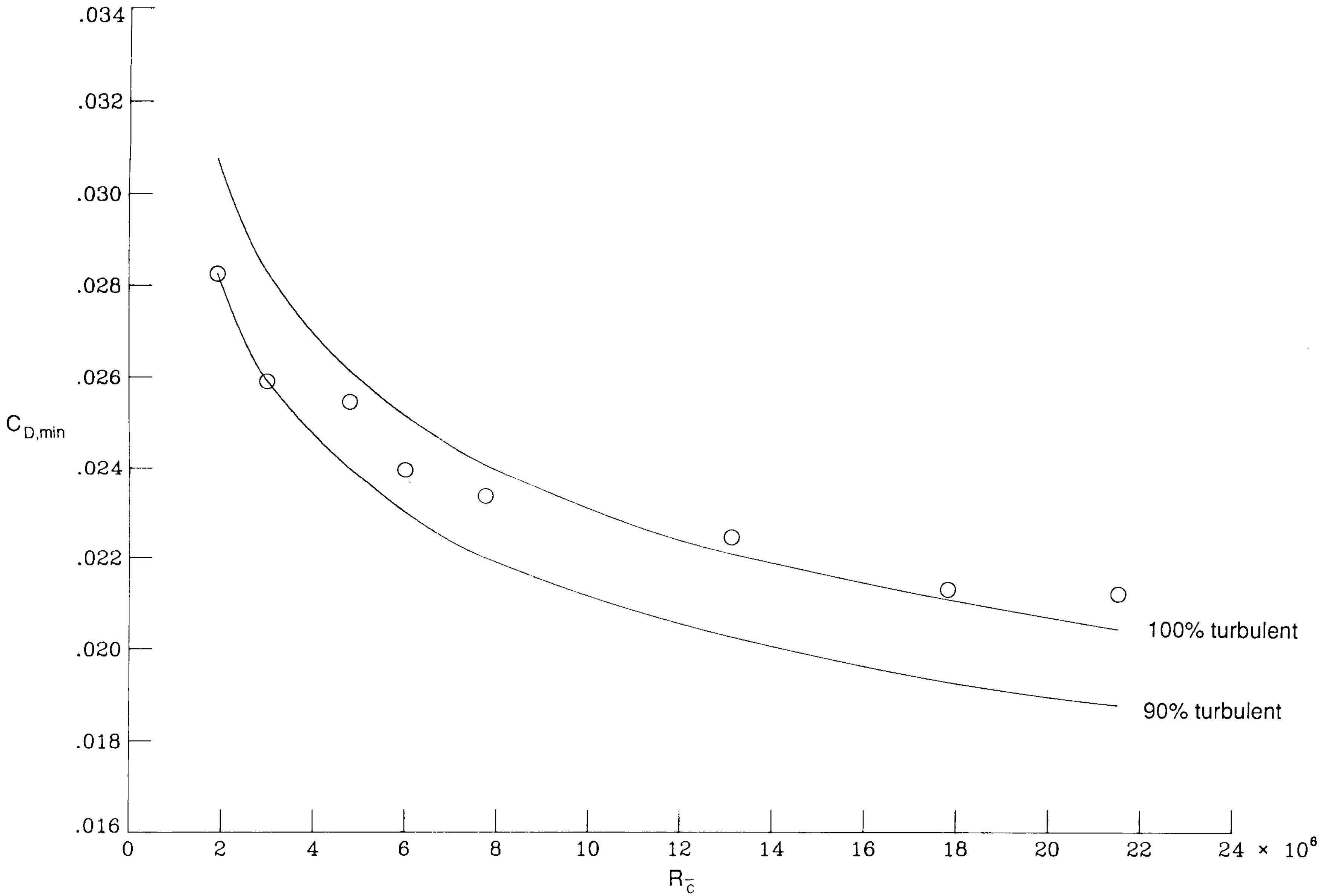

Figure 18. Estimation of trip drag penalty at $M = 0.82$.

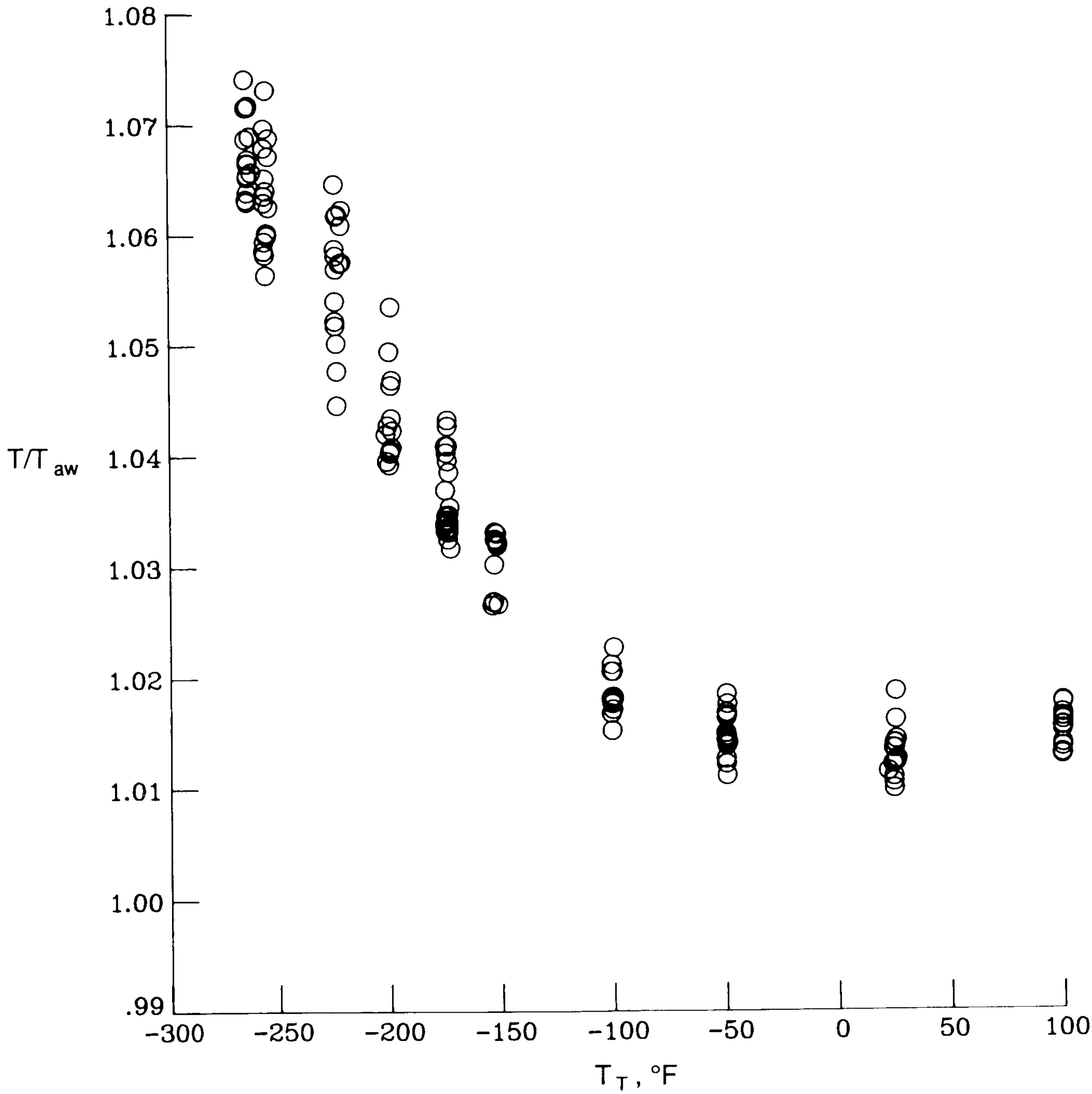

(a) $\eta = 0.2$.

Figure 19. Wing thermocouple data at $M = 0.82$ with $x/c \approx 0.4$.

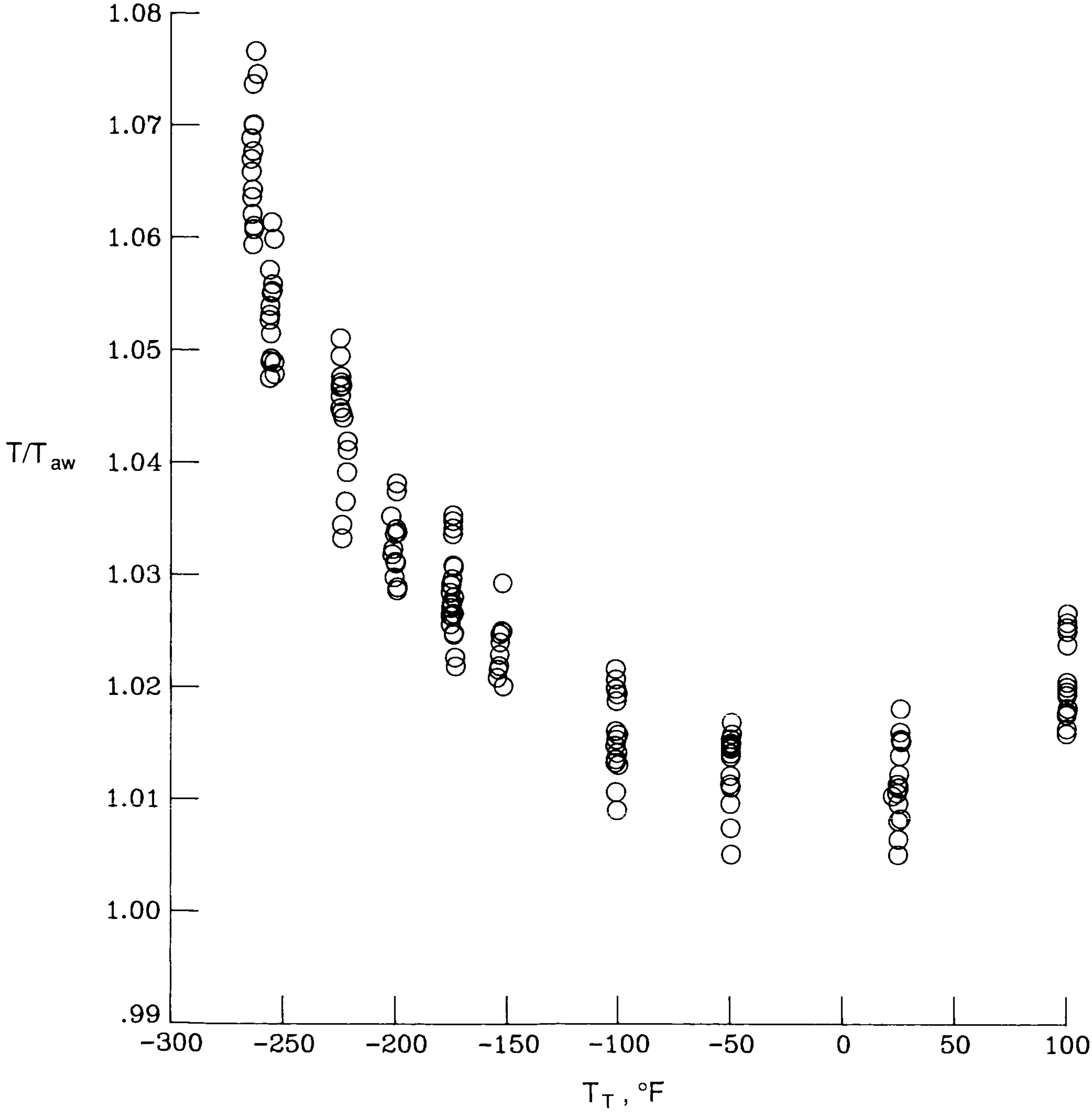

(b) $\eta = 0.5$.

Figure 19. Continued.

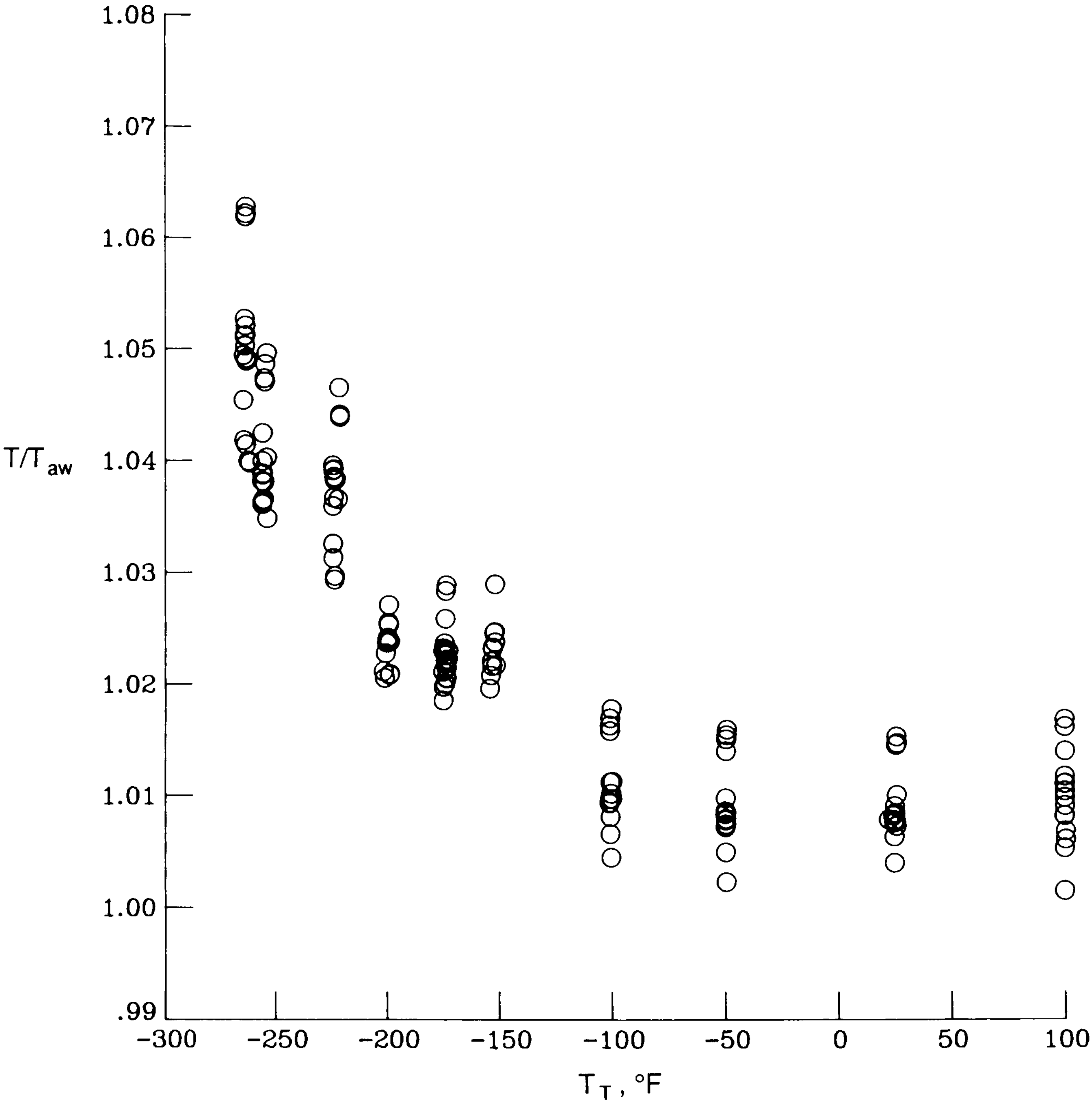

(c) $\eta = 0.8$.

Figure 19. Concluded.

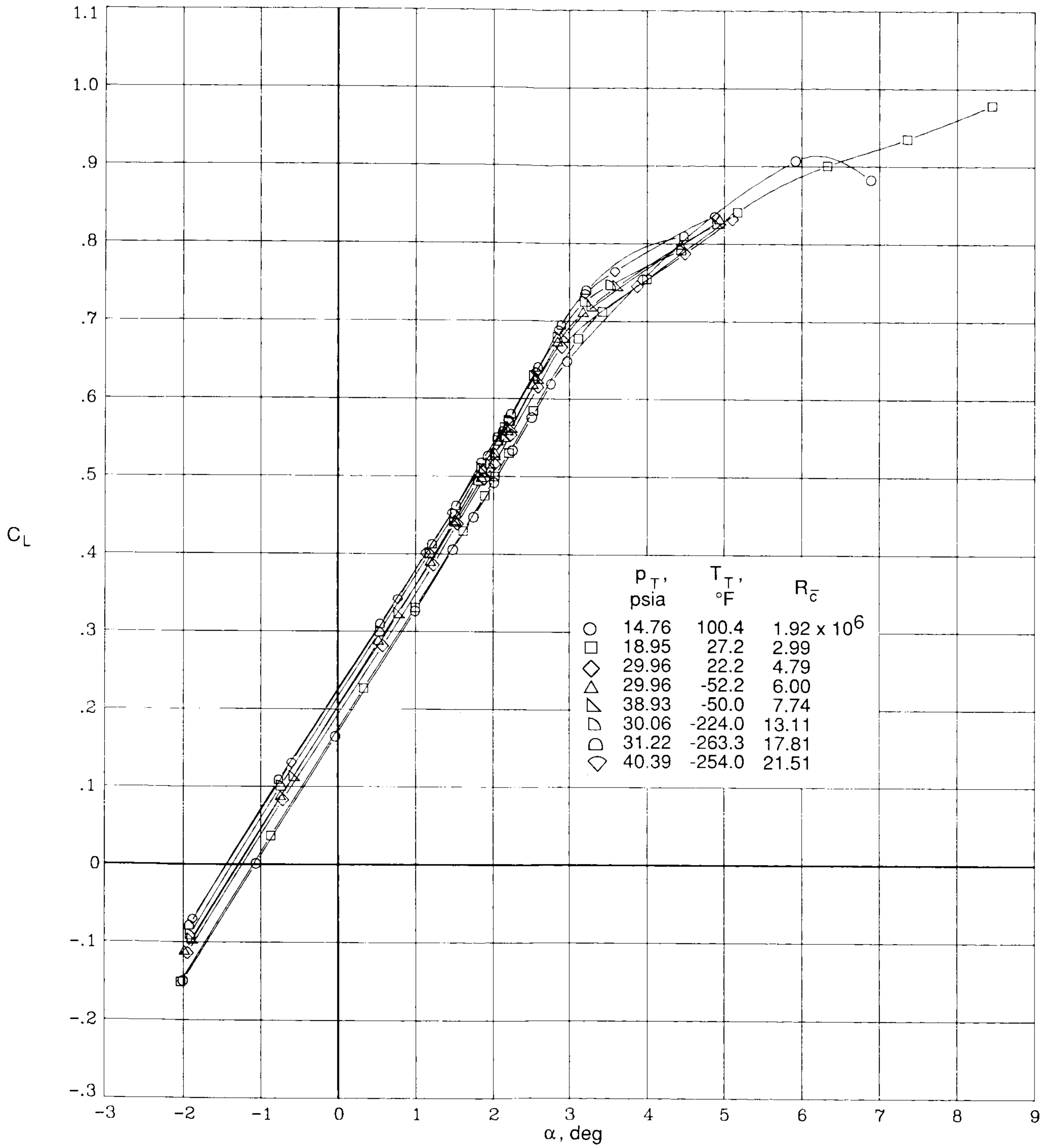

Figure 20. Reynolds number effects on lift coefficient versus angle of attack at $M = 0.82$.

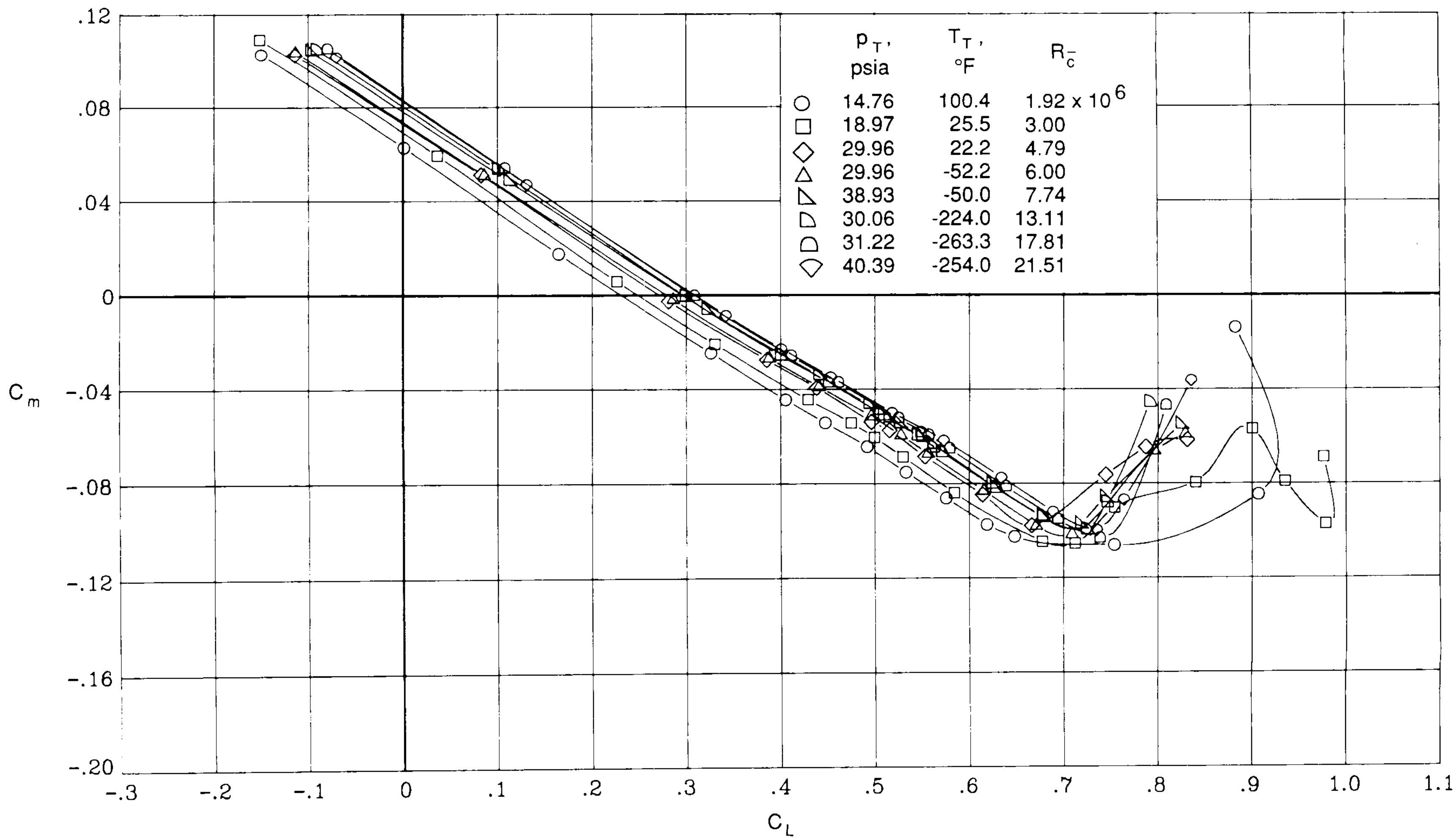

Figure 21. Reynolds number effects on pitching-moment coefficient versus lift coefficient at $M = 0.82$.

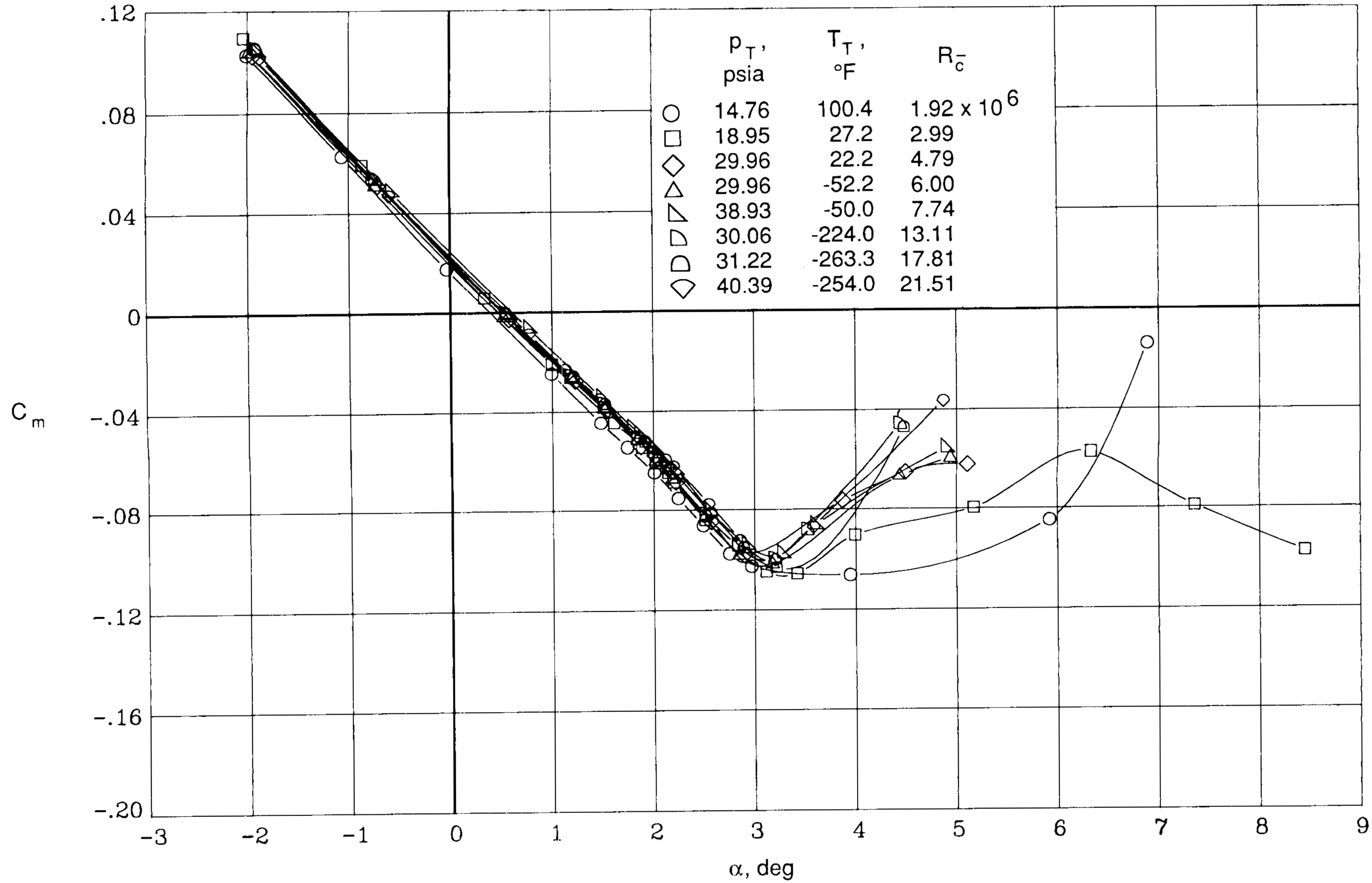

Figure 22. Reynolds number effects on pitching-moment coefficient versus angle of attack at $M = 0.82$.

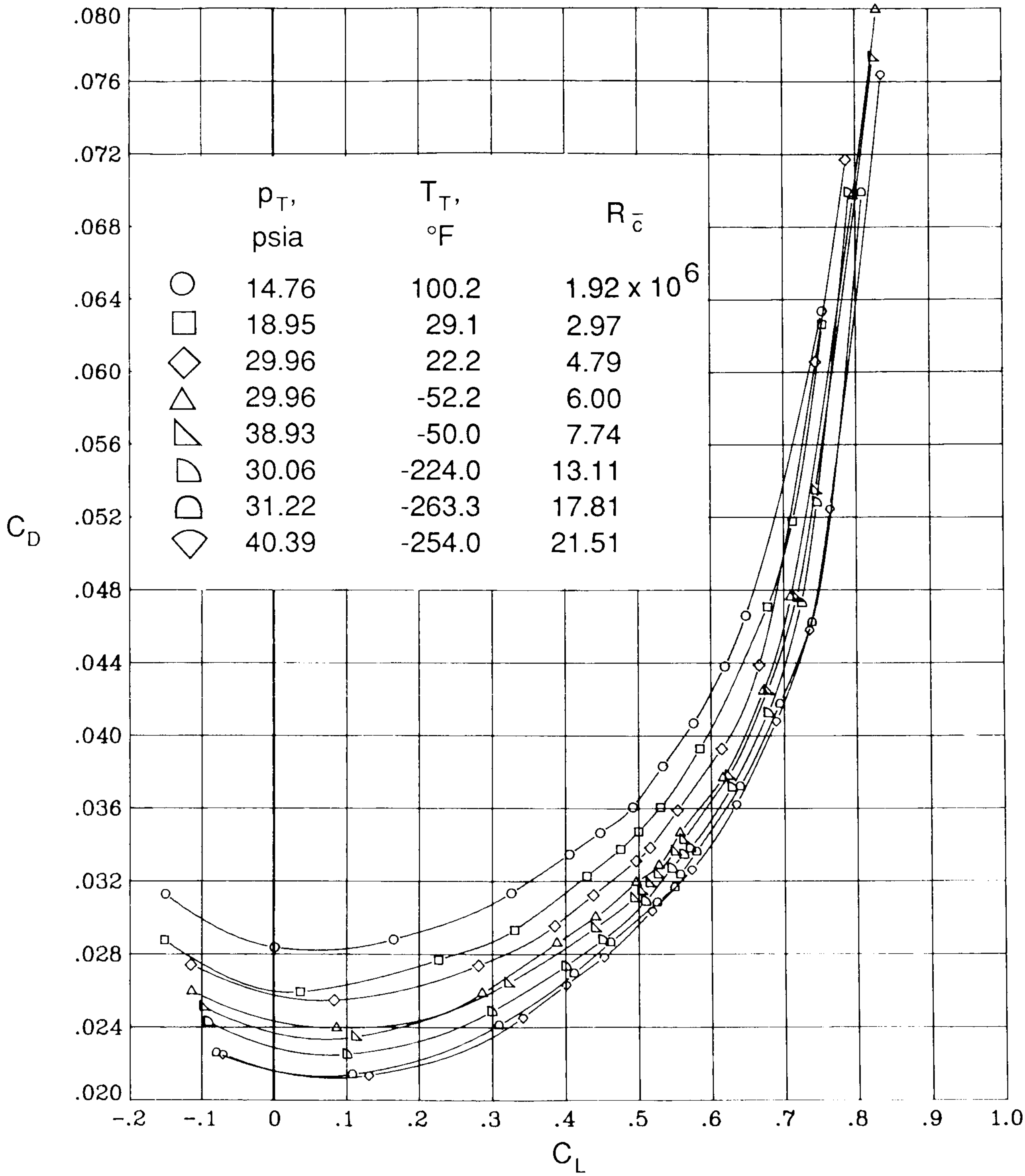

Figure 23. Reynolds number effects on drag coefficient versus lift coefficient at $M = 0.82$.

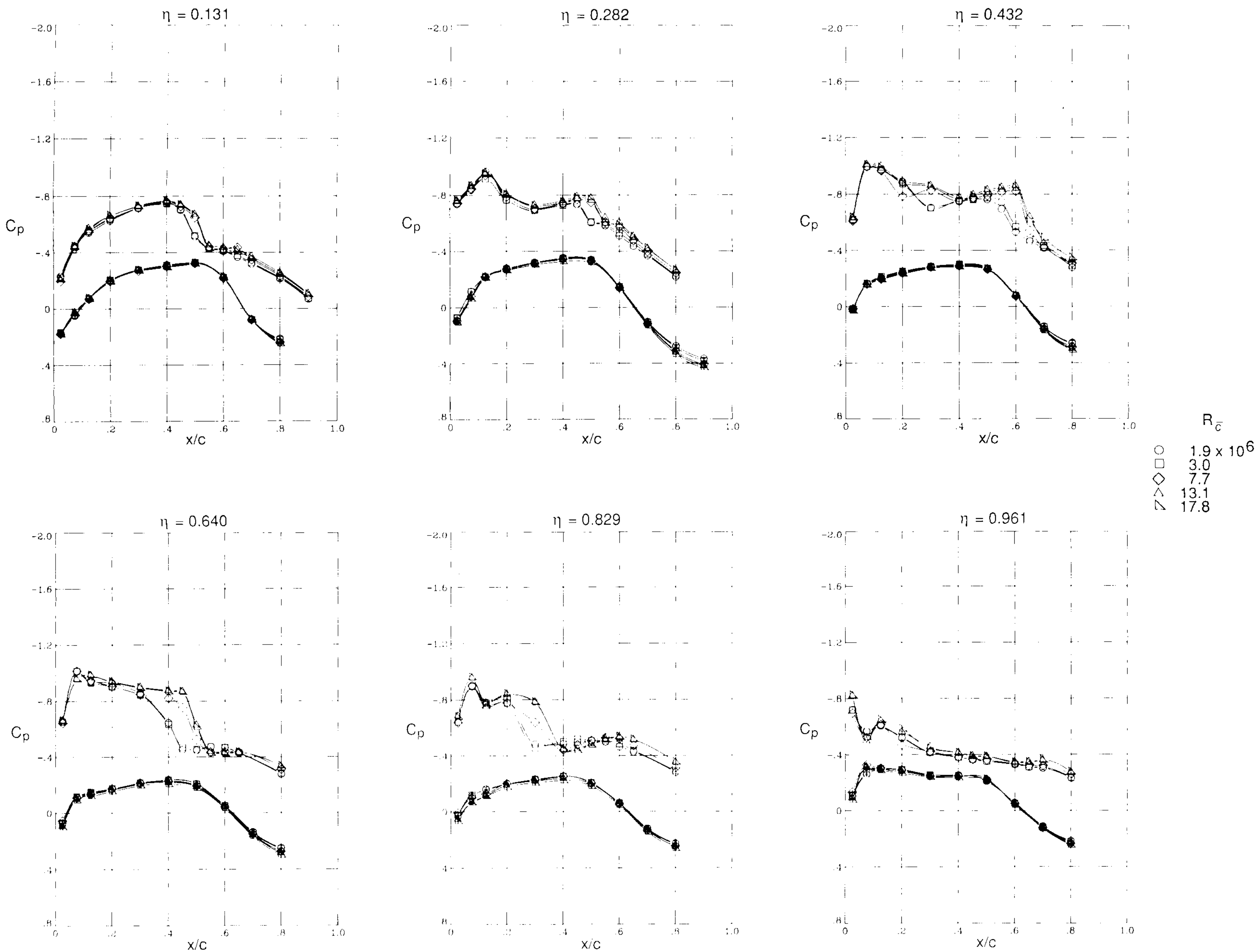

Figure 24. Reynolds number effects on wing chordwise pressure distributions at $M = 0.82$ and $\alpha = 2.0°$. Centered symbols (⊕, ⊡) represent wing lower-surface pressures.

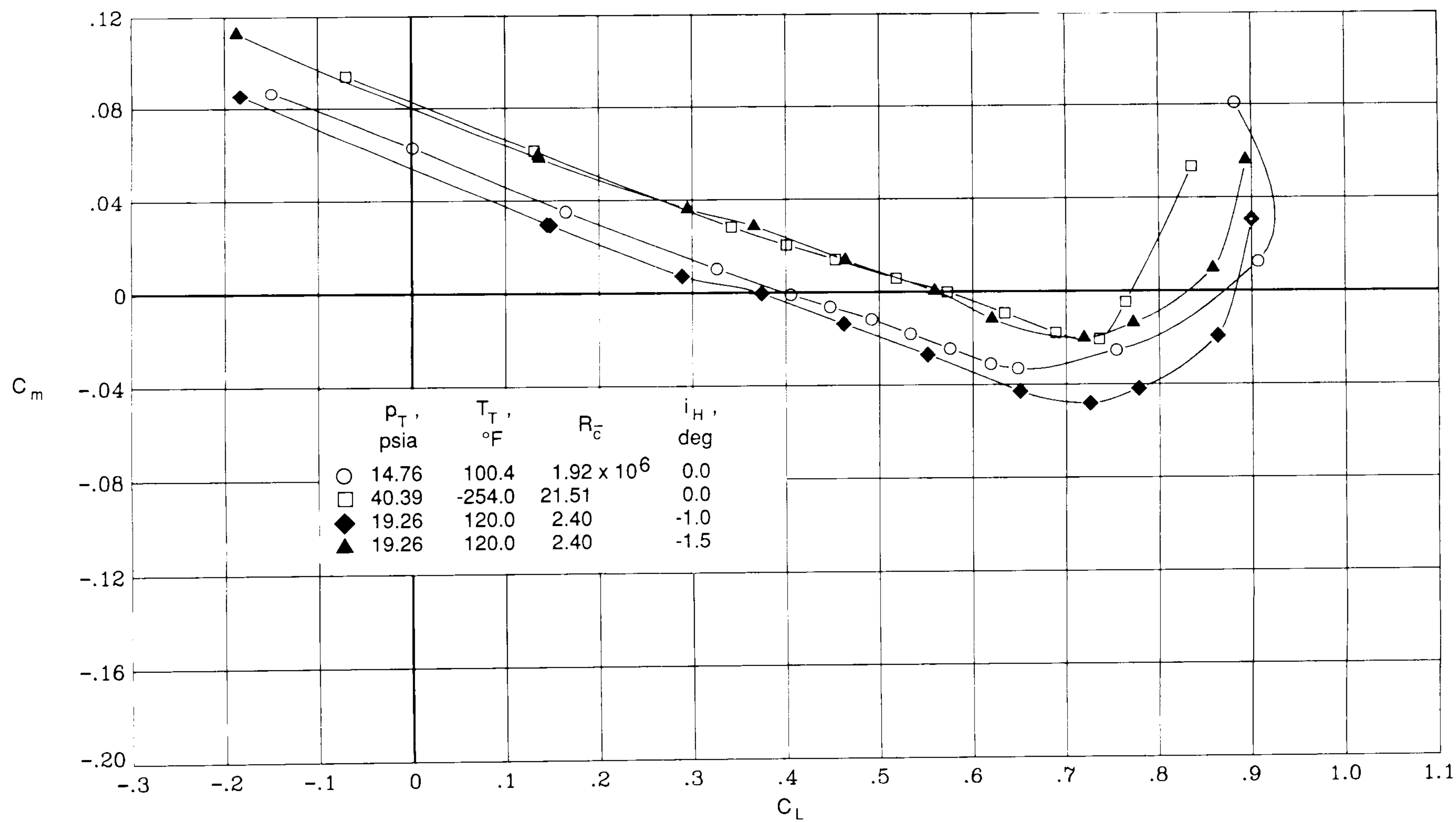

Figure 25. Comparison of pitching-moment coefficient data for Pathfinder I and Pathfinder I prototype at $M = 0.82$. Solid symbols represent Pathfinder I prototype from reference 2.

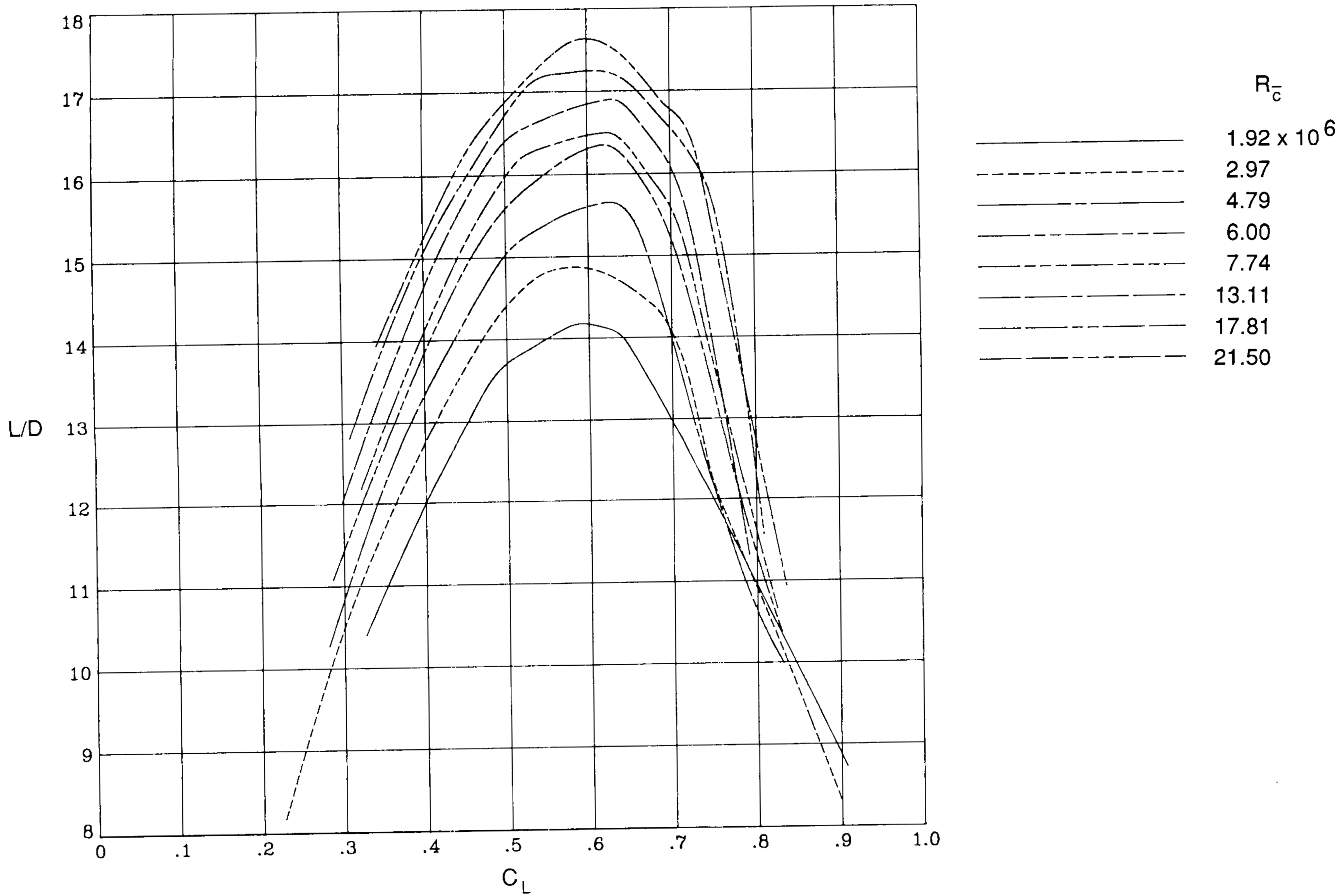

Figure 26. Reynolds number effects on untrimmed lift-drag ratio versus lift coefficient at $M = 0.82$.

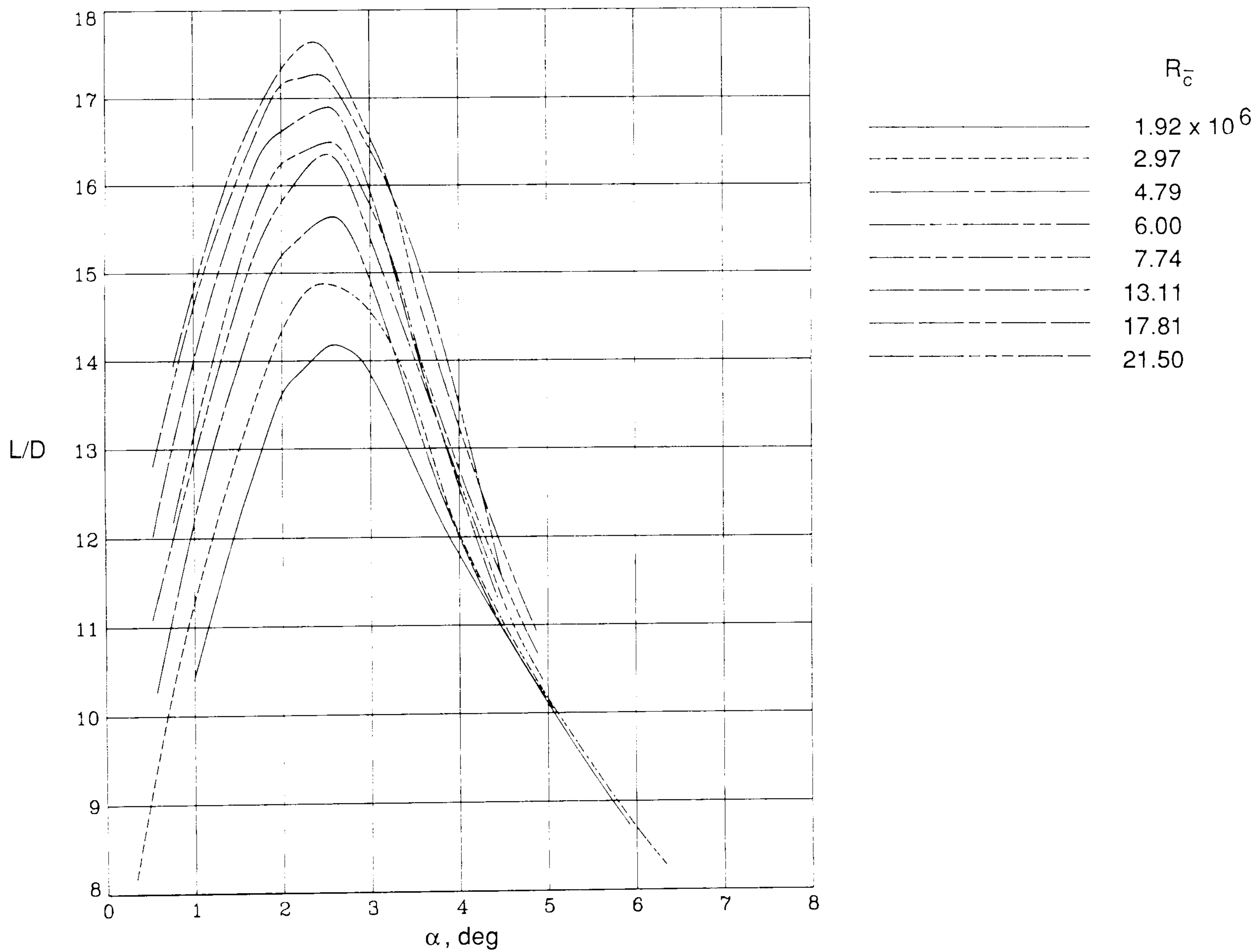

Figure 27. Reynolds number effects on untrimmed lift-drag ratio versus angle of attack at $M = 0.82$.

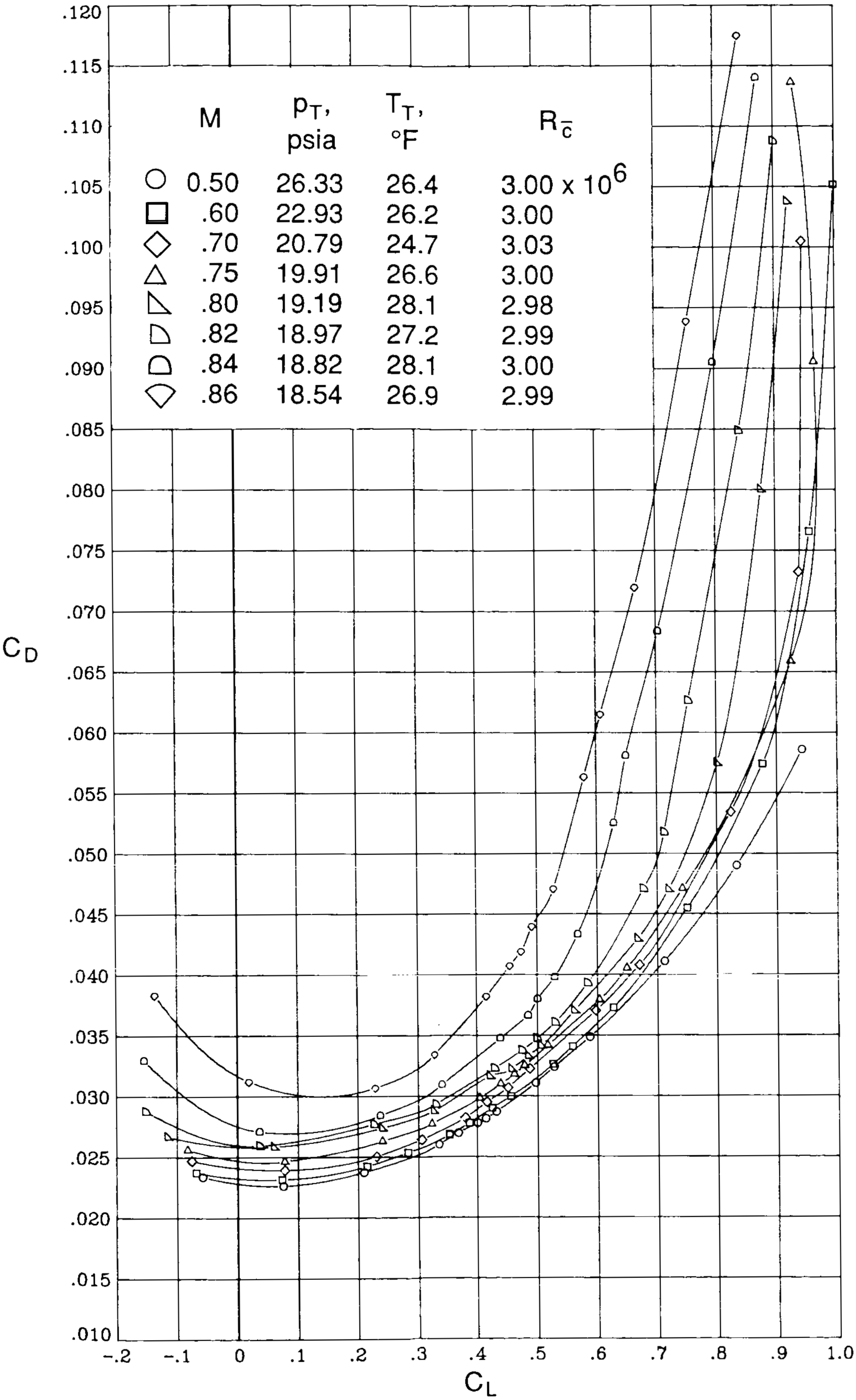

(a) $R_{\bar{c}} = 3.0 \times 10^6$.

Figure 28. Mach number effects on drag coefficient versus lift coefficient.

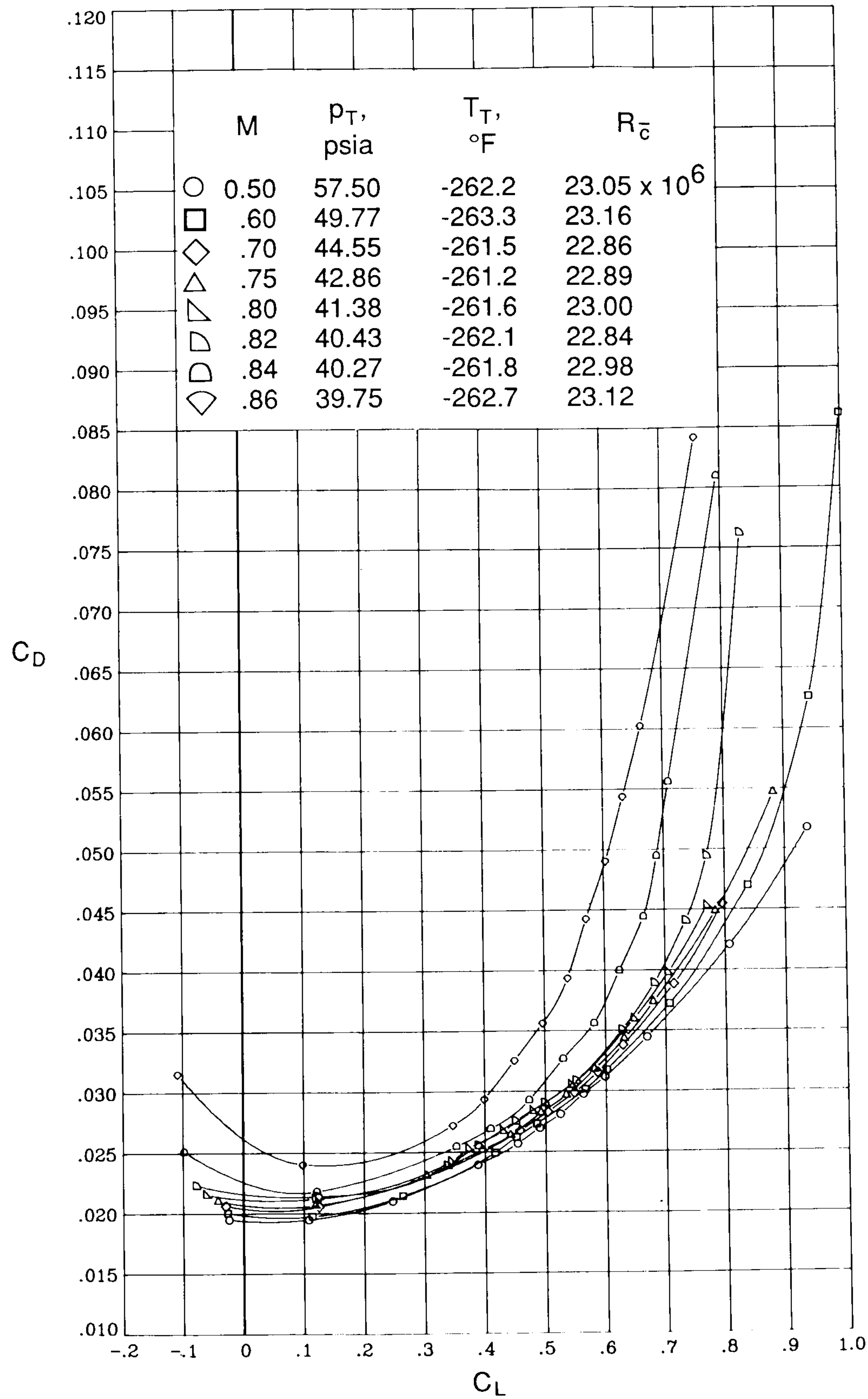

(b) $R_{\bar{c}} \approx 23.0 \times 10^6$.

Figure 28. Concluded.

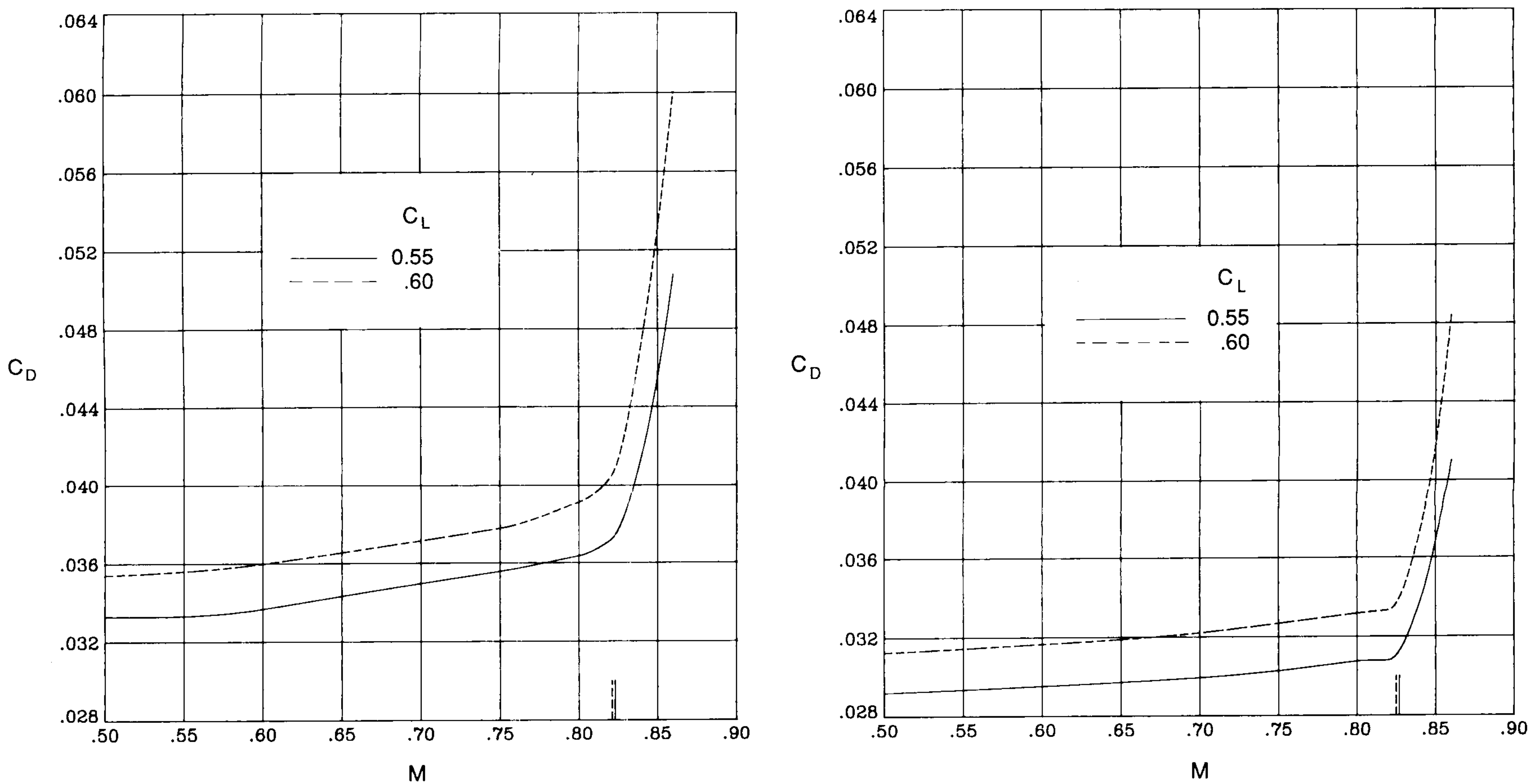

(a) $R_{\bar{c}} = 3.0 \times 10^6$.

(b) $R_{\bar{c}} = 23.0 \times 10^6$.

Figure 29. Variation of drag coefficient with Mach number. Tick marks on Mach number scale indicate drag-divergence Mach number.

NASA
National Aeronautics and Space Administration

Report Documentation Page

1. Report No.	2. Government Accession No.	3. Recipient's Catalog No.
NASA TP-2922		

4. Title and Subtitle	5. Report Date
Longitudinal Aerodynamic Characteristics of a Subsonic, Energy-Efficient Transport Configuration in the National Transonic Facility	August 1989
	6. Performing Organization Code
7. Author(s) Peter F. Jacobs and Blair B. Gloss	8. Performing Organization Report No. L-16569
9. Performing Organization Name and Address NASA Langley Research Center Hampton, VA 23665-5225	10. Work Unit No. 505-61-21-03
	11. Contract or Grant No.
12. Sponsoring Agency Name and Address National Aeronautics and Space Administration Washington, DC 20546-0001	13. Type of Report and Period Covered Technical Paper
	14. Sponsoring Agency Code

15. Supplementary Notes

16. Abstract

An investigation has been conducted in the National Transonic Facility (NTF) at the Langley Research Center to determine Reynolds number, aeroelasticity, boundary-layer transition, and nonadiabatic wall temperature effects for a subsonic, energy-efficient transport model. The model was tested over a Mach number range from 0.50 to 0.86 and a Reynolds number range from 1.9×10^6 to approximately 23.0×10^6 (based on mean geometric chord). The majority of the data were taken using cryogenic nitrogen. (Data at a Reynolds number of 1.9×10^6 were taken in air.) Longitudinal force and moment, wing pressure, and wing thermocouple data are presented in this report. The data indicate that increasing the Reynolds number resulted in greater effective camber of the supercritical wing and horizontal tail, thus resulting in greater lift and pitching-moment coefficients at nearly all angles of attack for a Mach number (M) of 0.82. As Reynolds number was increased, untrimmed lift-drag ratio (L/D) increased, the angle of attack for maximum L/D decreased, drag creep was reduced significantly, and drag-divergence Mach number increased slightly. Data repeatabilty for both modes of operation of the NTF (air and cryogenic nitrogen) was generally very good, and nonadiabatic wall effects were estimated to be small. Transition-free and transition-fixed configurations had significantly different force and moment data at $M = 0.82$ for low Reynolds numbers, and very small differences were noted at high Reynolds numbers.

17. Key Words (Suggested by Authors(s))	18. Distribution Statement
Cryogenic wind tunnel Energy-efficient transport (EET) Supercritical wing Reynolds number effects Nonadiabatic wall effects	FEDD Subject Category 02

19. Security Classif. (of this report)	20. Security Classif. (of this page)	21. No. of Pages	22. Price
Unclassified	Unclassified	68	

NASA FORM 1626 OCT 86

NASA Langley, 1989